



# Modélisation de la Variabilité Spatiale du Champ Sismique pour les Etudes d'Interaction Sol-Structure

Angkeara Svay

## ► To cite this version:

Angkeara Svay. Modélisation de la Variabilité Spatiale du Champ Sismique pour les Etudes d'Interaction Sol-Structure. Autre. Université Paris Saclay (COMUE), 2017. Français. NNT : 2017SACLC016 . tel-01544447

**HAL Id: tel-01544447**

**<https://theses.hal.science/tel-01544447>**

Submitted on 21 Jun 2017

**HAL** is a multi-disciplinary open access archive for the deposit and dissemination of scientific research documents, whether they are published or not. The documents may come from teaching and research institutions in France or abroad, or from public or private research centers.

L'archive ouverte pluridisciplinaire **HAL**, est destinée au dépôt et à la diffusion de documents scientifiques de niveau recherche, publiés ou non, émanant des établissements d'enseignement et de recherche français ou étrangers, des laboratoires publics ou privés.

NNT : 2017SACLC016

THESE DE DOCTORAT  
DE  
L'UNIVERSITE PARIS-SACLAY  
PREPAREE A  
"CENTRALESUPELEC"

ECOLE DOCTORALE N° 579  
**Sciences Mécaniques et Energétiques, Matériaux et Géosciences**

Spécialité de doctorat : **Génie Civil**

Par

**M. Angkeara SVAY**

**Modélisation de la Variabilité Spatiale du Champ Sismique pour  
les Etudes d'Interaction Sol-Structure**

Thèse présentée et soutenue à CentraleSupélec, Chatenay-Malabry, le 22 février 2017 :

**Composition du Jury :**

M, LABBE Pierre	Professeur, ESTP Paris	Président
M, SEMBLAT Jean-François	Directeur de Recherche, IFSTTAR	Rapporteur
Mme, CORNOU Cécile	Chargée de Recherche, ISTERre	Rapporteur
M, CLOUTEAU Didier	Professeur, CentraleSupélec	Directeur de Thèse
Mme, ZENTNER Irmela	Ingénieur de Recherche-Experte, EDF Lab	Encadrant
M, COTTEREAU Régis	Chargé de Recherche, CNRS/MSSMat	Co-Encadrant
M, PAOLUCCI Roberto	Professeur, Politecnico di Milano	Examineur
Mme, FOERSTER Evelyne	Ingénieur de Recherche, CEA-Paris-Saclay	Examineur





# ACKNOWLEDGEMENT

If this doctoral thesis can be submitted and validated, it is simply because of the help of all the people around me.

First of all, I would like to express my sincere gratitude to Professor Didier CLOUTEAU, for his continuous confidence on me by permitting me to realize this interesting work under his supervision and by giving me all the liberties to realize what I wish to do, and especially to be autonomous. His precious scientific knowledge did help me all along these three years.

The second person to be mentioned here is Dr. Irmela ZENTNER. Many thanks for her time she spent with me to guide me in the right direction, especially, at the beginning of the work. I was sometimes lost in the intersection between seismology and engineering since there were so many directions to go, but she was always there to rectify my direction. Thanks for accepting me as an intern in the world of “Spatial Variability of Seismic Ground Motions” which lets me discover that passionate world.

The third person who contributed a lot in this work is Dr. Régis COTTEREAU. Originally considered as a helper in numerical simulation, his aides were finally in all parts of this work : experimental, theoretical, numerical as well as methodological. Many thanks for his simplicity, his advices and criticisms (especially when I started using SEM3D) which were the important elements pushing me forward to reach this goal. His comments were sometimes hurtful but completely meaningful and it was a remarkable memory to work with him during these three years.

Another person that I cannot forget to mention here is Dr. Fernando Lopez-Caballero. He was not listed in the paper as my official supervisor, but I can say that he involved in most of the work I realized for this doctoral thesis. His simple and friendly personality did permit me to approach him to uncountable meaningful discussions which are useful for this work.

I also cannot forget the assistance from some of my colleagues, both at MSSMAT laboratory and at EDF, especially, Lucio, Luciano, Filippo and Zouhair. There is no word to describe our friendship, and you all did take part of the important people involving in this doctoral work. As what we used to lark together, Lucio is not preparing only his doctoral thesis, but also three other theses in the same time, including mine. He does deserve the title of our “Grand Prof”. Many thanks are also for Luciano for his wonderful library of stochastic field generation. The numerical analysis part of this work could be achieved by using that library. For Filippo, his hard work habits did influence me a lot. The most interesting memories are about working at the laboratory during the weekends, and some useful discussions by Skype which were sometimes at 3 AM. And now, it is about Zouhair. He got officially the title of my best and my worst “colleague of the office” because we were only two in the office at EDF. There were commonly so many things we did to help each other.

Another person who can be considered as the most important one is my girlfriend, Vattey. I would like to thank her for everything she did for me during the third year of this work. Thanks for always being next to me during all the stressful moments, and thanks for cherishing my life whenever I felt that I failed down. Thanks for the food you prepared for me every day, particularly for the special day : the defense of this doctoral thesis.

I am beholden to Dr. Jean-François SEMBLAT and Dr. Cécile CORNOU who confirmed to be the reporters of this manuscript, and who permitted this work to be presented, defended and

validated. I can say that I discovered the domain of “Soil-Structure Interaction” because of Jean-François since he was the supervisor of my first research project when I was in the second year at the Ecole Polytechnique. Many thanks to Pr. Pierre LABBE, Pr. Roberto PAOLUCCI and Dr. Evelyne FOERSTER who approved to be respectively president and members of jury for assessing and legitimizing this doctoral work.

I also want to extend my appreciation to many friends, students, professors, and research engineers with whom, somehow, I shared time and lots of enjoyable moments. For their generosity, help and friendship, I am highly grateful to : Vinicious, Ahmed, Shahram, Alex, Zhiyi, Naoufal, Diana, Silvana, Ioana, Rafael, Alfonso, Andrea, Thiago, Eric, Georges, François, Nicolas, Maroua, Sara, Zaki, Baptiste, Khalil, Romain, Hélène, Guillaume, Aurélien, Sylvie, Marc, Vincent, Fabrice, Pierre-Yves, Marion, Catherine, Aurore, Denis, Mike, Xue, Anne-Sophie, Chetra and many others that will certainly remain in my memories for ever. Thanks to my EDF managers, Vincent, Stéphane and Alexandre, who left me the freedom to pursue my own research unfettered by the actual industrial interests, and allowing me to do not only a profitable but also scientifically rigorous work !

Last, but not least, my respect is awarded to H.E Dr. Widhya CHEM, ambassador of Cambodia in France, and H.E Sophann KET, ambassador of Cambodia to UNESCO who spent their valuable time attending my thesis defense. It was my great honor to see their presence !

Finally, I am highly indebted to my two most important people : my parents and all my brothers and sister ! Thanks dad and mum for everything you did for this child. Thanks for giving me opportunity to get a proper education, from primary school until university, while almost all other children in our village did not have that chance beside going to the rice fields or working in the factory. Thank you for always allowing me to pursue my studies to catch my dream. You are poor, but you tried to save money just to help your children have a good education. You deserve to be remembered not only in this manuscript but in my whole life !

Paris, February 23rd, 2017

Angkeara

# RÉSUMÉ

Dans les analyses d'interaction sol-structure (ISS), la pratique commune en génie civil est de considérer un mouvement uniforme du champ libre à tous les points situés à la surface du sol. Néanmoins, cette considération n'est pas tout à fait réaliste parce que les signaux sismiques sont spatialement différents grâce à l'effet de passage d'ondes, à l'effet de site et aussi aux dispersions et réflexions des ondes qui propagent dans des milieux hétérogènes aléatoires ("incohérence pure"). Ainsi, pour répondre aux problèmes de sécurité des bâtiments et équipements, il est important de faire une analyse d'interaction sol-structure dans la manière plus réaliste. Cela peut être acquis par prendre en compte la variabilité spatiale du champ sismique dans les études d'ISS. Un grand nombre d'études dans la littérature montrent que la prise en compte de la variabilité spatiale du champ sismique dans les études d'ISS peut avoir des effets importants sur la réponse de structures.

L'incohérence spatiale du champ sismique due aux dispersions et réflexions des ondes (incohérence pure) peut généralement être modélisée pour ce genre d'études dans le cadre probabiliste par une fonction de cohérence.

Le but principal des études réalisées dans cette thèse de doctorat est de construire une description stochastique de la variabilité spatiale du champ sismique par un modèle de cohérence. Ce modèle devrait avoir une relation avec les propriétés physiques et statistiques de milieux considérés.

En s'appuyant sur les analyses théoriques de la propagation des ondes sismiques dans des milieux hétérogènes aléatoires, les analyses des données expérimentales obtenues par des enregistrements sur des sites sismiques, ainsi que sur les modélisations numériques de propagation des ondes sismiques dans des milieux hétérogènes aléatoires, un modèle de cohérence est validé dans le cadre des études de cette thèse de doctorat pour représenter la variabilité spatiale du champ sismique dans les études d'interaction sol-structure. L'influence de la variabilité spatiale du champ sismique sur la réponse de structure est également analysée.

# ABSTRACT

In seismic soil-structure interaction studies (SSI), the common practice in Civil Engineering is to consider a uniform movement of free field at any point on the ground surface. However, that assumption is not completely realistic since the seismic ground motions can vary spatially due to wave passage effects, dispersions and reflections of wave propagating in the random heterogeneous media "pure incoherence" and site effects. Therefore, in order to increase the security of buildings and equipment, it is important to do an analysis of seismic soil-structure interactions in the most realistic way. This can be achieved by taking into account the spatial variability of seismic ground motions. Several studies in the literature show that taking into account the spatial variability of seismic ground motions in SSI analyses can have remarkable effects on the structural responses.

The spatial incoherence of seismic ground motions due to dispersions and reflections of wave "pure incoherence" can generally be modelled in such analysis by a "coherency function" in frequency domain.

The principal goal of this Ph.D thesis is to construct a stochastic description of spatial variability of seismic ground motions by means of coherency functions. Accurately, it aims to propose a parametrical coherency model of spatial variability of seismic ground motions. This later should be related to some physical and statistical properties of the soil at the application sites so that it can be applied in any types of sites.

Based on theoretical considerations on coherency of seismic wave propagation in random heterogeneous media, on experimental data analyses, and on numerical modelling of seismic wave propagation in random heterogeneous media, a coherency model is validated and proposed for the analyses of soil-structure interactions. The influence of spatial variability of seismic ground motions on the structural responses are also pointed out by using the validated coherency model.

# Contents

<b>Acknowledgement</b>	<b>3</b>
<b>Résumé</b>	<b>5</b>
<b>Abstract</b>	<b>6</b>
<b>Contents</b>	<b>7</b>
<b>List of Figures</b>	<b>10</b>
<b>List of Tables</b>	<b>13</b>
<b>Introduction</b>	<b>15</b>
<b>1 An overview on spatial variability of seismic ground motions</b>	<b>19</b>
1.1 Introduction . . . . .	19
1.2 Causes of spatial variability of seismic ground motions . . . . .	19
1.3 Effects of spatial variation of seismic ground motions on the responses of structures . . . . .	20
1.4 Spatial variability of seismic ground motions in SSI analysis . . . . .	21
1.5 Coherency functions . . . . .	24
1.5.1 Types of coherency functions . . . . .	26
1.5.2 Statistical properties of coherencies . . . . .	29
1.5.3 Coherency models proposed in the literature . . . . .	31
1.5.4 On the theoretical considerations for defining coherency of plane waves propagating in a random heterogeneous medium . . . . .	39
1.5.5 Conclusions on coherency models . . . . .	42
<b>2 Spatial Coherency of Seismic Ground Motions estimated from Argostoli Database</b>	<b>45</b>
2.1 Introduction . . . . .	45
2.2 Argostoli Earthquakes in 2014 and Argostoli Dense Array . . . . .	46
2.3 Spatial coherency estimated from Argostoli database . . . . .	51
2.3.1 Determination of plane-wave propagation directions . . . . .	51
2.3.2 Spatial coherency estimated from strong motion windows . . . . .	51
2.3.3 Spatial coherency estimated from coda of seismic signals . . . . .	54
2.3.4 Influence of the strong motion durations on spatial coherency . . . . .	56
2.3.5 Influence of the number of earthquake events on spatial coherency . . . . .	56
2.4 Comparison between insitu spatial coherency and existing coherency models . . . . .	57
2.5 Conclusions on spatial coherency of Argostoli earthquake database . . . . .	61
<b>3 Numerical modelling of seismic wave propagation in heterogeneous media</b>	<b>63</b>
3.1 Introduction . . . . .	63
3.2 Introduction to the Spectral Element Method and Software SEM3D . . . . .	63
3.2.1 Generalities on software SEM3D . . . . .	64

3.2.2	Generation of random heterogeneous properties of the media . . . . .	65
3.2.3	Representation of earthquake source in numerical modelling . . . . .	65
3.2.4	A simple case-study with SEM3D . . . . .	66
3.3	Influence of the physical and statistical parameters of soil properties on the spatial coherency of earthquake ground motions . . . . .	68
3.3.1	Influence of the depth of heterogeneous layer . . . . .	69
3.3.2	Influence of shear-wave velocity . . . . .	72
3.3.3	Influence of coefficient of variation of elastic properties . . . . .	72
3.3.4	Influence of correlation length of medium . . . . .	75
3.4	Modelling of spatial variability of seismic ground motions for Argostoli dense array .	75
3.5	Conclusions on validation of coherency model and numerical assessment of spatial variability of seismic ground motions . . . . .	78
<b>4</b>	<b>Spatial variability of seismic ground motion in soil-structure interaction analysis</b>	<b>79</b>
4.1	Introduction . . . . .	79
4.2	Descriptions of the case-study . . . . .	80
4.2.1	Finite element model of reactor building . . . . .	81
4.2.2	Modelling of soil surrounding the building . . . . .	81
4.2.3	Earthquake signals (input motion) . . . . .	83
4.3	Methodology of Soil-Structure Interaction analysis accounting for incoherent input motions . . . . .	85
4.3.1	Soil-Structure Interaction analysis in frequency domain . . . . .	85
4.3.2	Accounting for spatial variability of seismic ground motions . . . . .	86
4.3.3	Power spectral density of structural responses and transfer function . . . . .	87
4.3.4	Transient analysis of structural responses . . . . .	88
4.4	Influence of spatial variability of seismic ground motions on the responses of KK reactor building . . . . .	88
4.5	Conclusion on the industrial application case study . . . . .	89
	<b>Summary and Conclusions</b>	<b>93</b>
	<b>Perspectives</b>	<b>95</b>
	<b>Appendices</b>	<b>97</b>
<b>A</b>	<b>Spectral densities of seismic signals and their smoothing</b>	<b>99</b>
<b>B</b>	<b>Verification of coherency estimator</b>	<b>103</b>
<b>C</b>	<b>Distributions of station pairs for different distances of separation of Argostoli dense array</b>	<b>107</b>
<b>D</b>	<b>Introduction to spectral element method and software SEM3D</b>	<b>109</b>
D.1	Equation of motions . . . . .	109
D.2	Weak formulation . . . . .	110
D.3	Spatial discretizations . . . . .	110
D.4	Diagonal mass matrix . . . . .	113
D.5	Time discretization . . . . .	113
D.6	Perfect Match Layer (PML) . . . . .	115
D.7	Stochastic field generations for random heterogeneous media . . . . .	116
D.8	Earthquake source . . . . .	118
<b>E</b>	<b>Descriptions of reactor building of KK power plant</b>	<b>121</b>

## Bibliography

124



# List of Figures

1.1	Three principal causes of spatial variation of seismic ground motions: a) wave passage effects; b) Site response effects; c) Scattering effects [Zentner, 2013] . . . . .	20
1.2	Comparison of the response spectra at a point of the internal structures in a reactor building for the case of coherent ground motions and incoherent ground motions. Above : embedded structure. Below : surface founded structure. [EPRI, 2006a] . . .	22
1.3	Coherent (left) and Incoherent (right) Membrane Forces in the 30 ft Embedded Concrete Structure Walls (embedment covers the lower 5 element layers) [Ghiocel et al., 2010]	23
1.4	Strong motion window used for estimating coherency of earthquake ground motions	25
1.5	Comparison between plane-wave coherency and lagged coherency of Abrahamson model [Abrahamson et al., 1991] estimated from Lotung database . . . . .	29
1.6	Dependence of the Variability of the Plane-Wave Coherency With Frequency (above) and Independence of the Variability of the Transformed Plane-Wave Coherency With Frequency (below) (from [EPRI, 2007a]) . . . . .	30
1.7	Plane wave coherency of Abramson models for soil sites and hard rock sites horizontal component . . . . .	35
1.8	Variation of $\eta$ as a function of station separation distance (above) and of frequency (below) [Konakli et al., 2013] . . . . .	37
1.9	Plane-Wave propagation in random layer of soil . . . . .	39
2.1	Location of studied site. a) Location of Kefalonia island with respect to Greece. b) Location of the Argostoli area with respect to Kefalonia island. c) Location of the Argostoli rock site dense array on the local geological map [Cushing et al., 2016] . .	46
2.2	Argostoli rock site dense array geometry mapped on aerial photography (source : Google Earth). Each red dot represents one sensor . . . . .	47
2.3	Epicenters of aftershocks recorded by the Argostoli rock-site dense array (approximately 2000 well recorded events from February 6th, 2014 to March 10th, 2014). Different colors indicate magnitude values: the white color circles present the earthquake events with magnitudes smaller than 2. The black star represents the location of array. . . . .	48
2.4	Epicenters of aftershocks recorded by the Argostoli rock-site dense array and used in the present study (selection of 93 earthquakes out of approximately 2000 well recorded events from February 6th, 2014 to March 10th, 2014). Colors indicate magnitude values. The black star represents the location of array. . . . .	49
2.5	Distribution of selected earthquake in terms of epicentral distances (X-axis), magnitudes (Y-axis) and Peak Ground Velocity (color scale). . . . .	49
2.6	Velocities captured at Argostoli dense array (event 2014-02-06-185141, Mw=3.0, Epicentral distance = 17.4 Km) . . . . .	50
2.7	Shear wave velocity profiles estimated beneath the Argostoli rock site dense array. These profiles are computed using surface-wave based methods. In blue: "best estimated" profile, in red: other possible profiles.) . . . . .	50
2.8	Distribution of angle $\phi$ representing the directions of plane-wave propagation. The center of circle corresponds to the station array . . . . .	52

2.9	Dispersions of horizontal plane-wave coherencies estimated from 93 events of Argostoli database for 10m, 30m, 55m and 100m of separations. The blue bold line represents the average of plane-wave coherencies	52
2.10	Spatial Incoherency estimated from Argostoli database for 10m, 30m, 55m and 100m of separations	53
2.11	Residuals of $\tanh^{-1}(\text{coherencies})$ of horizontal component from 93 earthquake events for 10m, 30m, 55m and 100m of separations	54
2.12	Comparison between coherencies estimated from strong motion windows and from coda parts of signals for 10m, 30m, 55m and 100m of separations	55
2.13	Residual of $\tanh^{-1}(\text{coherencies})$ estimated from coda window of ground motion signals for 10m and 100m of station separations	55
2.14	Comparison between coherencies estimated from different strong motion durations of signals for 10m and 100m of separations	56
2.15	Comparison between coherencies estimated from different numbers of earthquake events for 10m and 100m of separations	57
2.16	Comparison between coherencies estimated from Argostoli database and existing coherency models for 10m, 30m, 55m and 100m of separations	58
2.17	The values of parameters used for fitting existing coherency models with Argostoli coherencies. Left: $f_c$ as a function of station separations (for Abrahamson model). Right: $\alpha$ as a function of station separations (for the Model of Luco&Wong).	59
2.18	Comparison between coherencies estimated from Argostoli database and modified (fitted) coherency models for 10m, 30m, 55m and 100m of separations	60
2.19	Coherencies with respect to $d/\lambda$	60
2.20	Comparison between coherencies estimated from Argostoli database and constant-parameter coherency models for 10m, 30m, 55m and 100m of separations	61
3.1	Free surface elastic homogeneous medium	66
3.2	Smoothed Heaviside Step Function to be applied on the free surface of the medium	66
3.3	Half space medium surrounded by PML (left) and the free surface seen from above (right)	67
3.4	Magnitude of displacement at $t = 0.0025$ (left) and $t = 0.015$ (right)	67
3.5	Comparison between analytical solution with the solution given by SEM3D modelling	68
3.6	The representation of the medium modelled in SEM3D for analysing the influence of physical and statistical parameters on the spatial variability of earthquake ground motions	69
3.7	30m spatial coherencies for the case of $V_s = 700\text{m/s}$ ; $\ell_c = 40\text{m}$ , $COV = 15\%$ and $Z = 50\text{m}$ (left) or $Z = 100\text{m}$ (right)	70
3.8	Influence of $Z$ on the spatial coherency of earthquake ground motions and comparison between synthetic coherencies and theoretical coherency	70
3.9	Influence of $Z$ on the spatial coherency of earthquake ground motions and comparison between synthetic coherencies and theoretical coherency for the case of big value of $Z$ (for $V_s = 700\text{m/s}$ ; $\ell_c = 40\text{m}$ , $COV = 15\%$ )	71
3.10	Comparison of synthetic coherencies with the model of Sato in the case that $Z \geq 4 \times \ell_c$ (for $V_s = 700\text{m/s}$ ; $\ell_c = 40\text{m}$ , $COV = 15\%$ )	72
3.11	20m spatial coherencies for different shear-wave velocities presented with standard deviations and compared to the modified coherency model	73
3.12	influence of shear-wave velocity on spatial coherency for soil site for 20m, 30m and 40 of separations (for $\ell_c = 30\text{m}$ ; $\xi = 0.15$ )	73
3.13	influence of coefficient of variation (COV) of random properties on spatial coherency for soil site for 20m, 30m and 40 of separations (for $\ell_c = 30\text{m}$ ; $V_s = 800\text{m/s}$ )	74
3.14	influence of correlation length on spatial coherency for soil site and rock site (for $V_s = 800\text{m/s}$ ; $\xi = 0.15$ )	75

3.15 Comparisons between the <i>insitu</i> coherencies of Argostoli database, the synthetic coherencies estimated from synthetic signals of SEM3D and the modified coherency model . . . . .	77
4.1 Kashiwazaki and Kariwa Nuclear Power Plant, in Japan [IDN, 2015] . . . . .	80
4.2 Y-Z view of Unit 7 [IAEA, 2013] . . . . .	81
4.3 X-Z and Y-Z views of reactor building in Unit 7 [IAEA, 2013] . . . . .	82
4.4 Finite element mesh of reactor building . . . . .	82
4.5 Interfaces between reactor building and soil . . . . .	83
4.6 Three components of signals used for input motion . . . . .	84
4.7 FFT of the three components of signals used for input motion . . . . .	84
4.8 Dynamic sub-structuring method . . . . .	86
4.9 spectral accelerations of a point at the top of internal structure . . . . .	90
4.10 spectral accelerations of the point R1 . . . . .	90
4.11 Comparison between the coherencies obtained from different coherency models . . . . .	90
A.1 Hamming windows for $M = 1, 3, 5, 7, 9$ and $11$ . . . . .	101
B.1 Power Spectral Density of Clough & Penzien . . . . .	104
B.2 Comparison between the coherency model of Luco&Wong and the coherency estimated from simulated realizations . . . . .	104
D.1 8-node hexahedral reference element and the mapping function . . . . .	111
D.2 Positions of GLL points on a 2D element of order 9 [Aubry, 2016] . . . . .	112
D.3 Lagrange polynomial of order 9 [Aubry, 2016] . . . . .	112
D.4 A half space domain surrounded by PML materials . . . . .	115
D.5 Real and imaginary parts of the decay factor. The real parts controls the attenuation inside the absorbing layer and it is an increasing function reaching asymptotically the value 1. The imaginary part represents a phase shift, maximum at $\omega = \omega_c$ and decreasing to zero for both $\omega = 0$ and $\omega \rightarrow \infty$ [Festa and Vilotte, 2005] . . . . .	116
D.6 Modulus of the velocity at three different instants [Festa and Vilotte, 2005] to show about the absorbing properties of PML . . . . .	117
D.7 Geometry of a point shear-dislocation source, where $\mathbf{n}$ is a normal to the fault and $\mathbf{s}$ represents the fault slip direction . . . . .	118
D.8 Physical representation of each element of moment tensor matrix . . . . .	119
D.9 Different kinds of earthquake sources following different mement tensor matrix . . . . .	120
E.1 Maps of KK nuclear power plant [IAEA, 2012] . . . . .	122
E.2 Maps of Unit 7 [IAEA, 2012] . . . . .	122

# List of Tables

1.1	Autocorrelation function and its power spectral density function. . . . .	24
1.2	Parameters of Abrahamson model (1990) for soil site (second column) and the modified Abrahamson model after [Ancheta et al., 2011] (third column) . . . . .	32
1.3	Parameters of Abrahamson model (2006) for all types of soil . . . . .	33
1.4	Parameters of Abrahamson model (2007) for hard rock site . . . . .	34
1.5	Parameters of Abrahamson model (2007) for soil site, horizontal component . . . . .	34
2.1	Parameters of Abrahamson model for Argostoli dense array . . . . .	58
2.2	Fitted values of $Z$ of Sato model for different station separations . . . . .	59
3.1	Relative error in $\mathbb{L}^2$ between insitu coherencies and synthetic coherencies obtained by each couple of statistical parameter. The bold numbers are the smallest relative errors. . . . .	76
4.1	Stratigraphy of Unit 7 of KK site [IAEA, 2012] . . . . .	83
C.1	Distributions of station pairs for different separations . . . . .	108
E.1	Vertical coordinate of each floor of the reactor building . . . . .	121
E.2	Principal structural components of reactor building . . . . .	121
E.3	Material properties used for the construction of reactor building . . . . .	123
E.4	Distribution of mass inside the structural building . . . . .	123



# Introduction

*“Earthquakes do not kill people, structures do.”*

NORMAN AHMED, 2011

Earthquakes are one of the most devastating of all natural disasters. Many people are killed every year around the world by damaged structures which are destroyed by earthquakes. In order to reinforce the structures in earthquake zones, a refined analysis of Soil-Structure Interactions (SSI) is necessary. For such analysis, a common practice in Civil Engineering is to consider a uniform motion of free field on the ground surface which means that all points on the ground surface move together. An accelerogram is properly selected to represent the seismic force to apply on the structure at any point of the ground surface. However, that assumption is not always realistic [DerKiureghian and Neuenhofer, 1992], [Harichandran, 1999] since the seismic ground motions can vary spatially due to many factors including topological, geographical and physical factors. For a given site, the difference between the ground movements of two observation points during an earthquake is described by a term called "spatial variability of seismic ground motions". The spatial variation of the seismic ground motions can result from the relative surface-fault motion for sites located on either side of a causative fault, soil liquefaction, landslides, and from the general transmission of the waves from the source through the different earth strata to the ground surface (wave scattering). These principal causes of the spatial variability of seismic ground motions can be classified into the deterministic causes (site-response effects and wave passage effects) and the random causes (wave scattering : dispersions and reflections of seismic waves due to wave propagation in heterogeneous media).

Many studies reported in the literature these last three decades show the important effects of the spatial variability of seismic excitations on the structural responses for both extended structures [Luco and Wong, 1986]; [Ghiocel and Ostadan, 2007]; [Tseng et al., 2013]; [Jeremic et al., 2013]; [Zentner and Devesa, 2011]; [Mezouer et al., 1998]; [EPRI, 2006a] and multi-supported structures [Hong, 1993]; [DerKiureghian and Neuenhofer, 1992]; [Bi and Hao, 2013]; [Saxena et al., 2000]. For the favourable effects, one can observe the filtering of movements of translation at high frequencies. The introduction of the spatial variability of seismic excitations can lead to reduce the floor response-spectra. But the spatial variation of seismic ground motion can also generate additional forces known as pseudo-static forces, which are absent when the structure is subjected to a uniform support motion [DerKiureghian and Neuenhofer, 1992], [Konakli and DerKiureghian, 2011]. By taking into account the different soil site conditions, [Ghiocel et al., 2010] concluded, on their applications on a large size shear wall structure, that the seismic incoherent motions can increase bending moments in the base-mats and increase the shear wall forces in the external walls for the large foundation sizes. For their applications on a deeply embedded concrete pool structure, the authors found that the incoherent seismic input motions can reduce the global resultant of the local pressures but might locally produce “hot-spot” pressures for deeply embedded structures.

To take into account the spatial variability of seismic ground motions in the soil-structure interactions analysis, different causes of spatial variability of seismic ground motions need to be considered. The deterministic causes, such as site-response effects or wave passage effects, can be directly taken into account in the analysis by establishing the structural model, the seismic source models or the soil model corresponding to the analysed case. However, the random causes, which can also be called in the literature as *pure incoherence effects* due to the dispersions and reflections of seismic waves propagating in the heterogeneous media, cannot be taken into account in the deterministic analysis. Hence, it is necessary to develop an appropriate tool to characterize those fluctuations and their effects on the structural dimensioning analysis.

The spatial incoherence of seismic ground motions due to dispersions and reflections of seismic waves (*wave scattering*) can be modelled in a "probabilistic framework" by a coherency function. The "coherency function" is a normalized function obtained by the ratio between the crossed spectral density and the power spectral densities of two accelerograms at two separated stations. The literature proposed several coherency functions which can be empirical or semi-empirical. The semi-empirical models refer to those models whose expressions are obtained not only by analytical considerations but also by statistical analyses of data from some earthquake sites. The empirical models are those models whose expressions are only obtained empirically by statistical analyses of data from some earthquake sites. These coherency functions have been used in the Soil-Structure Interaction analysis of extended structures or multi-support structures such as dams, bridges, pipelines and also nuclear power plants in this last decade.

The modelling of the spatial variability of seismic ground motions in the analysis of Soil-Structure Interaction (SSI) has been used in earthquake engineering in the USA since the last 10 years. An empirical coherency model proposed by Abrahamson [EPRI, 2007a] has been accepted by the United States Nuclear Regulatory Commission (USNRC) for use in the designs of nuclear power plants. The methodology for taking into account the spatial variation of seismic movements in the soil-structure interaction analysis can be considered to be mature. Many validation studies have been realized with the SSI software SASSI and CLASSI by EPRI (Electric Power Research Institute, USA) [EPRI, 2005], [EPRI, 2006a], [EPRI, 2007a], [EPRI, 2007b]. The methodology implemented in the software SASSI was also accepted by the USNRC.

Nevertheless, although several coherency functions have been proposed and used in the literature for taking into account the spatial variability of earthquake ground motions in the soil structure interaction analyses, the applications of those functions are still limited. Some of them are purely empirical and do not have a proper relation to the physical properties of sites. This might provide unsatisfactory estimations of the actual site-specific coherency values. For the semi-empirical functions, although their expressions are formed by theoretical considerations with parameters which can be determined from the earthquake data, still several recent studies prove their limitations by comparing them to the coherencies estimated from earthquake sites [Konakli et al., 2013].

The main goal of this Ph.D thesis is to construct a stochastic description of spatial variability of seismic ground motions by means of coherency functions. The latter should be related to the physical and statistical properties of the soil at the application sites so that it can be applied in any types of sites.

In order to construct and validate this parametric model of the spatial variability of seismic ground motion, 3 important paths should be analysed:

1) **Determination of the functional form of coherency model:** The functional form of coherency model should be constructed by analysing the existing coherency models based on

analytical considerations of coherencies caused by the fact that the seismic waves propagate in a heterogeneous medium. A stochastic framework will be chosen for our analyses.

2) ***Statistical analysis of experimental data from available earthquake sites:*** The seismic signals recorded on the rock site at Argostoli town (Kefalonia Island, Greece) from the earthquakes that happened in the beginning of 2014 (magnitude 6Mw) are chosen to be analysed in these studies. The distances between different stations range from 10m to 360m (spatial variation of seismic ground motions for short distances) corresponding to the industrial applications.

3) ***Numerical simulations of seismic wave propagating in heterogeneous media:*** It is essential to model numerically the seismic wave propagation in heterogeneous media since it permits us to understand about different phenomena which can contribute to the spatial variability of seismic ground motions. The numerical modellings can also validate the coherency model which is constructed in the first path of this work.

This manuscript describes different studies realized with the aim of constructing a parametrical coherency model and showing the importances of taking into account the spatial variability of seismic ground motions in the soil-structure interaction analyses. The manuscript is arranged as follows.

Chapter 1 describes an overview on the spatial variability of seismic ground motions and on coherency functions which are proposed and used in the literature. The causes of spatial variability of seismic ground motions are presented in details and some significant effects of spatial variability of earthquake ground motions on the structural responses are also pointed out. The chapter is also dedicated to the presentation and discussion of different types of coherencies which can be used for engineering applications. Several widely used coherency models in the literature are cited and the limitations of each existing coherency model are discussed based on some recent works in the literature. The methodology for estimating coherencies from seismic signals is also presented, and finally, some theoretical considerations to define a coherency function of seismic wave propagating in random heterogeneous media are presented and discussed.

Chapter 2 presents the results of the statistical analysis of spatial coherencies estimated from the real earthquakes signals recorded on a rock site at Argostoli town, on the island of Kefalonia, Greece. A brief description of Kefalonia earthquakes in 2014 and of Argostoli dense array is presented. Some possible factors influencing the spatial coherency of seismic ground motions are analysed and discussed by using those *insitu* results. The coherencies estimated from Argostoli database are then compared to the existing coherency models to discuss on the limitations of those models and to conclude on the possibility of selecting a coherency model which can be conformed the most to the theoretical aspects as well as practical aspects.

With the introductions of coherency functions in Chapter 1 and the comparisons to the *insitu* results in Chapter 2, we can conclude on which coherency model should be taken into considerations, and Chapter 3 is principally dedicated to the verifications and validations of coherency model by using numerical modellings. Since the numerical tests are realized with spectral element method, the numerical method and software are briefly introduced in the beginning. Several numerical tests realized to understand more precisely about how each physical and statistical property of the soil influence the spatial variability of earthquake ground motions and to validate the selected coherency model are then presented. At the end of the chapter, the numerical modelling of seismic wave propagation at the Kefalonia island is presented to compare the spatial coherencies estimated from Argostoli database (*insitu* coherencies) with those estimated from numerical modelling. This numerical test can help us to conclude on the possible values of some physical and statistical



parameters of the heterogeneous rock site which can give a full validation of the selected coherency model.

Chapter 4 is dedicated to the importance of taking into account the spatial variability of seismic ground motions in the soil-structure interaction analyses. The Kashiwasaki-Kariwa power plant in Japan is chosen to be analysed. The results of soil structure interaction analysis with spatial variability of seismic ground motions by using the proposed coherency model are presented and discussed.

Conclusions arising from this doctoral work and suggestions for future works are presented in the last part of this manuscript, followed by the appendices.

# Chapter 1

## An overview on spatial variability of seismic ground motions

*“A people without knowledge of their past history, origin and culture is like a tree without roots.”*

MARCUS GARVEY

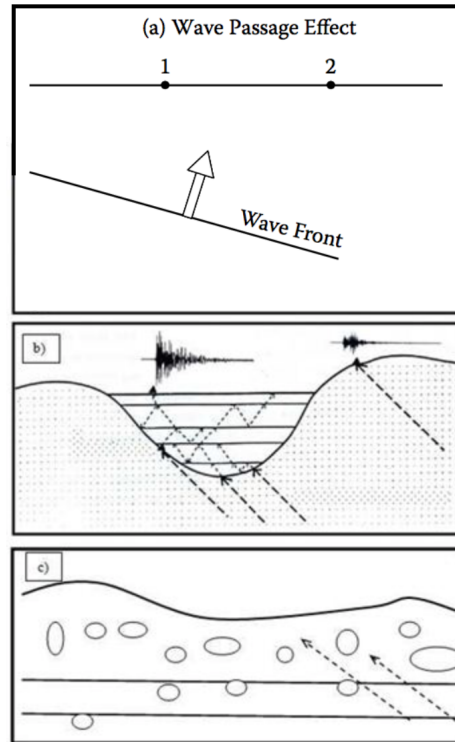
### 1.1 Introduction

The term "spatial variation of seismic ground motions" denotes the differences in the amplitude and phase of seismic motions recorded at two different locations of the ground. The spatial variability of seismic ground motions results from the general transmission of the waves from the source through the different earth strata to the ground surface can be represented by a term called "coherency function" in a probabilistic framework. The latter one is used in the soil-structure interaction analyses to account for the spatial incoherence of seismic ground motions. This chapter begins with some generalities on spatial variability of seismic ground motions: its causes, and its effects on structural responses. After that, different types of coherencies used in engineering applications are presented. Methodologies used in the literature to estimate coherencies from earthquake ground signals are also presented. Several coherency models proposed in the literature are reviewed. Finally, a theoretical consideration to define a coherency function of seismic motions due to wave propagation in heterogeneous media is presented.

### 1.2 Causes of spatial variability of seismic ground motions

The important factors creating the spatial variability of seismic ground motions can be divided in 3 groups [[Harichandran, 1999](#)]:

1) **Wave Passage Effects:** It refers to the difference in the arrival times of waves at separate stations. One can generally recognize this factor for the inclined incident plane waves. The figure [1.1.a](#) illustrates this factor. The wave passage time delay between two locations will introduce a



**Figure 1.1** – Three principal causes of spatial variation of seismic ground motions: a) wave passage effects; b) Site response effects; c) Scattering effects [Zentner, 2013]

shift in the Fourier phases of the earthquake ground motions (see Figure 1.1.a)

2) **Local site effects**: This term refers to the difference in local site conditions at each station that can be site geology and site geometry (e.g sedimentary valleys). This factor can be represented in figure 1.1.b. This term can alter the amplitude and frequency content of the bedrock motions differently. For the sedimentary valleys, the seismic waves get trapped within the valley and surface waves develop at the basin edge leading to large amplification on the sediment sites compared to the rock site.

3) **Scattering effects**: Also called *pure incoherence effects* in the literature, refers to the result of the refraction and the reflection of seismic wave (wave scattering) that occur as waves propagate in a heterogeneous medium and also the results of the superposition of waves arriving from different parts of an extended site (Figure 1.1.c).

### 1.3 Effects of spatial variation of seismic ground motions on the responses of structures

The effects of the spatial variation of seismic ground motions on structural responses have been largely analysed in the literature in these last three decades. Those analyses can be described from the simplest structures (beams) to the most complicated structures (bridges, nuclear power plants, ...etc). This section presents some examples of studies and their conclusions.

The inclusion of spatial variability of seismic ground motions in the dynamic analysis of soil-

structure interaction can lead to the reduction of structural response spectra (floor response spectra) at high frequencies. Mostly, we can remark this effect for the frequency higher than 10 Hz. The amount of response spectra reduction increases as spectral frequency increases. Figure 1.2 presents the structural response at a point of a nuclear power plant building for the case of surface founded and embedded structure, analysed by EPRI ([EPRI, 2006a]). For both surface founded and embedded structures, one can remark the important differences between structural response spectra for the case of coherent and incoherent ground motions. For low frequencies, the difference is almost negligible but it becomes significant for frequencies higher than 10 Hz.

For long-span structures, the variability in the support motions usually tends to reduce the inertia-generated forces within the structures, as compared to the forces generated in the same structure when the supports move uniformly. However, differential support motions generate additional forces, known as pseudo-static forces, which are absent when the structure is subjected to the uniform support motion [DerKiureghian and Neuenhofer, 1992]. By taking into account the different soil site conditions, [Ghiocel et al., 2010] concluded, on their applications on a large size shear wall structure, that the seismic incoherent motions can increase bending moments in the base-mats and increase the shear wall forces in the external walls for the large foundation sizes. For their applications on a deeply embedded concrete pool structure, the authors found that the incoherency seismic input motions can reduce the global resultant of the local pressures but might locally produce “hot spot” pressures for deeply embedded structures (Figure 1.3). From a simple application of seismic incoherent excitations to a simple structure, [Mezouer et al., 1998] noted that it is important to consider the spatial variation of earthquake ground motions since it can reduce translational and rotational responses of structures but increase the vertical responses. The latter conclusion should be investigated more precisely for other types of structures. The same authors also mentioned that the effects of spatial variation are more significant for low shear wave propagation velocity. For the application of seismic excitations on a skewed, 3 spans, RC highway bridge, [Lou and Zerva, 2005] concluded that the uniform input motion of the largest peak displacement still sometimes underestimates the structural responses and suggested that the spatially variable input motions should be applied as excitations at the bridge supports.

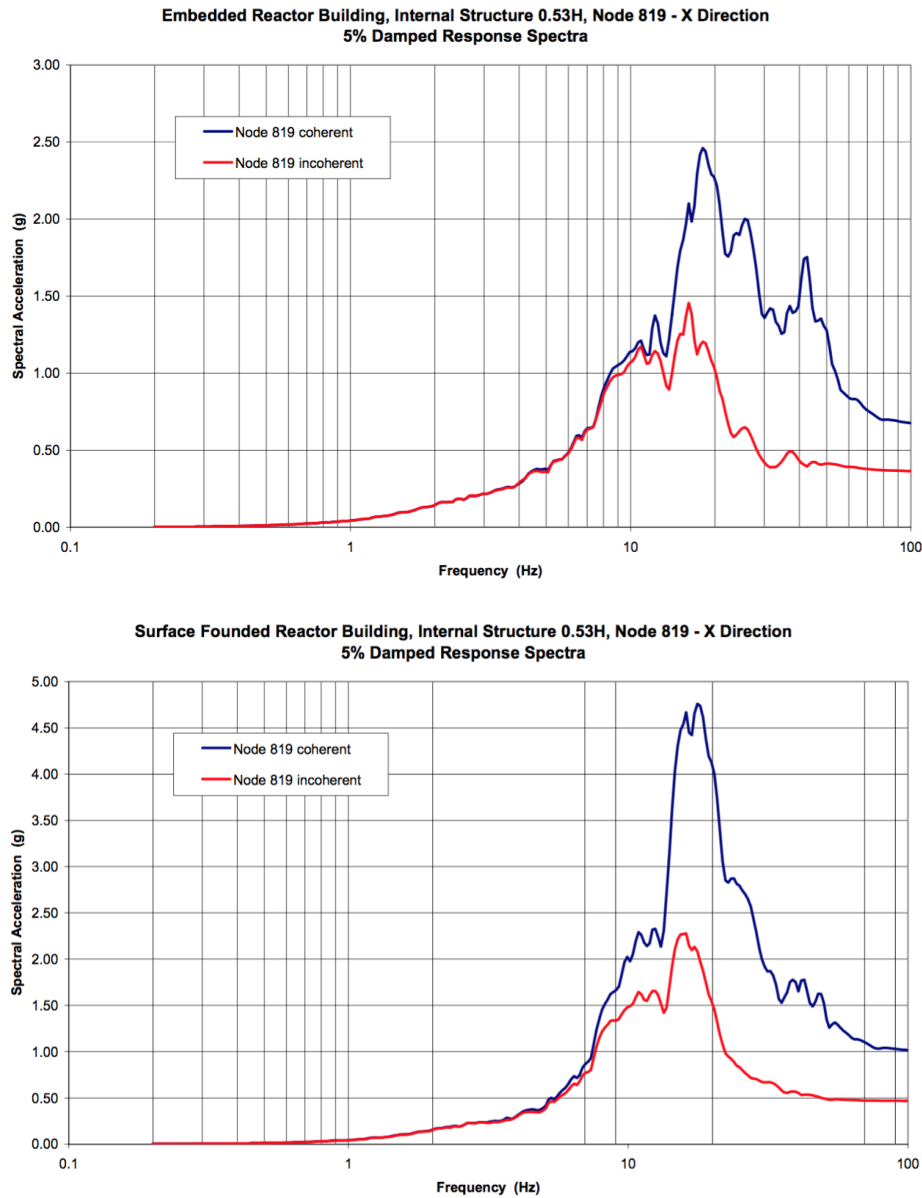
Finally, after [DerKiureghian, 1996], the differential support motions of structures often do not create a critical design situation, as the spatial variability effect usually tends to reduce the demand on the structures. But, the spatial variation of seismic ground motions caused by the site-response effect could pose a serious problem for short-span, stiff structures that are situated in the regions with rapidly varying soil profiles.

All aforementioned studies recommended that for long span structures like bridges, pipelines, tunnels and also nuclear power plants, it is important to take into account the spatial variation of seismic ground motions.

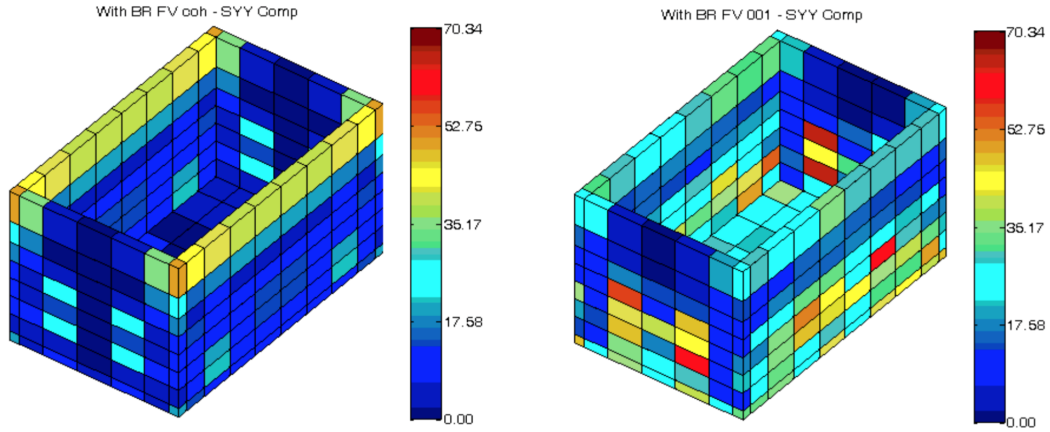
## 1.4 Spatial variability of seismic ground motions in SSI analysis

To take into account the spatial variability of seismic ground motions in the soil-structure interactions analysis, different causes of spatial variability of seismic ground motions need to be considered. The deterministic causes, such as site-response effects or wave passage effects, can be directly taken into account in the analysis by establishing the structural model, the seismic source models or the soil model corresponding to the analysed case.

With the nature of the earth’s crust which is significantly heterogeneous, the *pure incoherence*



**Figure 1.2** – Comparison of the response spectra at a point of the internal structures in a reactor building for the case of coherent ground motions and incoherent ground motions. Above : embedded structure. Below : surface founded structure. [EPRI, 2006a]



**Figure 1.3** – Coherent (left) and Incoherent (right) Membrane Forces in the 30 ft Embedded Concrete Structure Walls (embedment covers the lower 5 element layers) [Ghiocel et al., 2010]

effects due to the dispersions and reflections of seismic waves propagating in the earth's crust (wave scattering) can be correctly analysed when the values of physical properties (such as Young modulus  $E$ , mass density  $\rho$ , Lamé constants  $\lambda$  and  $\mu$ , bulk modulus  $\kappa$ ...etc) at each point in the media are provided. But those values at exactly each point of the space are rarely known. Anyway, the probabilistic approaches permit to give the values of physical properties at each point of the space by using only their statistical properties, i.e, less information is needed. Hence, the wave scattering in a heterogeneous medium can be analysed in a probabilistic framework by modelling the medium as a random heterogeneous medium.

The *pure incoherence effects* can be, therefore, taken into account in Soil-Structure Interaction analysis (in probabilistic framework) by coherency function whose definition is given in the section 1.5. More details about mathematical formulations to incorporate coherency function in the SSI analysis will be provided in the Chapter 4.

To get a full comprehension in a coherency function as well as its parameters who are related to the physical and statistical properties of random heterogeneous media, it is preferred to start our analyses by giving the statistical descriptions of a random heterogeneous medium.

Mathematically, the random medium can be described by spatial statistical distributions of its physical properties, e.g. P- and S-wave velocities or density, etc. The velocity field of a heterogeneous medium can be described as a superposition of a deterministic part  $V_o$  (mean velocity) and a fluctuating part  $V_o \cdot \xi(\mathbf{x})$ :

$$V(\mathbf{x}) = V_o(1 + \xi(\mathbf{x})) \quad (1.1)$$

where  $\mathbf{x} = (x, y, z)$  is the spatial position vector and  $\xi(\mathbf{x})$  is the fractional fluctuation of the velocity.

To describe statistically a random heterogeneous medium, the autocorrelation function is introduced. The autocorrelation function (ACF) is a statistical measure of the spatial correlation and the magnitude of the fluctuations in the medium. It describes the degree of similarity of the medium's parameters in dependence on the positions and the distance between two different points in the medium. In geophysics, the correlation functions of random media are of principal importance for understanding and inverting the properties of seismic waves propagating in geological structures [Klimes, 2002]. The autocorrelation function of a physical property (such as mass

Type	ACF	PSDF
Gaussian	$R(r) = \xi^2 \exp(-\frac{r^2}{\ell_c^2})$	$S(k) = \xi^2 \ell_c^3 \sqrt{\pi^3} \exp(-\frac{k^2 \ell_c^2}{4})$

**Table 1.1** – Autocorrelation function and its power spectral density function.

density  $\rho$  or P-and S-wave velocities  $V_p$  and  $V_s$ ) can be defined by:

$$R_{VV}(\mathbf{x}, \mathbf{x}') = R_{VV}(\mathbf{x} - \mathbf{x}') = \langle \xi(\mathbf{x}) \xi(\mathbf{x}') \rangle \quad (1.2)$$

in which,  $\langle \rangle$  is the mathematical expectation.

The correlation function depends only on the distance between the two points ( $r$ ), and not on the positions of those points:

$$R_{VV}(\mathbf{x}, \mathbf{x}') = R_{VV}(\mathbf{x} - \mathbf{x}') = R_{VV}(|\mathbf{x} - \mathbf{x}'|) = R_{VV}(r) \quad (1.3)$$

The magnitude of the velocity fluctuations is given by the mean square of the fractional fluctuation:

$$\epsilon^2 = R_{VV}(0) = \langle \xi^2(\mathbf{x}) \rangle \quad (1.4)$$

with the variance  $\epsilon^2$  and the standard deviation  $\epsilon$ . Beside the variance or standard deviation which are the measures of the fluctuation magnitude, the correlation functions are characterized by a length scale that is called the correlation length  $\ell_c$ . Physically, the correlation length can be imagined as the distance beyond which the values of the random field are almost uncorrelated. It can be considered as the typical size of the random heterogeneities.

The Fourier transform of correlation function gives the Power Spectral Density Function (PSDF) in wave number domain:

$$S(\mathbf{k}) = \int_{-\infty}^{\infty} \int_{-\infty}^{\infty} \int_{-\infty}^{\infty} R_{VV}(\mathbf{x}) e^{i\mathbf{k}\mathbf{x}} d\mathbf{x} \quad (1.5)$$

where  $\mathbf{k}$  is the wave number vector.

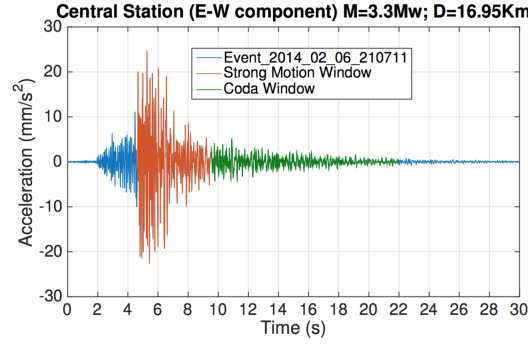
There are many correlation models proposed in the literature to represent the random physical random properties of the media, along which: Exponential, Gaussian, Power-law, Triangular and Low-pass white noise, etc. An extended analysis of different correlation models might be found in [Klimes, 2002]. Among many correlation models found in the literature, the most commonly used model in the literature might be the Gaussian correlation function. The autocorrelation function and power spectral density function of the Gaussian model are presented in Table 1.1.

To be noted that different definitions of  $\ell_c$  can be found in the literature (see for example [Shinozuka and Deodatis, 1988]). For what follows, we define the correlation length of a random heterogeneous medium as twice the zeroth-order moment of the autocorrelation function:

$$\ell_c = \frac{2}{\epsilon^2} \int_0^{\infty} R_{VV}(x) dx \quad (1.6)$$

## 1.5 Coherency functions

The coherency function is generally used in the literature to model the spatial incoherence of seismic ground motions. By definition, the coherency function is a normalized function obtained by



**Figure 1.4** – Strong motion window used for estimating coherency of earthquake ground motions

the ratio between the smoothed-cross spectral density (cross spectrum  $S_{jk}$ ) and the smoothed-power spectral density (power spectra:  $S_{jj}$  and  $S_{kk}$ ) of two observed accelerograms at  $j$  and  $k$ :

$$\gamma(d_{jk}, \omega) = \frac{\overline{S}_{jk}^M(\omega)}{\sqrt{\overline{S}_{jj}^M(\omega) \cdot \overline{S}_{kk}^M(\omega)}} \quad (1.7)$$

where  $d_{jk}$  is the distance between  $j$  and  $k$ ,  $\omega$  is the cycle frequency and over-line with  $M$  represent the smoothing of power spectra. More details about smoothing of spectral densities can be found in Appendix A.

To be noted that the coherency function (1.7) depends only on the distance between two stations  $j$  and  $k$ , and does not depend on their locations. This property results from a hypothesis in which the stationary process of earthquake signals are considered. The notions of spectral densities can be used also because of that hypothesis. But the earthquake ground motion signals are not stationary. Hence, only the strong motion windows of signals are used for the estimations of spatial coherencies since it is assumed that the signals are stationary in strong motion windows [Abrahamson et al., 1990]. The strong motion window can be obtained by using Arias intensity (AI) which represents the energy of earthquake signals. That Arias intensity is evaluated following the expression used by Abrahamson [EPRI, 2007a] :

$$AI(\tau) = \frac{\int_{T_p}^{\tau} (V_1^2(t) + V_2^2(t))dt}{\int_{T_p}^{T_p+25} (V_1^2(t) + V_2^2(t))dt} \quad (1.8)$$

where  $T_p$  is the arrival time of P-wave, i.e, the beginning of earthquake signals, and  $V_1(t)$  and  $V_2(t)$  are the both signal velocigrams in the horizontal component. The beginning and the end of the strong motion window are considered to be at the moment when Arias Intensity reaches a value of 0.1 and 0.9. An example of the strong motion window for an earthquake event is presented in figure 1.4. The red part of the signal represents the strong motion window used for evaluating the coherency of seismic ground motions.

With the definition defined by equation 1.7, a coherency function generally depends on frequency and station-separation distance. It is a complex-valued function since the cross spectral density  $S_{jk}(\omega)$  is complex. The real part of the complex coherency function  $\gamma_{jk}(\omega)$  describes the similarity of the two ground motions without any adjustment for inclined wave propagation and therefore includes the effect of the deviation from vertical plane wave propagation [Abrahamson, 1992].



### 1.5.1 Types of coherency functions

From the complex coherency function presented in equation 1.7, one can find in literature, different types of coherency definitions: lagged coherency, unlagged coherency, and plane-wave coherency. In order to avoid the confusion of these coherency types, the complex coherency function will be represented by  $\gamma_{jk}(\omega)$  (or  $\gamma(d_{jk}, \omega)$ ), the lagged coherency function by  $|\gamma_{ij}(\omega)|$  (or  $|\gamma(d_{ij}, \omega)|$ ), the unlagged coherency by  $\gamma_{jk}^U(\omega)$  (or  $\gamma^U(d_{jk}, \omega)$ ) and the plane-wave coherency is represented by  $\gamma_{jk}^{PW}(\omega)$  (or  $\gamma^{PW}(d_{jk}, \omega)$ ). One can distinguish these three types of coherency by their definitions described in the following subsections.

#### Lagged Coherency

The complex coherency (equation 1.7) has an amplitude and a phase for each frequency band. The lagged coherency is simply the modulus term (amplitude) of the complex coherency:

$$|\gamma(d_{jk}, \omega)| = \left| \frac{\bar{S}_{jk}^M(\omega)}{\sqrt{\bar{S}_{jj}^M(\omega) \cdot \bar{S}_{kk}^M(\omega)}} \right| \quad (1.9)$$

The lagged coherency is a measure of "similarity" in the seismic motions, and indicates the degree to which the data recorded at the two stations are related. The lagged coherency reflects, at each frequency, the correlation of the motions. It is expected that at low frequencies and short separation distances, the motions will be similar and therefore, theoretically, the lagged coherency will tend to unity as frequency or station separation distance tend to zero. On the other hand, for uncorrelated processes, lagged coherency becomes zero. Hence, at large frequencies and long station separation distances, whose motions become uncorrelated, the lagged coherency will become zero ([Zerva, 2009]). However, in the estimation of lagged coherency from given seismic ground motion signals, the lagged coherency does not go to zero at large separations and high frequencies due to one important reason. After Abrahamson [Abrahamson et al., 1991], a segment of earthquake signals can contain wave components in addition to the plane wave. At high frequencies, the scattered energy or noise contribute significantly to the records. The correlation of these additional wave components will be reflected in the lagged coherency and will not let estimated lagged coherency approach zero at high frequencies and large separations.

#### Unlagged Coherency

The unlagged coherency  $\gamma^U(d_{jk}, f)$  is simply the real part of the complex coherency estimated in equation (1.7):

$$\gamma^U(d_{jk}, f) = \Re(\gamma(d_{jk}, f)) \quad (1.10)$$

It measures the coherency assuming no time lag between locations [Abrahamson et al., 1991]. This corresponds *only* to the assumption of vertical wave propagation for which there is no wave passage effects on the spatial variability of seismic ground motions. The unlagged coherency is given by the real part of the complex coherency.

The coherent part of the wave passage effect can lead to negative value of the unlagged coherency. Negative values indicate that the ground motions at the two stations are out of phase. An unlagged coherency of  $-1$  indicates that the ground motion is  $180^\circ$  out of phase due to wave passage effects [EPRI, 2006a].

## Plane Wave Coherency

As described in section 1.5.1, after Abrahamson [Abrahamson et al., 1991], the lagged coherency cannot approach zero at high frequencies and large separations of stations due to the presence of some wave components (in the analysed segments of earthquake signals) in addition to the plane wave. Another point is that the lagged coherency describes only the deviations of the ground motions from plane wave propagation at *each* frequency, but doesn't consider the deviation of the motions from a single plane wave at *all* frequency. More precisely, the lagged coherency allows for different frequencies to have their own wave speed and direction of wave propagation. Since soil-structure interaction applications always consider a single plane wave speed and single direction at *all* frequencies, the lagged coherency is not consistent with these applications [Abrahamson et al., 1991] [EPRI, 2006b].

Therefore, Abrahamson [Abrahamson et al., 1991] is interested in another type of coherency called *Plane-Wave Coherency*  $\gamma^{PW}(d_{jk}, \omega)$  which measures the coherency relative only to a single plane wave velocity for each earthquake. The Plane-Wave Coherency can be estimated from the time histories by taking the real part of the cross-spectrum after aligning the ground motions based on the best plane-wave velocity:

$$\gamma^{PW}(d_{jk}, \omega) = \Re \left[ \frac{\bar{S}_{jk}^M(\omega)}{\sqrt{\bar{S}_{jj}^M(\omega) \cdot \bar{S}_{kk}^M(\omega)}} \right]_{plane\_wave\_direction} \quad (1.11)$$

To estimate this plane wave coherency, we need to:

- (i) evaluate the direction of plane wave propagation
- (ii) rotate the signals into the direction of plane wave propagation evaluated in (i)
- (iii) align the signals for each station pair in the direction of plane wave propagation to remove the wave passage effects
- (iv) estimate the smoothed cross-spectral density, the smoothed power spectral densities and finally, the coherencies (equation 1.11)

The direction of plane-wave propagation can be found from the earthquake ground motion signals by determining an angle  $\phi$  for which the correlation coefficient between the two horizontal components (after being rotated by angle  $\phi$ ) is equal to zero. It is considered that 3rd principal component is the vertical direction.

The coefficient of correlation between the two horizontal components ( $a_1$  and  $a_2$ ) of earthquake signals is given by [Rezaeian and DerKiureghian, 2011]:

$$\rho_{1,2} = \frac{\int_0^\tau a_1(t) a_2(t) dt}{\sqrt{\int_0^\tau a_1^2(t) \int_0^\tau a_2^2(t)}} \quad (1.12)$$

where  $\tau$  here indicates the end of signals.

After [Abrahamson et al., 1991], for a plane wave, the phase difference is given by :

$$\theta(d_{jk}^r, \omega) = \omega d_{jk}^r / c, \quad (1.13)$$

where  $d_{jk}^r$  is the separation distance between stations  $j$  and  $k$  in the direction of plane wave propagation (radial component) and  $c$  is the apparent velocity best-fit plane wave. The term  $d_{jk}^r/c$  is the time shift between the two time histories at  $j$  and  $k$ . The phase difference of the "coherent" motion can be partitioned to isolate the part of the ground motion that can be described by a single plane wave at all frequencies:

$$\exp[i\theta(d_{jk}^r, \omega)] = h(d_{jk}^r, \omega) \exp[i\omega d_{jk}^r / c] + (1 - h(d_{jk}^r, \omega) \exp[i\eta(\omega/2\pi)]) \quad (1.14)$$

where  $h(d_{jk}^r, \omega)$  gives the relative power of the coherent wave field that can be described a single plane wave at all frequencies, and  $\eta(\omega/2\pi)$  is a random phase term. With that definition, the plane-wave coherency of a single plane wave at all frequencies is given by:

$$\gamma^{PW}(d_{jk}, d_{jk}^r, \omega) = |\gamma(d_{jk}, \omega)| h(d_{jk}^r, \omega). \quad (1.15)$$

It is also noted that the unlagged coherency for a single plane wave at all frequencies can simply be found by multiplying the plane-wave coherency by  $\cos(\omega d_{jk}^r / c)$ :

$$\gamma^U(d_{jk}, d_{jk}^r, \omega) = |\gamma(d_{jk}, \omega)| h(d_{jk}^r, \omega) \cos(\omega d_{jk}^r / c) \quad (1.16)$$

Therefore,  $h(d_{jk}^r, \omega)$  and apparent velocity of best-fit plane wave  $c$  can be found by:

$$h(d_{jk}^r, \omega) \cos(\omega d_{jk}^r / c) = \frac{\Re(\gamma(d_{jk}, \omega))}{|\gamma(d_{jk}, \omega)|} \quad (1.17)$$

By using non linear regressions, with the database from Lotung (LSST array), in Taiwan for the earthquakes in 1985 and 1986, [Abrahamson et al., 1991] proposed to take  $h(d_{jk}^r, \omega)$  in the form:

$$h(d_{jk}^r, \omega) = \frac{1}{1 + (\frac{\omega}{2\pi l})^n} \quad (1.18)$$

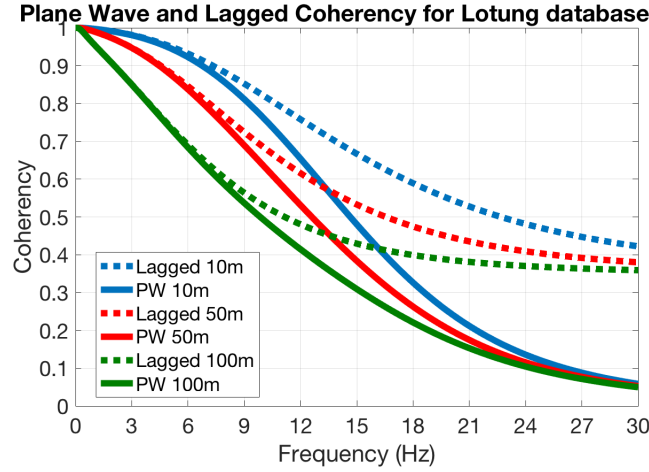
where  $l$  and  $n$  are to be determined from the ratio of equation 1.17. One can remark that  $h(d_{jk}^r, \omega)$  doesn't finally depend on  $d_{jk}^r$ .

With equations 1.15 and 1.16, by knowing the unlagged coherency and by knowing the apparent velocity of the best-fit plane wave, the plane wave coherency can also be defined by:

$$\gamma^{PW}(d_{jk}, d_{jk}^r, \omega) = \frac{\gamma^U(d_{jk}, d_{jk}^r, \omega)}{\cos(\omega d_{jk}^r / c)} \quad (1.19)$$

Since the real part of the smoothed cross-spectrum will have both positive and negative values, the plane-wave coherency will approach zero at high frequencies and large separation distances. The values of plane-wave coherency are less than or equal to the lagged coherency.

Figure 1.5 shows the difference between *lagged coherency* and *plane-wave coherency* for the coherency model of Abrahamson [Abrahamson et al., 1991] constructed by using database from earthquakes at Lotung in Taiwan in 1986. One can remark the important difference between the two aforementioned coherencies: the two coherencies have the same value for low frequencies, but



**Figure 1.5** – Comparison between plane-wave coherency and lagged coherency of Abrahamson model [Abrahamson et al., 1991] estimated from Lotung database

at high frequencies, the lagged coherency stays constant while the plane-wave coherency keeps decreasing toward zero.

Since soil-structure interaction analyses generally assume a single plane wave, the plane wave coherency is consistent with the intended application. In other words, the *plane wave coherency* function can be used to evaluate the standard engineering practice of modelling the wave-field by a single plane-wave.

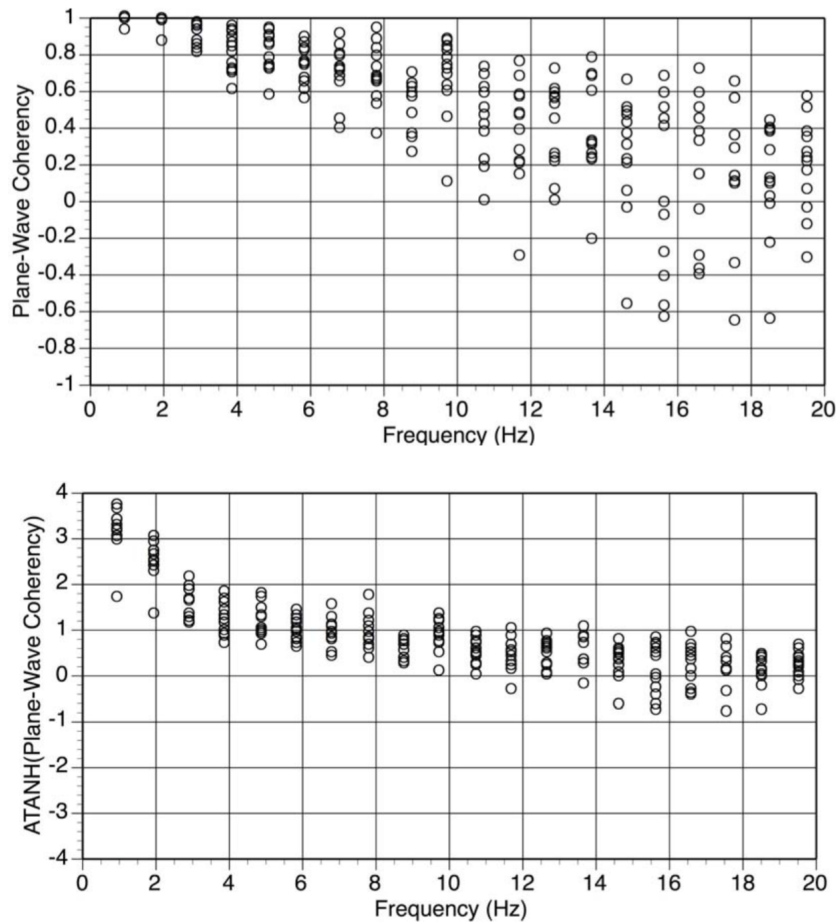
### 1.5.2 Statistical properties of coherencies

The estimations of coherency by using the stochastic method can lead to a bias and a variance. The statistics of the (smoothed) coherency estimate  $|\gamma(d_{jk}, \omega)|$  or  $\gamma^{PW}(d_{jk}, \omega)$  are not simple as discussed by [Abrahamson, 1992] and [Zerva, 2009]. Figure 1.6(above) presents the dependency of the variability of the plane-wave coherency with frequency. It is noted that the uncertainty of coherency depends on its own values: the uncertainty increases as  $|\gamma_{ij}(\omega)|$  and  $\gamma^{PW}(d_{jk}, \omega)$  decreases (the coherency is not homoscedastic). Therefore, [Abrahamson et al., 1991] proposed to do the statistical analysis on  $\tanh^{-1}|\gamma(d_{jk}, \omega)|$  and  $\tanh^{-1}[\gamma^{PW}(d_{jk}, \omega)]$  since the uncertainty of the transformation  $\tanh^{-1}$  is approximately constant. If the value of  $|\gamma_{ij}(\omega)|$  is not small, the distribution of  $\tanh^{-1}|\gamma_{ij}(\omega)|$  is considered to be a normal distribution. The dependency becomes less significant for the case that plane-wave coherency is presented in the  $\tanh^{-1}$  transform (Figure 1.6(below)).

Therefore, after Abrahamson [EPRI, 2007a], the average of coherency should be evaluated after the  $\tanh^{-1}$  transform are applied to the plane-wave coherencies estimated from different events and different station pairs. Mathematically,

$$\gamma^{PW}(d_{jk}, \omega)|_{mean} = \tanh[\mathbb{E}(\tanh^{-1}(\gamma_n^{PW}(d_{jk}, \omega)))] \quad (1.20)$$

where  $n$  indicates different realization of coherencies (from different events or from different station pairs).



**Figure 1.6** – Dependence of the Variability of the Plane-Wave Coherency With Frequency (above) and Independence of the Variability of the Transformed Plane-Wave Coherency With Frequency (below) (from [EPRI, 2007a])

### 1.5.3 Coherency models proposed in the literature

This section presents some semi-empirical and empirical coherency models that have been proposed and widely used in the literature. The expression "semi-empirical functions" refers to the functions which are formed by theoretical considerations and also by using the analyses of data from earthquake sites. They are sometimes called "parametrical models" since their expressions are given by theoretical considerations and their parameters are given by using recorded data from earthquake sites. On the other hand, the expression "empirical functions" refers to the functions given directly by using statistical analyses of recorded data without using physical theories.

For more detail reviews of coherency function models, reader can be referred to the analyses of [Zerva and Zervas, 2002].

Generally, the seismic incident fields are considered to be homogeneous, hence, the stochastic description of seismic incident field depends only on the distance between two observed points and not on the location of those points. Consequently, for all of the coherency models presented in the following, the coherency are written as a function of distance  $d$  and frequency  $\omega$  ou  $f$  with  $\omega = 2\pi f$ .

#### Empirical coherency function models

Most of the studies of spatial coherency are based on evaluation of the ground motions from the dense array located in Taiwan, at Lotung due to the extensive database that is available from the SMART-1 array [Abrahamson et al., 1987]. By using data from that array, a significant number of coherency models have been developed by different authors, along which: [Abrahamson, 1993], [Harichandran and Vanmarcke, 1986], [Harichandran, 1988], [Harichandran, 1991], [Loh, 1985], [Loh and Yeh, 1988], [Loh and Lin, 1990], [Novak, 1987], [Oliveira et al., 1991], [Ramadan and Novak, 1993], [Verno et al., 1991], [Zerva and Zhang, 1997], [Hao et al., 1989], [Abrahamson et al., 1990].

The first two remarkable empirical coherency models might be those of [Abrahamson et al., 1990] and [Harichandran and Vanmarcke, 1986]. The latter developed an isotropic model for the horizontal component of the *lagged coherency* based on data from a single far-field event recorded by the Strong Motion Array in Taiwan, phase 1 (SMART-1), located at Lotung. Their model of *lagged coherency*, applicable for separation distances greater than 100 m, is given by:

$$|\gamma(d, \omega)| = A \exp \left[ -\frac{2d}{\alpha\theta(\omega)}(1 - A + \alpha A) \right] + (1 - A) \exp \left[ -\frac{2d}{\theta(\omega)}(1 - A + \alpha A) \right] \quad (1.21)$$

where  $\theta(\omega) = k[1 + (\omega/\omega_o)^b]^{-1/2}$ ,  $A = 0.736$ ,  $\alpha = 0.147$ ,  $k = 5210$ ,  $\omega_o/2\pi = 1.09$  and  $b = 2.78$ .

To be noted that this lagged coherency model is validated only for the distances more than 100 m; therefore, for some structures such as nuclear power plants whose diameters of foundations are around 100m, this model cannot be applied.

[Konakli et al., 2013] compared the aforementioned model with data recored by the UPSAR array during the 2004 Parkfield earthquake. In their investigations, for station separation distances 100 - 300 m, the empirical model of [Harichandran and Vanmarcke, 1986] is in fair agreement with the UPSAR estimates for frequencies up to approximately 4 Hz but for separation distances greater than 300 m, the UPSAR coherency estimate tends to be greater than that given by the

Parameters	Abramson 1990	Modified by Ancheta 2011
$a$	$2.54 - 0.012d$	$3.79 - 0.499 \ln d$
$b$	$-0.115 - 0.00084d$	$-0.115 - 0.00084d$
$c$	$1/3$	$1/3$
$g$	$0.878$	$0.878$
$k$	$0.35$	$0.35$

**Table 1.2** – Parameters of Abrahamson model (1990) for soil site (second column) and the modified Abrahamson model after [Ancheta et al., 2011] (third column)

empirical model. It is then concluded that this empirical coherency model overestimates the spatial incoherence for the case of recorded data from the UPSAR array.

Located within the SMART-1 array, the Large Scale Seismic Test (LSST) array allows investigations of spatial variability for horizontal separations as small as 6 m. Using data from fifteen earthquakes of magnitude 3.7 - 3.8 of LSST array, [Abrahamson et al., 1990] proposed a *lagged coherency* model for horizontal component which is applicable for separation distances smaller than 100 m:

$$\tanh^{-1} |\gamma(d, f)| = a(d) \exp \left[ b(d) \frac{f}{2\pi} \right] + c(d) \left( \frac{f}{2\pi} \right)^{g(d)} + k \quad (1.22)$$

where the parameters are given in Table 1.2.

This model was derived for frequencies higher than 1 Hz, but can be safely extrapolated to zero frequency. But on the basis of comparison with SMART-1 coherencies, [Abrahamson et al., 1990] noted that extrapolation to distances greater than 100 m will underestimate the coherency. By comparing this model with data from dense arrays in Japan and California for station separation up to 100 m, [Schneider et al., 1992] concluded that for arrays located on soil, the agreement of the model with coherency estimates of data was considered satisfactory, but for arrays located on rock, the coherency estimates of data were lower than those predicted by the model. The coherency obtained from the soil sites is normally smaller than that obtained from the rock sites due to the fact that the soil sites possess much more non-linearities and heterogeneities than the rock sites.

For the same data and same separation distances, Abrahamson [Abrahamson, 1992] also developed another *plane-wave coherency* model. The comparison between the *lagged coherency* and *plane-wave coherency* of Abrahamson obtained from the LSST arrays is presented in figure 1.5.

[Ancheta et al., 2011] revisited the *lagged-coherency* model of [Abrahamson et al., 1990] by comparing this model with data from BVDA arrays (Borrego Valley Differential Array) in California. The authors found that the model fit to the BVDA data is good for the separation distance  $d \geq 30$  m for all frequencies, but underestimates coherency for  $d = 10$  m and  $d = 20$  m and frequencies less than 10 Hz. From a parametric study, only the coefficient  $a(d)$  of Abrahamson lagged coherency model (equation 1.22) is proposed to be changed by the authors and other coefficients are conserved to be the same to the original model. For the aforementioned coefficient, the change is done from linear expression  $a(d) = 2.54 - 0.012d$  to log-linear expression  $a(d) = 3.79 - 0.499 \ln d$  since the log-linear function produces a higher coefficient of determination than a linear fit (see Table 1.2).

[Konakli et al., 2013] recently compared the model of [Ancheta et al., 2011] with data recorded by the UPSAR array during the 2004 Parkfield earthquake. The author concluded that for separation distances smaller than 100 m, the UPSAR coherency estimate tends to be greater than that given



Parameter	Horizontal component	Vertical component
$a_1$	1.647	3.15
$a_2$	1.01	1.0
$a_3$	0.4	0.4
$f_c$	$-1.886 + 2.221 \cdot \ln\left(\frac{4000}{d+1} + 1.5\right)$	$\exp(2.43 - 0.025 \ln(d+1) - 0.048(\ln(d+1))^2)$
$n_1$	7.02	4.95
$n_2$	$5.1 - 0.51 \cdot \ln(d+10)$	1.685

**Table 1.3** – Parameters of Abrahamson model (2006) for all types of soil

by the empirical model in the entire frequency range examined. This concludes that the the lagged coherency model edited by [Ancheta et al., 2011] overestimates the incoherency of data from UPSAR arrays.

Finally, one of the most used *plane-wave coherency* model in the United States in these last 10 years is *plane-wave* Abrahamson model, [EPRI, 2006a]. The model is formed based on the by using non-linear regression of data from the earthquakes of 10 different sites: Lotung LSST (Soil), EPRI Parkfield (Soft Rock or Hard Soil), Chiba (Soil), Imperial valley (Soil), Hollister Differential (Soil), Stanford (Soil), Coalinga (Soft Rock or Hard Soil), Pinyon Flat (Hard Rock), SMART-1 (Soil), SMART-2 (Soil). The "*plane-wave coherency*" model of Abrahamson for all types of soil is given by:

$$|\gamma^{PW}(d, f)| = \left[ 1 + \left( \frac{f \cdot \tanh(a_3 d)}{f_c \cdot a_1} \right)^{n_1} \right]^{-0.5} \times \left[ 1 + \left( \frac{f \cdot \tanh(a_3 d)}{f_c \cdot a_2} \right)^{n_2} \right]^{-0.5} \quad (1.23)$$

with:

Many studies have been realized to validate this model, and also to integrate this model in to a software (SASSI) to account for spatial variation of seismic ground motions in the analysis of soil-structure interactions [EPRI, 2006a], [EPRI, 2007a], [EPRI, 2007b], [EPRI, 2006b], [EPRI, 2006c], [EPRI, 2005].

To be noted that this model was developed by Abrahamson for all types of soil since the formalution was obtained by means of coherencies from 10 differents sites described above. The first 8 sites are considered to be dense arrays since the station separation varies from 3 m to 340 m. The last two sites are large arrays because the station separation of SMART-1 varies from 100 m to 4000 m and that of SMART-2 varies from 200 m to 750 m.

Since this last model was developed for all types of soil, and since the coherency obtained from soil sites is much smaller than that from hard rock site, this model can sometimes overestimate or underestimate the coherency of some specific sites. Abrahamson [EPRI, 2007a] wanted then to develop 3 different coherency models which are corresponding to 3 different types of soil : normal soil, soft-rock and hard rock. The author devided the 8 dense arrays sites to 3 types: LSST, Chiba, Imperial Valley and Hollister Differential are put in the type of normal soil (shear wave velocity for the top 30 m was evaluated and varies from 180 m/s to 290 m/s for each site), EPRI Parkfield and Coalinga are put in the type of soft-rock (shear wave velocity for the top 30 m was evaluated to be around 400 m/s), and Pinyon Flat is put in the type of hard rock (shear wave velocity for the top 30 m was evaluated to be 1030 m/s). The *plane-wave coherency* model of Abrahamson for



Parameter	Horizontal component
$a1$	1.0
$a2$	40
$a3$	0.4
$f_c$	$27.9 - 4.82 \cdot \ln(d_{ij} + 1) + 1.24 \cdot (\ln(d_{ij} + 1) - 3.6)^2$
$n_1$	$3.8 - 0.04 \cdot \ln(d_{ij} + 1) + 0.0105 \cdot (\ln(d_{ij} + 1) - 3.6)^2$
$n_2$	16.4

Parameter	Vertical component
$a1$	1.0
$a2$	200
$a3$	0.4
$f_c$	$29.2 - 5.2 \cdot \ln(d + 1) + 1.45 \cdot (\ln(d + 1) - 3.6)^2$
$n_1$	$2.03 - 0.41 \cdot \ln(d + 1) - 0.078 \cdot (\ln(d + 1) - 3.6)^2$
$n_2$	10

Table 1.4 – Parameters of Abrahamson model (2007) for hard rock site

Parameters	Horizontal component	Vertical component
$a1$	1.0	1.0
$a2$	$15.8 - 0.044 \cdot d_{ij}$	100
$a3$	0.4	0.4
$f_c$	$14.3 - 2.35 \cdot \ln(d_{ij} + 1)$	$\exp(2.25 - 0.021 \cdot d_{ij})$
$n_1$	3.0	1.3
$n_2$	15.0	3.0

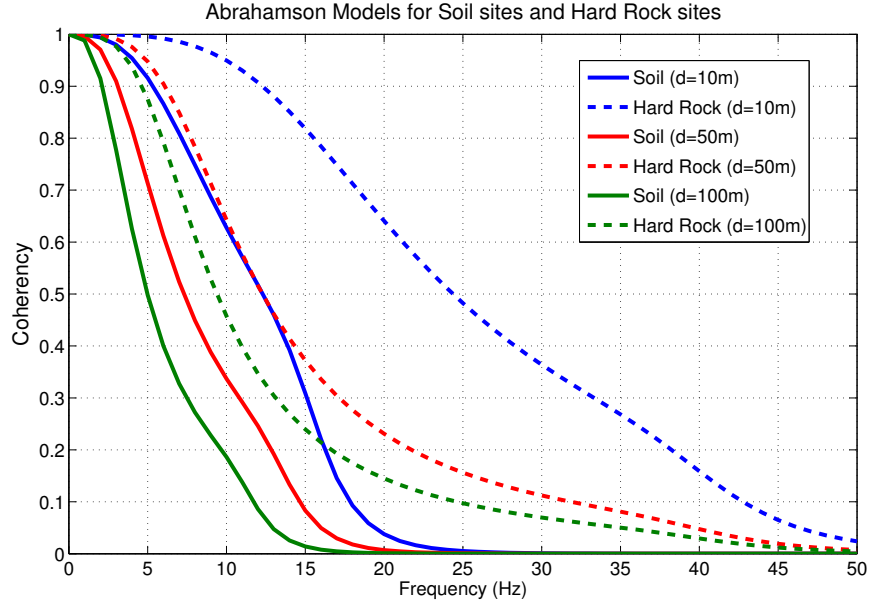
Table 1.5 – Parameters of Abrahamson model (2007) for soil site, horizontal component

*Hard Rock sites* and for *Soil sites* take almost the same functional form of equation 1.23 :

$$|\gamma^{PW}(d, f)| = \left[ 1 + \left( \frac{f \cdot \tanh(a_3 d)}{f_c \cdot a_1} \right)^{n_1} \right]^{-0.5} \times \left[ 1 + \left( \frac{f \cdot \tanh(a_3 d)}{a_2} \right)^{n_2} \right]^{-0.5} \quad (1.24)$$

For the **hard rock sites**, the parameters for horizontal and vertical component are respectively listed in Table 1.4. For the **soil sites**, the parameters of Abrahamson model for horizontal and vertical component are listed in Table 1.5.

For the *plane-wave coherency* model of the soft-rock sites (ou hard soil sites), Abrahamson couldn't formulate a rigorous model since he explained in [EPRI, 2007a] that the EPRI Parkfield site has a particular topography that can influence significantly the coherency of seismic ground motions. But the author mentioned that for SSI applications on soft-rock sites, it is recommended that the average between the soil coherency and the hard-rock coherency is used. Figure 1.7 presents the *plane-wave coherency* of Abrahamson model for soil sites and hard-rock sites for horizontal component.



**Figure 1.7** – Plane wave coherency of Abramson models for soil sites and hard rock sites horizontal component

### Semi-empirical coherency function models

Semi-empirical models are formed based on analytical considerations but include parameters that require estimation from recorded data. One of the most quoted coherency models is maybe the one introduced by [Luco and Wong, 1986] considering the propagation of shear waves in a random medium. For this model, the coherency for a pair of acceleration processes at two different stations with a separation distance  $d$  is given by:

$$\gamma^{PW}(d, f) = \exp \left[ - \left( \frac{2\pi \cdot \alpha \cdot f \cdot d}{V_s} \right)^2 \right] \quad (1.25)$$

where  $V_s$  is the average shear wave velocity of the ground medium along the wave travel path and  $\alpha$  the spatial variability factor varying generally between 0.1 and 1 and becoming 0 for the pure coherence case. With its properties, this model is classified in the category of *plane-wave coherency*. [Luco and Wong, 1986] introduced this model based on the theoretical analyses in which the parameter  $\alpha$  can be evaluated by:

$$\alpha = \xi \sqrt{\frac{Z}{\ell_c}} \quad (1.26)$$

where  $\xi$  is the coefficient of variation of elastic properties of the media,  $Z$  is the distance along which the seismic waves propagate in random heterogeneous medium, and  $\ell_c$  is the correlation length of random heterogeneous media. To be noted that the reference of theoretical analyses to obtain the functional form of that coherency model cannot be found.

Since  $\alpha$  and  $V_s$  are two constant parameters, the expression of model of [Luco and Wong, 1986] is often replaced by writing with only one parameter  $\eta$ , i.e.

$$\gamma^{PW}(d, f) = \exp \left[ -(2\pi\eta fd)^2 \right] \quad (1.27)$$

[Luco and Wong, 1986] suggested the typical values of  $\eta$  in the range from  $2 \times 10^{-4} \text{ s/m}$  to  $3 \times 10^{-4} \text{ s/m}$ . [Zerva and Harada, 1997] revisited the model of [Luco and Wong, 1986] with accounting for the site topography by a horizontally extended layer with random characteristics overlaying a half-space (bedrock). Their model includes the effects of wave passage with constant velocity on the ground surface, the loss of coherence due to scattering of the waves as they travel from the source to the site, and the local site effects, approximated by vertical transmission of shear waves through a horizontal layer with random properties. They proposed then to change the constant  $\alpha$  to an analytical expression which is function of the properties and the depth of soil layers at the given site.

The model of [Luco and Wong, 1986] was also revisited by [Konakli et al., 2013] by comparing this coherency model with the coherency estimated from accelerograms recorded by the UPSAR array during the 2004 Parkfield earthquake. The authors concluded that the parameter  $\eta$  cannot be constant as suggested by [Luco and Wong, 1986], but that latter one has to be dependent on both separation distance and frequency so that the model is compatible with the data of UPSAR. In their studies, to fit the coherency model of [Luco and Wong, 1986] with the coherency estimated from the UPSAR array, [Konakli et al., 2013] first determined  $\eta$  as a function of station separation distance  $d_{ij}$  and after that as a function of frequency. Figures 1.8 presents the value of  $\eta$  as a function of station separation distance and of frequency. Figure 1.8(above) show clearly that to fit the coherency model of [Luco and Wong, 1986] with the data from UPSAR array, the value of  $\eta$  is strongly dependent on the station separation distance. On the other hand, from Figure 1.8(below), the value of  $\eta$  also depends on the frequency but the dependency is less remarkable than the case of station separation distance.

Another semi-empirical model to be cited should be the one of [DerKiureghian, 1996]. With theoretical considerations, [DerKiureghian, 1996] gave the functional form of the coherency function, which accounts for three principle causes of spatial variation of seismic ground motions, by:

$$\gamma(d, \omega) = \gamma(d, \omega)^{incoherence} \cdot \gamma(d, \omega)^{wave-passage} \cdot \gamma(d, \omega)^{site-response} \quad (1.28)$$

$$\gamma(d, \omega) = |\gamma(d, \omega)| \cdot \exp \left\{ i \left[ \theta(d, \omega)^{wave-passage} + \theta(d, \omega)^{site-response} \right] \right\} \quad (1.29)$$

with:

$$|\gamma(d, \omega)| = \cos [B(d, \omega)] \exp \left\{ -0.5 [A(d, \omega)]^2 \right\} \quad (1.30)$$

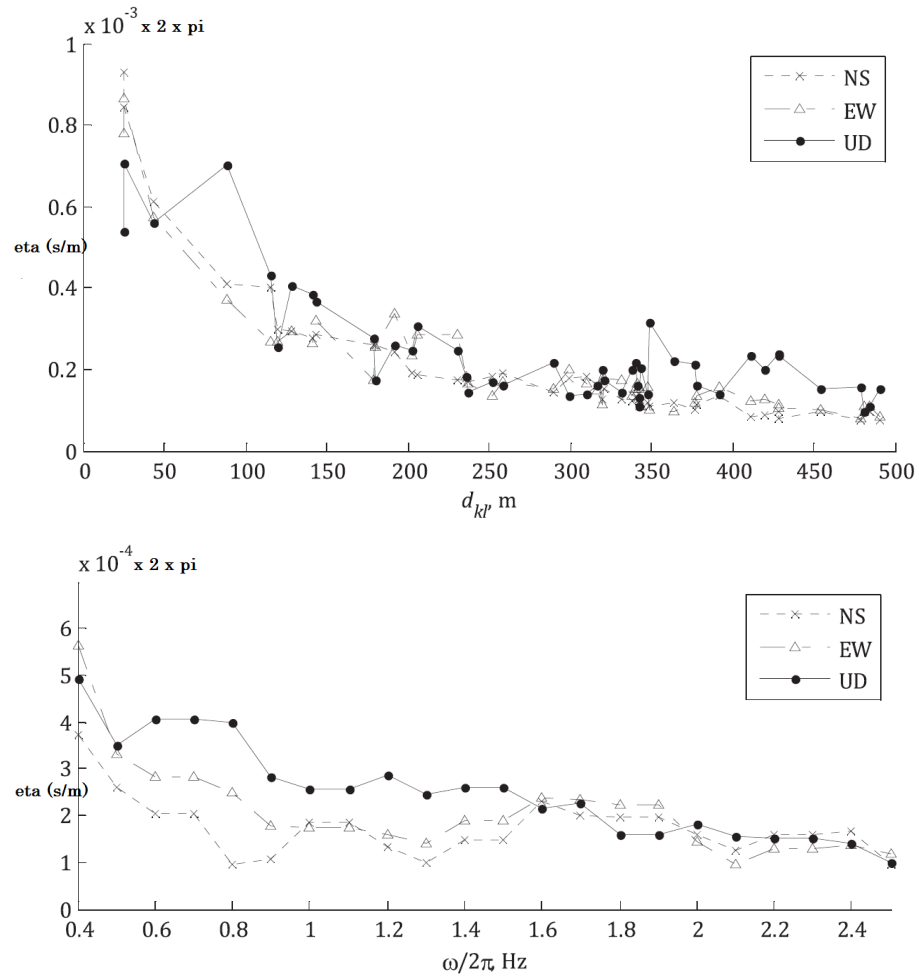
in which,  $A(d, \omega)$  is a function characterizing the difference between the phases of the two acceleration processes at frequency  $\omega$  and  $B(d, \omega)$  is a function characterizing the difference in the corresponding wave amplitudes;

$$\theta(d, \omega)^{wave-passage} = -\frac{\omega d^L}{v_{app}} \quad (1.31)$$

where  $d^L$  is the projected horizontal distance in the longitudinal direction of propagation of waves and  $v_{app}$  is the surface apparent wave velocity;

$$\theta(d, \omega)^{site-response} = \tan^{-1} \left\{ \frac{\text{Im} [H_i(\omega) H_j(-\omega)]}{\text{Re} [H_i(\omega) H_j(-\omega)]} \right\} \quad (1.32)$$

in which  $H_i(\omega)$  &  $H_j(\omega)$  are the frequency response functions (transfer functions) for the absolute acceleration response of the soil profile for the acceleration inputs at the bedrock level. The derivation of equation 1.32 is based on the assumption of linear (or linearised) soil behaviour and vertical wave propagation at each site. The expression of  $H_m(\omega)$  (for  $m = i, j$ ) can be determined by using the theoretical physics of wave propagation in the medium. Due to [Clough and Penzien, 1993], for



**Figure 1.8** – Variation of  $\eta$  as a function of station separation distance (above) and of frequency (below) [Konakli et al., 2013]

the single-degree-of-freedom filter idealization of the soil column, the frequency response function  $H_m(\omega)$  is given by:

$$H_m(\omega) = \frac{\omega_m^2 + 2i\zeta_m\omega_m\omega}{\omega_m^2 - \omega^2 + 2i\zeta_m\omega_m\omega} \quad (1.33)$$

where  $\omega_m$  and  $\zeta_m$  represent respectively the filter frequency and damping ratio for site  $m$ .

There are still anyway some mysteries in using the coherency model of [DerKiureghian, 1996] since some parameters are still not clarified until now.

Finally, another semi-empirical model of coherency which is not yet used in literature, but should be cited here, might be the one introduced in [Sato et al., 2012]. From theoretical considerations on seismic wave propagation in random heterogeneous media, which will be presented in details in the next subsection, [Sato et al., 2012] gave the functional form of coherency model as :

$$\gamma(d, f) = \exp \left[ -\sqrt{\pi}\xi^2\ell_c Z \frac{(2\pi f)^2}{V_o^2} [1 - \exp(-\frac{d^2}{\ell_c^2})] \right] \quad (1.34)$$

where  $\xi$ ,  $\ell_c$ ,  $V_o$  and  $Z$  are respectively the coefficient of variation of elastic properties in the media, the correlation length of heterogeneous media, the average velocity of wave propagation in the media, and the depth of the random heterogeneous layer.

The details of theoretical considerations to define that coherency function are provided in the next subsection. Without any precision about the origin of these theoretical analyses, we prefer calling the coherency function given by equation 1.34 as the model of Sato [Sato et al., 2012].

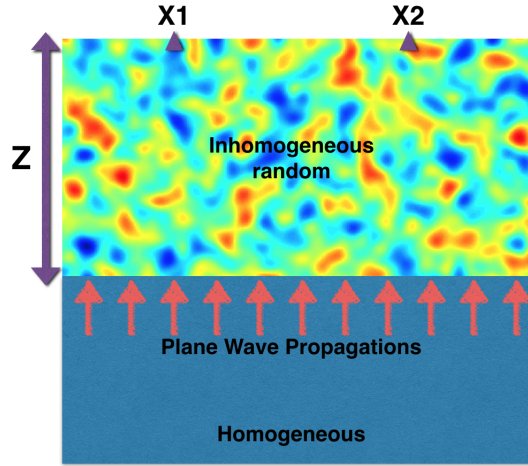
In the real application of seismic wave propagation in the random heterogeneous media, the main question is about the value of  $Z$  since one needs to determine from which depth, the medium is considered to be heterogeneous. Another things are about statistical parameters  $\ell_c$  and  $\xi$  because it is not easy to define clearly about their value for a site of interest. About the wave velocity, many studies in the literature and the common practices in Earthquake Engineering normally consider the value of  $V_{s30}$  (average value of shear-wave velocity for the first 30m vertically of the medium).

To be remarked that the functional form of the model introduced in [Sato et al., 2012] is simply similar to that of [Luco and Wong, 1986]. Accurately, in the case that  $d \ll \ell_c$ , with an obvious development, we will see that the equation 1.34 will give the functional form like:

$$\gamma(d, f) = \exp[-\sqrt{\pi}\xi^2 \frac{Z}{\ell_c} (\frac{2\pi \cdot f \cdot d}{V_o})^2] \quad (1.35)$$

which is almost the same to the model of [Luco and Wong, 1986].

One can say that the model of [Luco and Wong, 1986] is simply a particular case of model of [Sato et al., 2012]. To cover all possible cases, it should be more interesting to work with the model of [Sato et al., 2012]. In chapter 3, we use numerical modelling of wave propagation in random heterogeneous media to understand more about the influence of physical and statistical properties of the medium on the spatial variability of seismic ground motions, and to check for the possibility of validation of coherency model based on numerical case studies.



**Figure 1.9** – Plane-Wave propagation in random layer of soil

#### 1.5.4 On the theoretical considerations for defining coherency of plane waves propagating in a random heterogeneous medium

This section presents some mathematical considerations to define a theoretical coherency function of plane-wave propagating in a random heterogeneous medium. More precisely, we present the theoretical analyses to obtain the coherency model of Sato (equation 1.34) which can be found in [Sato et al., 2012].

These analyses are realized based on the statistical descriptions of a random heterogeneous medium presented in the section 1.4.

Consider an inhomogeneous random layer whose thickness is represented by  $Z$  (Figure 1.9). For the far-fault earthquakes, it is considered that the seismic wave arrive at first layer in form of plane-wave. To simplify this analysis, it is also considered that the plane-wave arrive in vertical direction. There is no, thus, wave passage effects.

Let a scalar plane wave  $u$  propagate in that inhomogeneous random layer with velocity  $V(\mathbf{x})$  such that:

$$V(\mathbf{x}) = \begin{cases} V_o & \text{for } Z \leq 0 \\ V_o(1 + \xi(\mathbf{x})) & \text{for } Z > 0 \end{cases} \quad (1.36)$$

in which,  $\xi(\mathbf{x})$  is the wave velocity fluctuation in the random medium ( $|\xi(\mathbf{x})| = COV$ , Coefficient Of Variation) and  $V_o$  is the wave velocity in the homogeneous layer.

In inhomogeneous random medium, the equation of a scalar wave  $u$  can be written as:

$$\left[ \Delta - \frac{1}{V^2(\mathbf{x})} \frac{\partial^2}{\partial t^2} \right] u(\mathbf{x}, t) = 0 \quad (1.37)$$

For the case of small fluctuation, i.e  $|\xi| \ll 1$ , equation 1.37 can be written as:

$$\left[ \Delta - \frac{1}{V_o^2(\mathbf{x})} \frac{\partial^2}{\partial t^2} \right] u(\mathbf{x}, t) + \frac{2}{V_o^2} \xi \frac{\partial^2 u(\mathbf{x}, t)}{\partial t^2} = 0 \quad (1.38)$$

At a point  $\mathbf{x}_t = (x, y)$  situated on the ground surface (transverse plane, orthogonal to the wave propagation direction "vertical direction"), the scalar wave-field can be written as a superposition of plane wave:

$$u(\mathbf{x}_t, Z, t) = \frac{1}{2\pi} \int_{-\infty}^{\infty} U(\mathbf{x}_t, Z, \omega) e^{i(k_o Z - \omega t)} d\omega \quad (1.39)$$

where wave number  $k_o = \omega/V_o$  and  $U(\mathbf{x}_t, Z, \omega)$  is the amplitude of plane wave with angular frequency  $\omega$ . To be noted here that it is about the superposition of different frequencies (and then, with also different corresponding wave numbers), but not about different angles.

Substituting 1.39 into 1.38, we get:

$$\frac{\partial^2 U}{\partial z^2} + 2i \cdot k_o \frac{\partial U}{\partial z} + \Delta_t U - 2k_o^2 \cdot \xi \cdot U = 0 \quad (1.40)$$

where  $\Delta_t = \frac{\partial^2}{\partial x^2} + \frac{\partial^2}{\partial y^2}$  is the Laplacian operator in the transverse plane (plane of the ground surface).

Consider  $\ell_c$  the correlation length of the heterogeneous random medium. In the case that  $\ell_c k_o \gg 1$ , the amplitude changes very slowly; the second derivative term in 1.40 can be neglected. We obtain:

$$2i \cdot k_o \frac{\partial U}{\partial z} + \Delta_t U - 2k_o^2 \cdot \xi \cdot U = 0 \quad (1.41)$$

Taking the ensemble average of 1.41, we obtain :

$$2i \cdot k_o \frac{\partial \langle U \rangle}{\partial z} + \Delta_t \langle U \rangle - 2k_o^2 \cdot \langle \xi \cdot U \rangle = 0 \quad (1.42)$$

From 1.41, the wave-field situated at  $z$  can be written in an integral form by using the wavefield at  $z - \Delta z$  where  $\Delta z > 0$ :

$$U(\mathbf{x}_t, z, \omega) = U(\mathbf{x}_t, z - \Delta z, \omega) + \frac{i}{2k_o} \int_{z-\Delta z}^z dz' [\Delta_t U(\mathbf{x}_t, z', \omega) - 2k_o^2 \xi(\mathbf{x}_t, z') U(\mathbf{x}_t, z', \omega)] \quad (1.43)$$

Suppose the existence of an intermediate scale  $\Delta z$  which is larger than the correlation distance  $\ell_c$  but smaller than the scale of variation of  $U$ . Then one can write :

$$U(\mathbf{x}_t, z, \omega) \approx U(\mathbf{x}_t, z - \Delta z, \omega) + \frac{i}{2k_o} \Delta z \Delta_t U(\mathbf{x}_t, z - \Delta z, \omega) - ik_o U(\mathbf{x}_t, z - \Delta z, \omega) \int_{z-\Delta z}^z dz' \xi(\mathbf{x}_t, z') \quad (1.44)$$

Multiplying  $\xi(\mathbf{x}'_t, z)$  and taking the ensemble average, one has:

$$\langle \xi(\mathbf{x}'_t, z) U(\mathbf{x}_t, z, \omega) \rangle \approx -ik_o \int_{z-\Delta z}^z dz' \langle \xi(\mathbf{x}'_t, z) \xi(\mathbf{x}_t, z') \rangle \langle U(\mathbf{x}_t, z - \Delta z, \omega) \rangle \quad (1.45)$$

$$\approx -ik_o \int_0^\infty dz_d R(\mathbf{x}_t - \mathbf{x}'_t, z_d) \langle U(\mathbf{x}_t, z, \omega) \rangle \quad (1.46)$$

$$= -\frac{i}{2} k_o A(\mathbf{x}_t - \mathbf{x}'_t) \langle U(\mathbf{x}_t, z, \omega) \rangle \quad (1.47)$$

where we put  $\langle U(\mathbf{x}_t, z - \Delta z, \omega) \rangle \approx \langle U(\mathbf{x}_t, z, \omega) \rangle$  in the right-hand side because the variation of  $U$  is small and  $\langle \xi(\mathbf{x}'_t, z) U(\mathbf{x}_t, z - \Delta z, \omega) \rangle = 0$  since there is no contribution of the inhomogeneity at  $z$  to

the wavefield at  $z - \Delta z$ , which means the neglect of backward scattering. The upper bound of the integral region for  $z_d = z' - z$  is changed from  $\Delta z$  to infinity since  $\Delta z \gg \ell_c$ . Function  $A$  defined by the longitudinal integral of autocorrelation function ( $R$ ) describing the correlation of media on the transverse plane. Mathematically, that function is given by:

$$A(\mathbf{x}_t) = \int_{-\infty}^{\infty} dz R(\mathbf{x}_t, z) \quad (1.48)$$

The coherency function of wavefield  $U$  at different locations ( $\mathbf{x}_1$  and  $\mathbf{x}_2$ ) on the ground surface is defined by:

$$\gamma(\mathbf{x}_1, \mathbf{x}_2, z, \omega) = \langle U(\mathbf{x}_1, z, \omega) U^*(\mathbf{x}_2, z, \omega) \rangle \quad (1.49)$$

Multiplying  $U^*$  by 1.41 and taking the ensemble average, one can write:

$$2ik_o \frac{\partial \gamma}{\partial z} + (\Delta_{t,1} - \Delta_{t,2})\gamma - 2k_o^2 \langle (\xi_1 - \xi_2) U_1 U_2^* \rangle = 0 \quad (1.50)$$

where  $U_1$  and  $U_2$  are respectively the modules at  $\mathbf{x}_1$  and  $\mathbf{x}_2$ . By using the same procedure as for the derivation of equations 1.45, 1.46 and 1.47, the third term of equation 1.50 can be written :

$$\langle (\xi_1 - \xi_2) U_1 U_2^* \rangle = -ik_o [A(0) - A(d)]\gamma \quad (1.51)$$

where  $d = |\mathbf{x}_1 - \mathbf{x}_2|$ .

The equation 1.50 can be written

$$2ik_o \frac{\partial \gamma}{\partial z} + (\Delta_{t,1} - \Delta_{t,2})\gamma + 2ik_o^3 [A(0) - A(d)]\gamma = 0 \quad (1.52)$$

Introducing, in the plane of ground surface (horizontal), center of mass coordinates  $\mathbf{x}_c = (\mathbf{x}_1 + \mathbf{x}_2)/2$  and difference coordinates  $\mathbf{x}_d = (\mathbf{x}_1 - \mathbf{x}_2)/2$ , Laplacian can be written as

$$\Delta_{t,1} = \Delta_{t,d} + \frac{1}{4} \Delta_{t,c} + \nabla_{t,c} \nabla_{t,d} \quad (1.53)$$

$$\Delta_{t,2} = \Delta_{t,d} + \frac{1}{4} \Delta_{t,c} - \nabla_{t,c} \nabla_{t,d} \quad (1.54)$$

Since the coherency function  $\gamma$  is independent of the center of mass coordinates, the second term of the left-hand side in 1.52 is equal to zero ( $(\Delta_{t,1} - \Delta_{t,2})\gamma = 0$ ), one can write

$$\frac{\partial \gamma}{\partial z} + k_o^2 [A(0) - A(d)]\gamma = 0 \quad (1.55)$$

With the initial condition  $\gamma(d, z = 0, \omega) = 1$  (the seismic wave-field is considered to be perfectly coherent in the bedrock layer), the equation 1.55 can be solved and the solution on the ground surface is

$$\gamma(d, Z, \omega) = \exp(-k_o^2 [A(0) - A(d)]Z) \quad (1.56)$$

In the case of a random medium described by Gaussian autocorrelation model (see Table 1.2), the function  $A$  can be defined by

$$A(d) = \sqrt{\pi} \xi^2 \ell_c \exp\left(-\frac{d^2}{\ell_c^2}\right) \quad (1.57)$$



Replacing 1.57 into 1.56, one can finally get the coherency function of seismic wave propagating in an heterogeneous medium:

$$\gamma(d, Z, \omega) = e^{-\sqrt{\pi}\xi^2\ell_c k_o^2 Z [1 - \exp(-\frac{d^2}{\ell_c^2})]} \quad (1.58)$$

$$\gamma(d, f) = e^{-\sqrt{\pi}\xi^2\ell_c Z \left(\frac{\omega}{V_o}\right)^2 [1 - \exp(-\frac{d^2}{\ell_c^2})]} \quad (1.59)$$

The equation 1.59 (which is already presented in equation 1.34) is called as the coherency model of Sato in this manuscript.

### 1.5.5 Conclusions on coherency models

Different definitions of coherency estimations and also different models of coherency used in the literature are reviewed and presented in this chapter. Among all models presented, the plane-wave coherency models of Abrahamson [EPRI, 2007a] (equation 1.24) and the coherency model of [Luco and Wong, 1986] (equation 1.25) are the most widely used.

For the different definitions of coherency, the *plane-wave coherency* and *lagged coherency* are the two coherencies which are commonly analysed in the literature. To be consistent with soil-structure interaction applications, the *plane-wave coherency* should be used since this coherency also assumes a single plane wave direction and single plane wave velocity for *all* frequencies. Therefore, in the analyses of this Ph.D thesis, only *plane-wave coherency* will be presented to represent the spatial coherency of seismic ground motions for soil-structure interaction applications.

Concerning the empirical models of Abrahamson [EPRI, 2007a] (equation 1.24), the formulations were constructed empirically without any physical considerations except the fact that the coherency tends to 1 at zero frequency and zero distance and tends to zero at large separation distances and high frequencies. Although Abrahamson constructed two different models for soil sites and rock sites, his models don't have a direct relation to the soil properties, and this might be somewhat unsatisfactory to apply these coherency models to arbitrary sites in soil-structure interaction applications as they may provide unsatisfactory estimations of the actual site-specific coherency values.

Alternatively, the model of [Luco and Wong, 1986] (equation 1.25) contains a soil property which is the shear wave velocity  $V_s$ . The latter parameter is generally considered in the literature to be  $V_{s30}$  which is the average of the shear wave velocity for the top 30 m of soil. But this parameter will be discussed in the future studies to conclude whether the average of the shear wave velocity for the top 30 m  $V_{s30}$  is a correct velocity to be used in this coherency model, or one should take the average of this shear wave velocity over the deeper layer of soil. About the parameter  $\alpha$  of this coherency model, although originally, this parameter is a function of other physical and statistical parameters ( $\ell_c$  correlation length of random medium,  $\xi$  coefficient of variation of elastic properties in the random medium, and  $Z$  the distance along which seismic waves propagate in random heterogeneous medium), until now, there is not any study can confirm exactly about the uses of those parameters. In the literature, this parameter  $\alpha$  is generally replaced by a constant. But due to the studies presented in the literature in these recent years, the constant value of  $\alpha$  cannot fit this coherency model to some *insitu* coherencies. Further analyses should be done in order to conclude on the value of this parameter. The comparison between the spatial coherencies estimated from Argostili database with this coherency model, which will be presented in Chapter 2 will give more comprehension about this model and its parameters.

Finally, a theoretical analysis on the determination of coherency function from seismic wave propagation in random heterogeneous media, existing in literature, is reviewed and summarised to give more comprehension on the physical and statistical aspects of coherency function. Those theoretical consideration are summarised from the analyses of [Sato et al., 2012], and the parametrical coherency model deduced from those analyses are called "model of [Sato et al., 2012]" in this manuscript. With this model, we can observe the existences of several physical and statistical properties of the random heterogeneous media, which can be verified directly by using numerical case-studies. It is remarked that the coherency model of [Luco and Wong, 1986] is simply the special case of the analysed model of [Sato et al., 2012] when  $d \ll \ell_c$ . Since this condition is not always true for the real applications, we keep the functional form of model of [Sato et al., 2012] and we will use numerical case-studies to understand more about the influence of each parameters in the model, and to check for the possibility of validating the model.



## Chapter 2

# Spatial Coherency of Seismic Ground Motions estimated from Argostoli Database

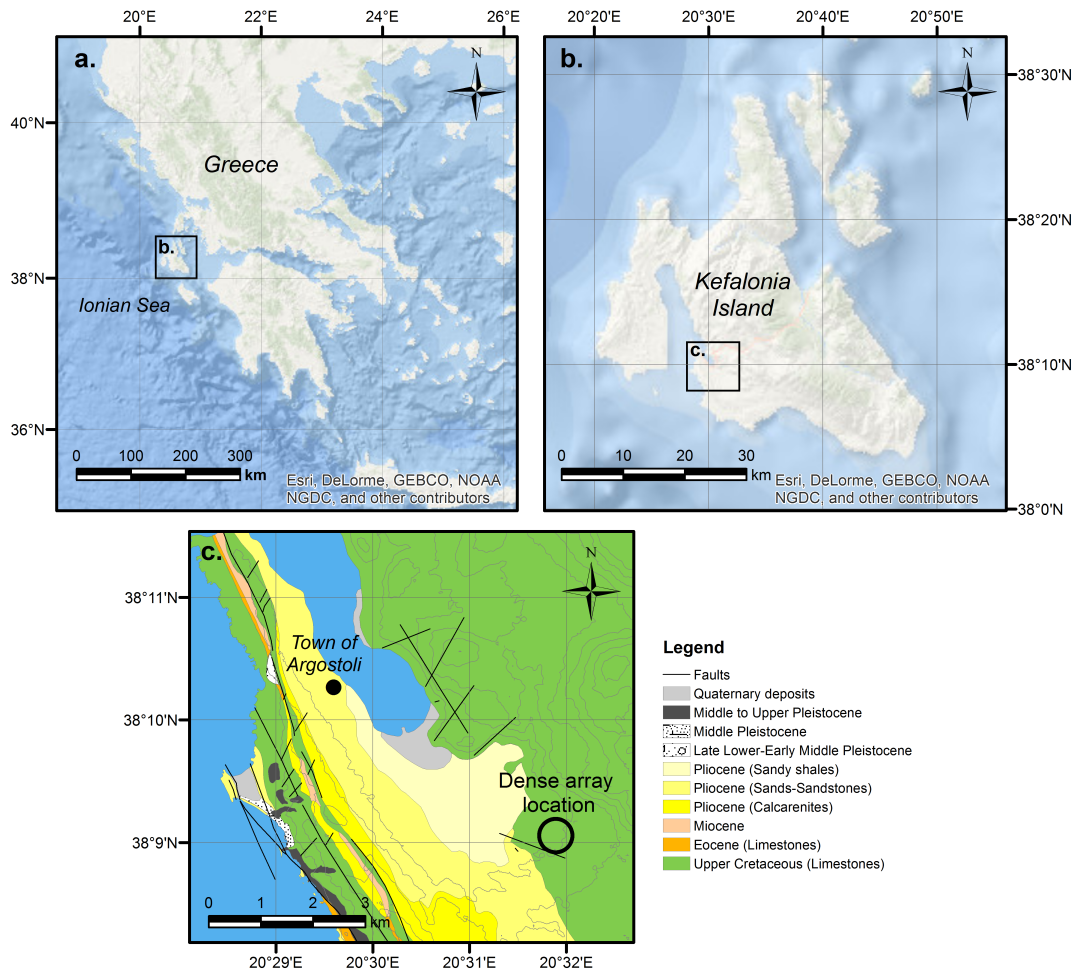
*“Data do not give up their secrets easily. They must be tortured to confess.”*

JEFF HOPPER AND BELL LABS

### 2.1 Introduction

This chapter presents the statistical analyses of the spatial coherency of seismic ground motions from a rock site dense array implemented during the Kefalonia 2014 aftershock sequence. To be noted that in the framework of SINAPS@ project, we participated in the seismic signal recording campaign at Kefalonia island after two important earthquakes in the beginning of 2014 (January 26th and February 3rd). We also participated in the preparation of the signal database which are used in our analyses on the spatial coherencies of seismic ground signals and presented in what follows.

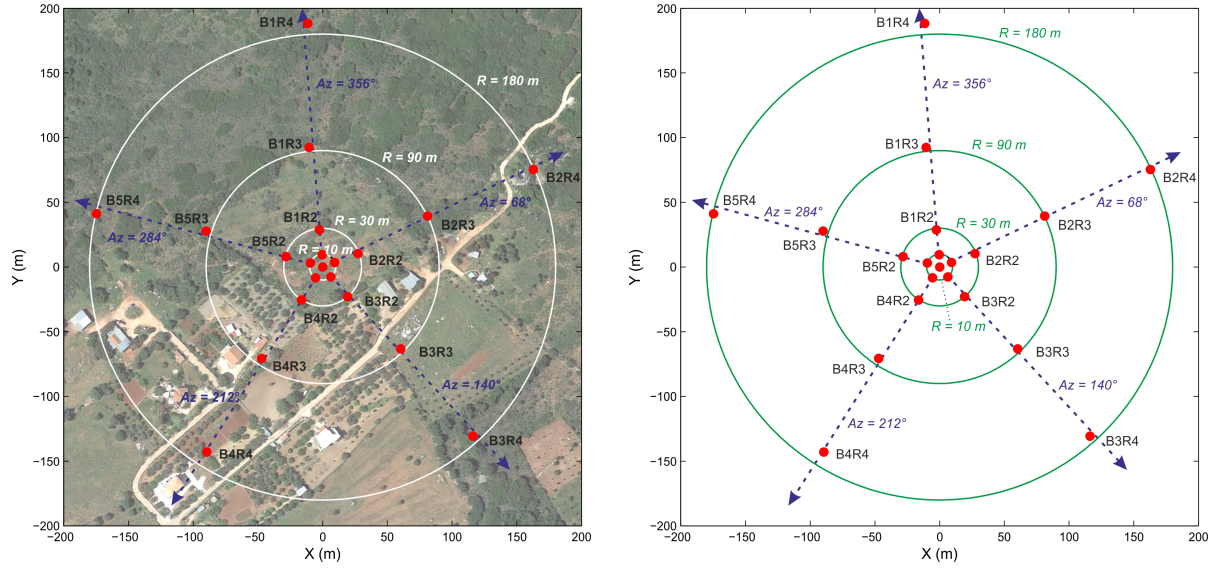
The chapter starts with the presentations of Kefalonia earthquakes in 2014 and Argostoli rock site dense array. After that, the spatial coherencies estimated from 93 different earthquake events and from different station pairs are presented to show the dispersions of coherencies. The presentation is followed by the comparison between the coherencies estimated from horizontal component and vertical component. The coherencies estimated from coda parts of earthquake ground signals are also compared to the coherencies estimated from strong motion windows of signals. After that comparison, the analyses are devoted to the influence of strong motion durations and earthquake event numbers on the average of the plane-wave coherency. Finally, the estimated coherencies are compared to the existing coherency models to discuss about their limitations, and the possibility of modifying some parameters of those coherency models to fit with the *insitu* coherency are also discussed.



**Figure 2.1** – Location of studied site. a) Location of Kefalonia island with respect to Greece. b) Location of the Argostoli area with respect to Kefalonia island. c) Location of the Argostoli rock site dense array on the local geological map [Cushing et al., 2016]

## 2.2 Argostoli Earthquakes in 2014 and Argostoli Dense Array

The island of Kefalonia, located in Ionian Sea, Greece, (Figure 2.1) is one of the most seismically active regions in the Euro-Mediterranean area, especially due to the proximity of the Kefalonia Transform Fault that plays a major role for the transition zone between the African subducting plate and the continental Apulian plate. Numerous earthquakes shook the area in the past (e.g. the major 1953, Mw 7.2 earthquake and induced an uplift up to meter of a great part of the Kefalonia island). Due to this high seismicity, as well as the presence of sedimentary basin, the area was chosen as a test site within the framework of the French Research Agency (ANR) PIA Sinaps@ project ([www.institut-seism.fr/projets/sinaps/](http://www.institut-seism.fr/projets/sinaps/)) [BergeThierry et al., 2016] in order to validate 3D non-linear computer codes through the installation of a permanent accelerometric vertical network within the basin (Koutavos area). The area benefits from a first geophysical survey conducted in September 2013 that allowed identifying and characterizing rock outcropping area, among other objectives.

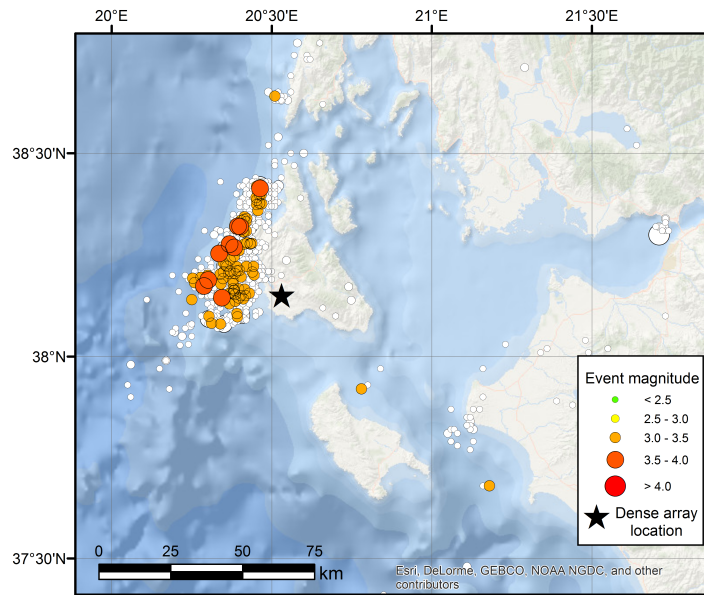


**Figure 2.2** – Argostoli rock site dense array geometry mapped on aerial photography (source : Google Earth). Each red dot represents one sensor

Then, the Kefalonia island was shaken by two significant earthquakes on January 26th, 2014 at 13:55:43 UTC ( $M_w=6.1$ ) and on February 3rd, 2014 at 03:08:45 UTC ( $M_w=6.0$ ) [Valkanotis et al., 2014], [Theodoulidis et al., 2016]. This sequence motivated the organisation of a post-seismic survey [Hollender et al., 2015a] that aimed to deploy on the site: (1) temporary accelerometer network (waiting the installation of the Sinaps@ project permanent accelerometric network), (2) a rotation sensor, and (3) a dense array located on the previously identified rock site (to be complementary to other previous datasets from soil sites). The analyses realized and presented in this Ph.D thesis are focused on the analysis of this last instrumentation.

The Argostoli rock-site dense array consists of 21 sensors, distributed 5 by 5 on 4 circles with respective radius of 10, 30, 90 and 180 m, plus a central station (Figure 2.2). On the left, the array is presented as in aerial photo to show how the stations were implemented on the observation site, and on the right, it is simply the same array without aerial photo to present more clearly about the geometry of array, as well as the different station separations. This geometry leads to a star with 5 branches (corresponding to 5 equally spaced azimuths) with 4 stations on each branch. Each station is identified by the ID of the branch and the ID of the radius (e.g. station B2R3 means "branch number 2 and radius number 3, B0R0 being the central station). All sensors were Guralp CMG6TD broadband seismometers with built-in digitizers that present a flat frequency response between 0.03 and 100 Hz. A 200 Hz sampling frequency is used for our measurements. This choice implies a good instrumental sensitivity that allows getting a good signal-to-noise ratio for low frequencies, but also induced saturation for strongest motions.

The stations were in operation and recorded in continuous mode from February 6th, 2014 to March 10th, 2014. By the use of seismicity catalogues, we extracted up approximately 2000 well recorded events from this continuous databank, with local magnitudes between 1 and 5. Figure 2.3 presents all well recorded events during one month from February 6th, 2014 to March 10th, 2014. From this whole database, 93 events were selected in order to process the statistical analysis on the estimation of the spatial coherency of earthquake ground motions. These 93 events are characterized by local magnitudes between 2.7 and 3.6 according to the NOA (National Observatory of Athens) catalogue. They present focal distances between 9 and 77 km as well as PGV (Peak Ground Velocity) from 0.05 to 2.4 mm/s. Figure 2.4 presents the map of the selected events. The distributions of the used events in terms of focal distance, magnitude and PGV are presented in



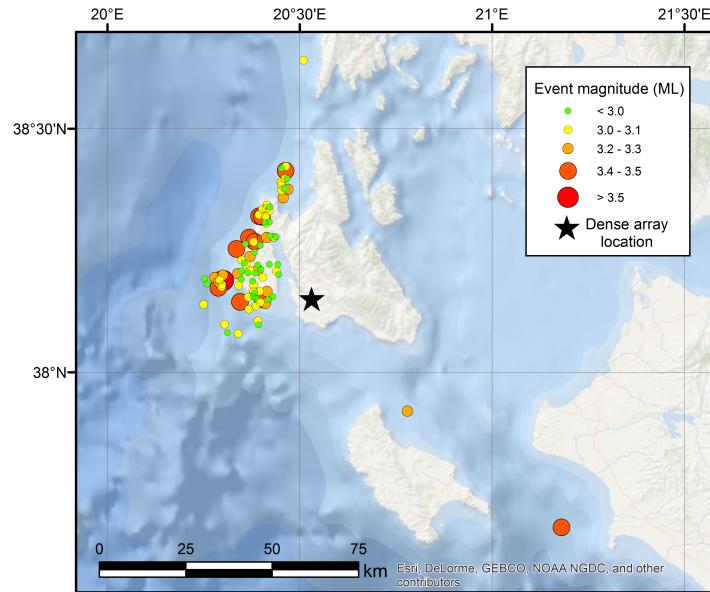
**Figure 2.3** – Epicenters of aftershocks recorded by the Argostoli rock-site dense array (approximately 2000 well recorded events from February 6th, 2014 to March 10th, 2014). Different colors indicate magnitude values: the white color circles present the earthquake events with magnitudes smaller than 2. The black star represents the location of array.

Figure 2.5.

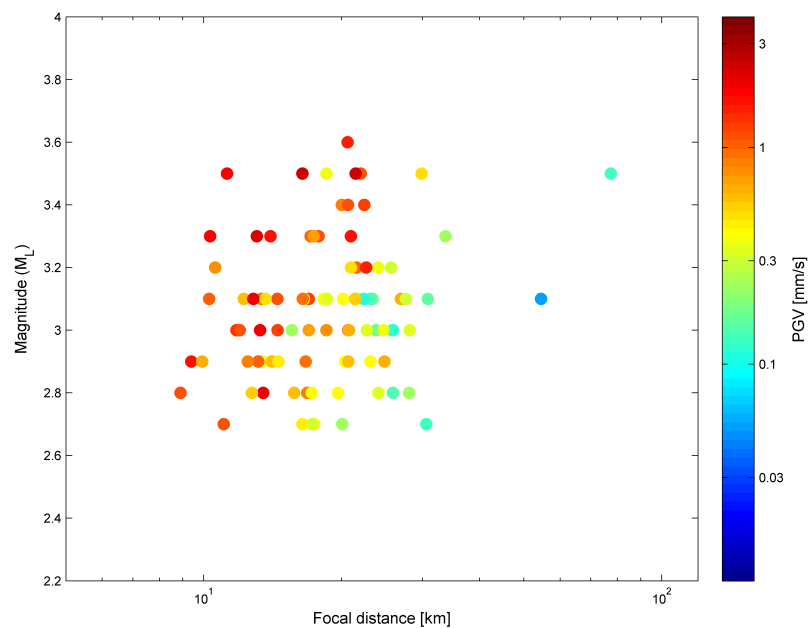
The smaller earthquakes were not used in these studies since that was desired to investigate the coherencies with motions as high as possible. Conversely, higher magnitudes induced saturation of sensors and were then not usable for coherency analysis. An example of 5 velocigrams along the branch B1 (Central station, B1R1, B1R2, B1R3, B1R4) for all the three directions for an earthquake event (event 2014-02-06-185141,  $M_w=3.0$ , epicentral distance = 17.4 km) is presented in Figure 2.6.

As described previously, the Argostoli rock-site dense array area took benefit from a previous geophysical survey that allowed determining velocity profiles beneath the site. This geophysical survey consisted in the implementation of methods based on the analysis of surface-wave dispersion [Foti et al., 2014]. The circular passive arrays of seismometers are deployed successively in order to record ambient vibration. These circles had radius from 5 m to 700 m. Using the Spatial Autocorrelation (SPAC) method, the analysis of these data allowed determining the dispersion curve of the fundamental mode of Rayleigh waves, that was then converted in velocity profile by inversion. Since the inversion process does not lead to unique solution, a set of possible velocity profile is showed in Figure 2.7. These profiles lead to  $V_{s30}$  value (shear-wave velocity for the top 30 m) of about  $830 \pm 35$  m/s.



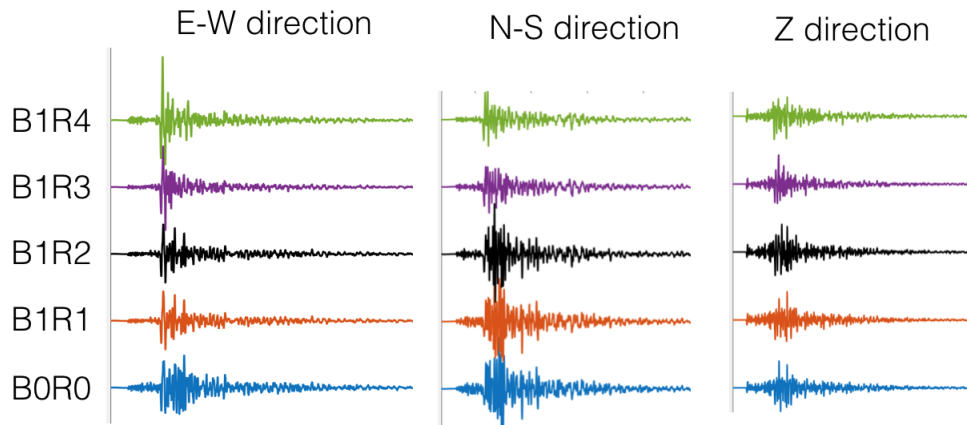


**Figure 2.4** – Epicenters of aftershocks recorded by the Argostoli rock-site dense array and used in the present study (selection of 93 earthquakes out of approximately 2000 well recorded events from February 6th, 2014 to March 10th, 2014). Colors indicate magnitude values. The black star represents the location of array.

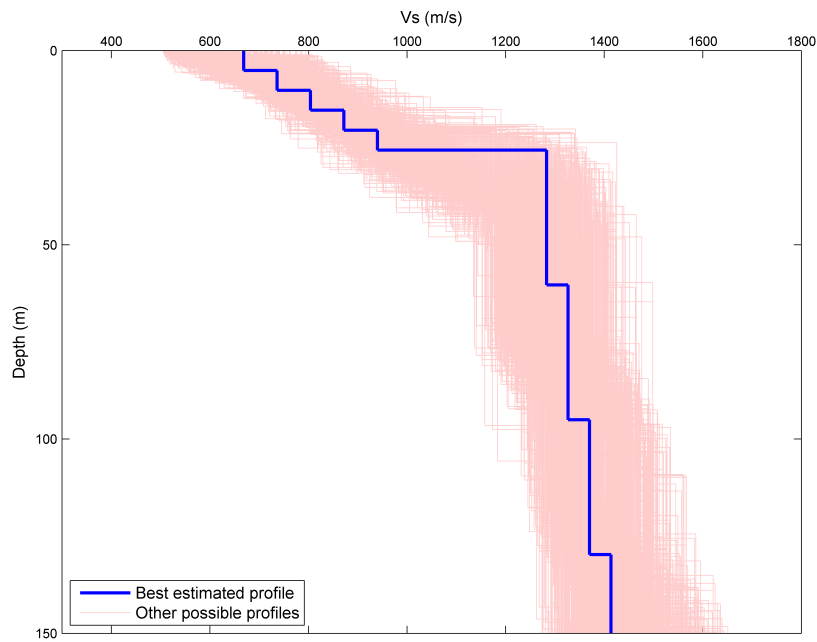


**Figure 2.5** – Distribution of selected earthquake in terms of epicentral distances (X-axis), magnitudes (Y-axis) and Peak Ground Velocity (color scale).





**Figure 2.6** – Velocities captured at Argostoli dense array (event 2014-02-06-185141,  $M_w=3.0$ , Epicentral distance = 17.4 Km)



**Figure 2.7** – Shear wave velocity profiles estimated beneath the Argostoli rock site dense array. These profiles are computed using surface-wave based methods. In blue: "best estimated" profile, in red: other possible profiles.)

## 2.3 Spatial coherency estimated from Argostoli database

The statistical analyses of spatial coherencies of seismic ground motions estimated from Argostoli database are presented in what follows. First of all, the spatial coherency estimated from strong motion windows is presented. For each separation of station pair, the dispersions of all coherencies estimated from 93 earthquake events are presented to show how the coherency varies for different earthquake events. After that, we aim to investigate the coherency estimated from coda part of earthquake ground motion signals. The dependencies of coherency with event number and strong motion duration are also discussed.

### 2.3.1 Determination of plane-wave propagation directions

As described in the section 1.5, to evaluate the plane-wave coherency, one needs to search for the direction of plane-wave propagation and best plane wave velocity for each earthquake event. Figure 2.8 presents the distribution of the angle  $\phi$  for the events used for estimating coherencies. It is reminded that the angle  $\phi$  is evaluated by letting the coefficient of correlation  $\rho$  be equal to zero (equation 1.12). Note that the found angles correspond very well to the azimuths of earthquake events presented in Figure 2.4 in which most of the earthquake sources are situated in the direction north-west of the station array. Some small differences between the azimuth and the angle  $\phi$  might be explained by the fact of assuming the vertical component as the 3rd principle component because it is possible that there are still some correlation between the horizontal components and vertical component. But the differences are not significant and can be neglected.

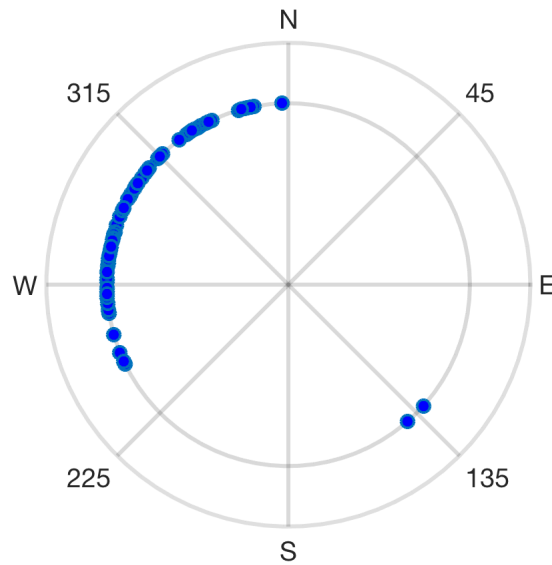
For each event, the signals are rotated to the direction of plane-wave propagation, and the "best-fit" plane wave velocity can be evaluated by aligning the stations to the direction of plane-wave propagation. As discussed by Abrahamson in [Abrahamson et al., 1991], it is possible that each event or each pair of stations can give different value of "best fit" plane wave velocity, but for the analyses of Argostoli database, it is observed that the "best fit" plane wave velocity is approximatively constant and gives the slowness to be around 0.175 s/km. In his analyses of Lotung site in Taiwan [Abrahamson et al., 1991], and of Pinyon Flat site in USA [EPRI, 2007a], Abrahamson also observed the constant apparent velocity of "best-fit" plane wave propagation.

### 2.3.2 Spatial coherency estimated from strong motion windows

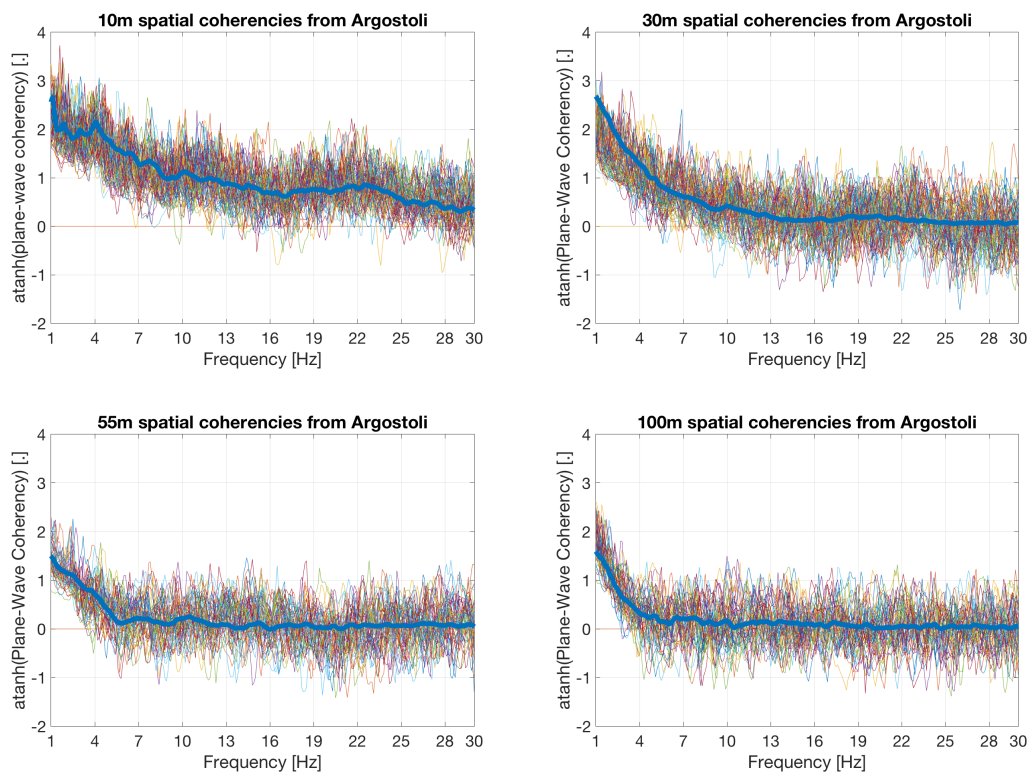
With the 93 earthquake events used for estimating coherencies, the strong motion windows which can be determined from 10%IA to 90%IA (equation 1.8) can vary from 1s to 10s depending on epicentral distance and magnitude of events. The length of strong motion windows increases in parallel with epicentral distances but for most of the analysed events, the strong motion durations are around 5s since many of the analysed events have almost the same epicentral distances (see Figure 2.5).

The plane-wave coherencies estimated from 93 different earthquake events are presented in Figure 2.9. The station separations of 10 m, 30 m, 55 m and 100 m for horizontal component are shown. The average of all coherencies estimated for the same station separations are also presented (the blue bold line). As discussed in the section 1.5.2, the plane-wave coherencies of all events are presented in  $(\tanh^{-1})$  transforms since its distribution is considered to be a normal distribution.

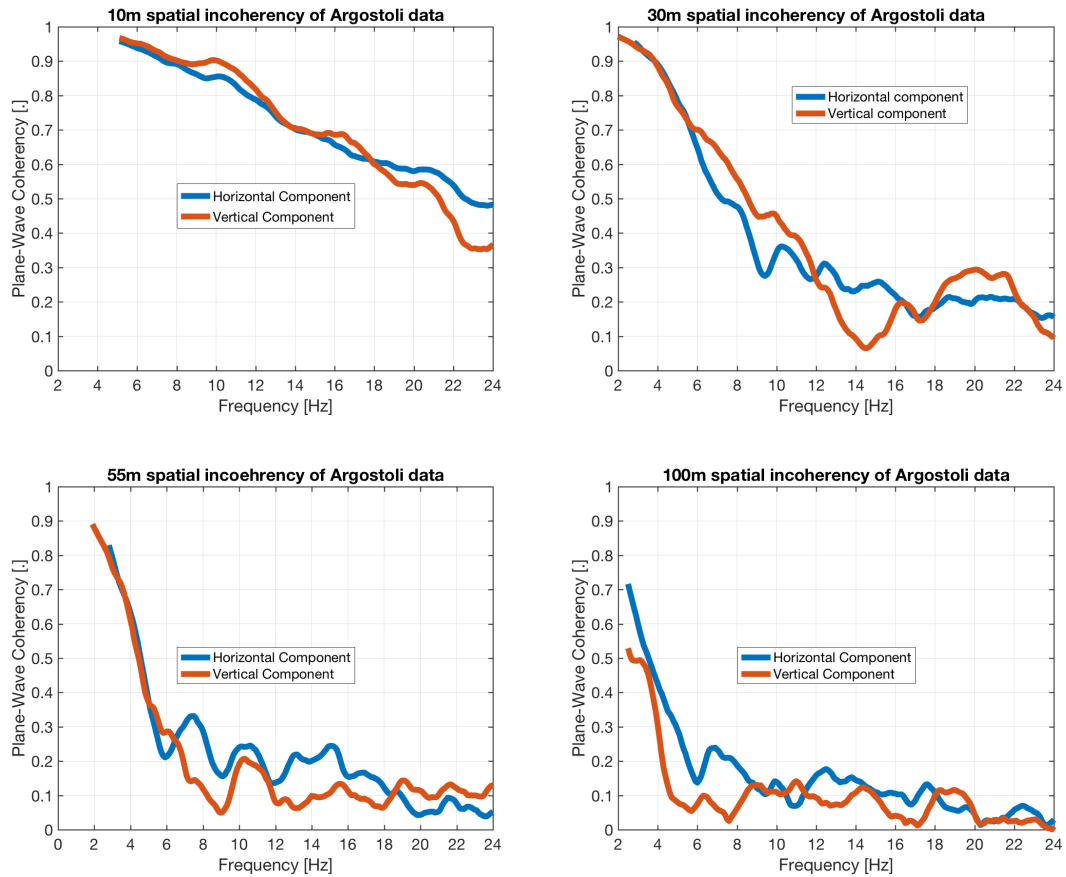
The plane wave coherencies for vertical components are also estimated with Argostoli database.



**Figure 2.8** – Distribution of angle  $\phi$  representing the directions of plane-wave propagation. The center of circle corresponds to the station array



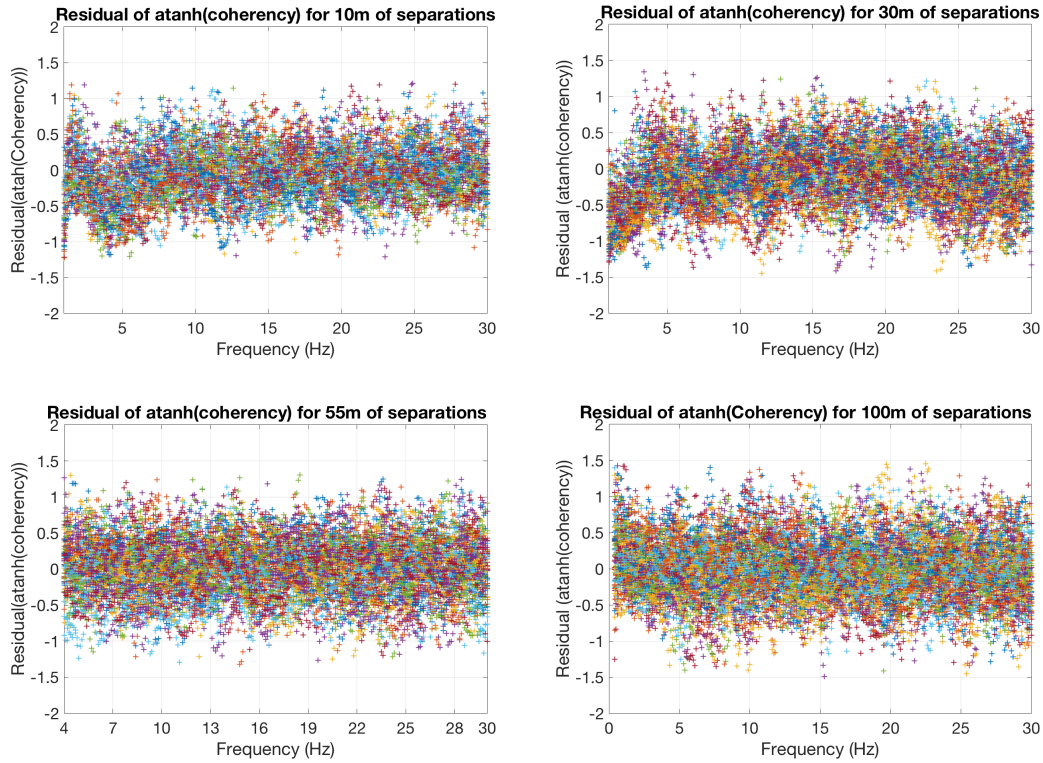
**Figure 2.9** – Dispersions of horizontal plane-wave coherencies estimated from 93 events of Argostoli database for 10m, 30m, 55m and 100m of separations. The blue bold line represents the average of plane-wave coherencies



**Figure 2.10** – *Spatial Incoherency estimated from Argostoli database for 10m, 30m, 55m and 100m of separations*

The comparisons between the averages of plane-wave coherencies estimated from horizontal component and those estimated from vertical component are shown in Figure 2.10. Once again, the station separations of 10 m, 30 m, 55 m and 100 m are presented. For each separation distance, the difference between two plane-wave coherencies estimated from horizontal component and vertical component of signals can be remarked. However, that difference does not seem significant compared to the dispersion of all coherencies estimated for same station separations presented in Figure 2.9. Hence, for Argostoli database, there is not an exact conclusion about whether the coherencies of horizontal components are bigger or smaller than those of vertical components. This might be explained by the fact that the Argostoli dense array is situated on a rock site where the soil can be considered to have isotropic properties.

The residuals of plane-wave coherencies estimated from 93 different earthquake events for horizontal component are also evaluated and presented in Figure 2.11. The residuals presented here are simply the difference between the plane-wave coherencies of different events and the average of plane-wave coherencies presented in Figure 2.10. With the transform  $\tanh^{-1}(\text{Coherency})$ , one can remark exactly that the variation of coherencies from different events remains approximatively constant with frequencies. From 10m to 100m of station separations, the difference in terms of residual of coherencies is not significant although the plane-wave coherency for 100m distance is very small compared to that of 10m of separations.

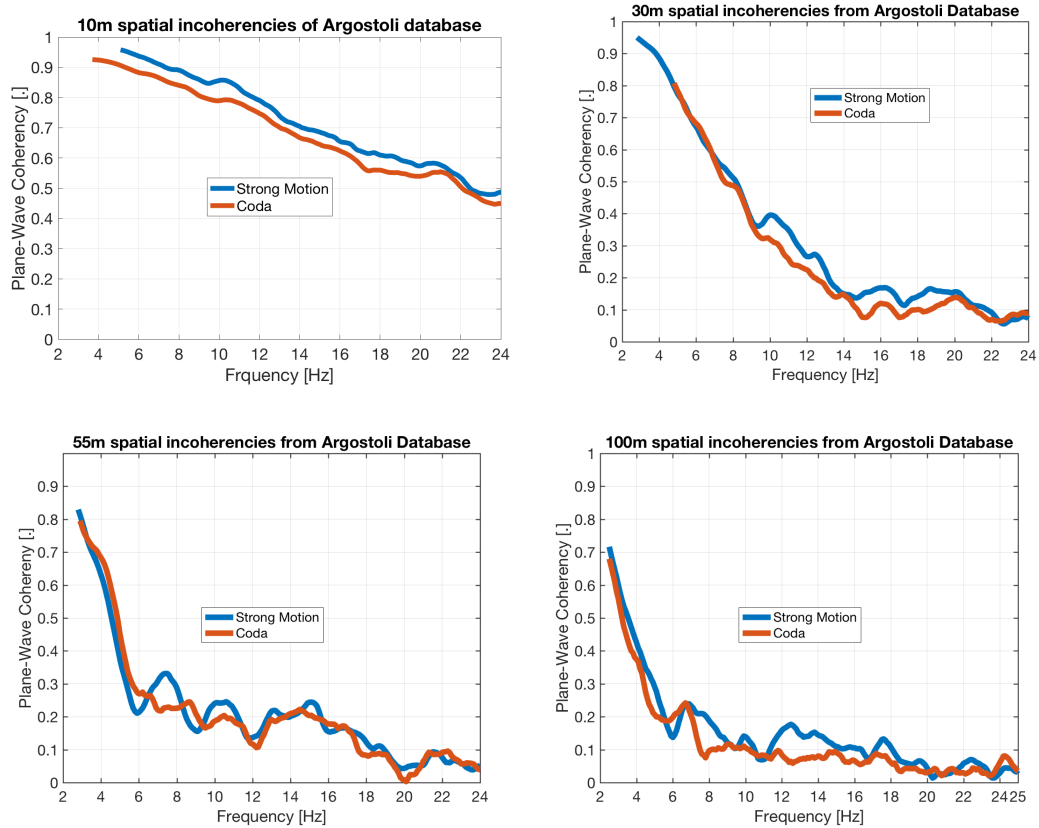


**Figure 2.11** – Residuals of  $\tanh^{-1}(\text{coherencies})$  of horizontal component from 93 earthquake events for 10m, 30m, 55m and 100m of separations

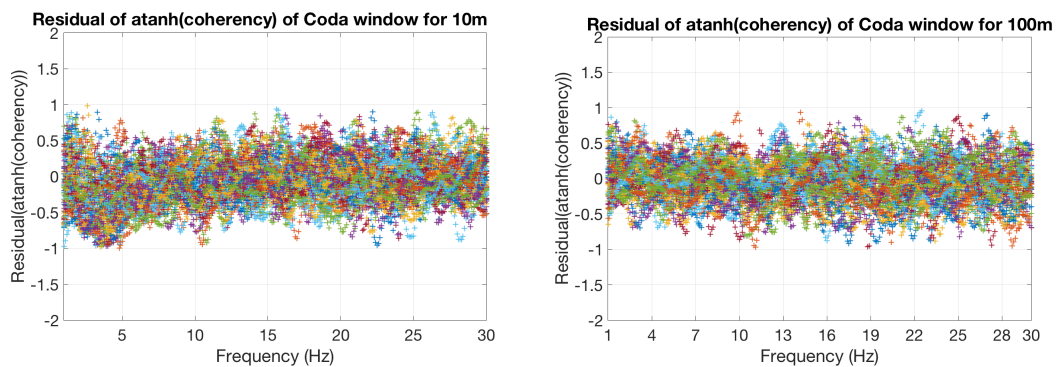
### 2.3.3 Spatial coherency estimated from coda of seismic signals

Another interesting point about spatial coherencies of earthquake ground motions is to investigate on the coda part of the ground motion signals. The coda part of signals refers to the last part of signals where the amplitude of the motions is significantly small compared to the strong motion window. First of all, the window of  $AI \geq 0.9$  (equation 1.8) is taken to represent the coda window of the signal (the green color part of Figure 1.4). The point of  $AI = 0.9$  is taken to be the beginning of coda windows since it is considered to be the end of strong motion window as described in section 2.3.2. But for some cases, it seems that at  $AI = 0.9$ , the coda window still consists of some high amplitudes of signals which are not consistent to the definition of coda window. Hence, for our analyses, to avoid the influence of strong motions of signal on coda window, the windows of  $AI \geq 0.97$  are considered to be coda window of signals for Argostoli database. With that definition, the length of coda windows varies from 3s to 10s. To estimate the plane wave coherency, the directions and velocities of plane wave propagation are considered to be the same as the case of strong motion window, and the spectral densities are also smoothed with an 11-Hamming window function as the case of strong motion windows.

Figure 2.12 presents the comparison of those two coherencies. It is shown that the difference is not really significant here and it can be considered to be in the range of standard deviation of coherencies estimated from strong motion windows (see Figure 2.9). One can also analyse the variability of coherencies estimated from coda windows by investigating the residual of  $\tanh^1(\text{coherency}(\text{coda}))$  (Figure 2.13). The first point to be concluded from that result by comparing to Figure 2.11 is that the variability of coherencies estimated from coda windows seems to be smaller than that estimated from strong motion windows.

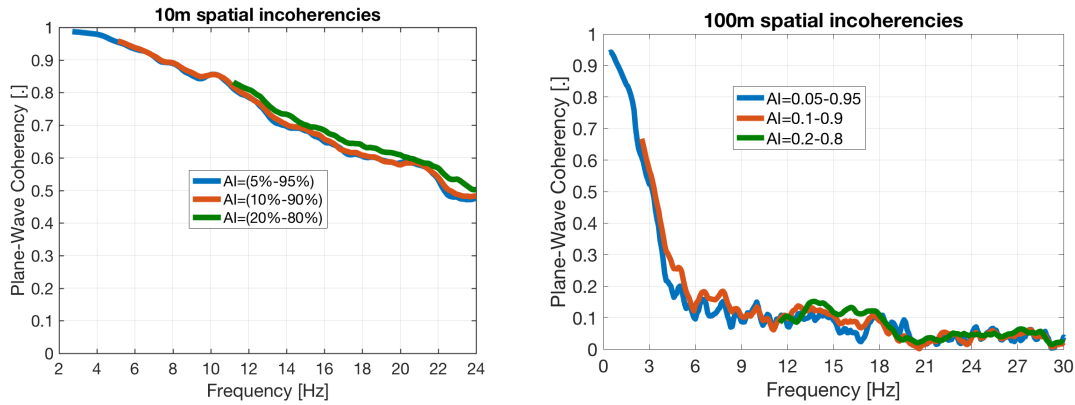


**Figure 2.12** – Comparison between coherencies estimated from strong motion windows and from coda parts of signals for 10m, 30m, 55m and 100m of separations



**Figure 2.13** – Residual of  $\tanh^{-1}(\text{coherencies})$  estimated from coda window of ground motion signals for 10m and 100m of station separations





**Figure 2.14** – Comparison between coherencies estimated from different strong motion durations of signals for 10m and 100m of separations

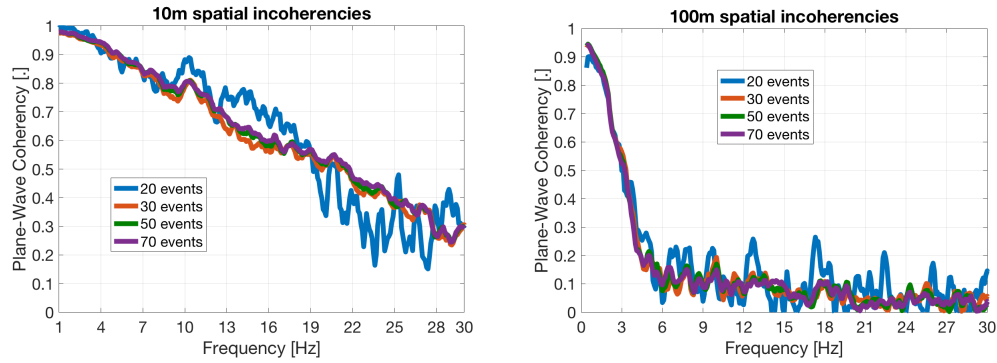
These results show that with a sufficient number of earthquake events, the coda windows and the strong motion windows of signals give the same spatial coherencies of earthquake ground motions. It is interesting in terms of engineering applications since it suggests that the plane-wave coherencies of earthquake signals on rock sites can be identified from the coda parts of signals which can be more or less estimated from some feasible experiments on a given site. This remarkable conclusion should be investigated more precisely for other earthquake sites.

### 2.3.4 Influence of the strong motion durations on spatial coherency

As described above, the coherencies of earthquake ground motions are estimated from strong motion windows of earthquake signals defined from Arias Intensity (equation 1.8). Another analysis which should be done is to investigate the influence of that duration on the spatial coherencies. To do so, the comparison between the coherencies estimated from different durations of strong motions is realized and presented in Figure 2.14. In that figure, the station separations of 10m and 100m are presented since they are respectively the smallest and the biggest separation distances which are analysed in our studies. Three different durations are presented : the window of  $AI = 0.05 - 0.95$ , the window of  $AI = 0.1 - 0.9$  and the window of  $AI = 0.2 - 0.8$ . One can remark that the strong motion duration does not strongly influence the coherencies. This result could be expected since no difference was found between the coherencies estimated from coda parts and strong motion windows. Nevertheless, the fact of taking a short strong motion duration can lead to loss the resolutions in frequency. It can be concluded from this analysis that the strong motion durations can be defined from  $AI = 0.05$  to  $AI = 0.95$  (or from  $AI = 0.05$  to  $AI = 0.9$ ) to get a high resolution in frequencies.

### 2.3.5 Influence of the number of earthquake events on spatial coherency

Since the coherencies of seismic ground motions presented above are obtained by statistical analyses from 93 different earthquake events, it is necessary to study the convergence of coherencies. Simply it aims to understand about the sufficient number of earthquake events which can give a good estimation of coherencies. This analysis is shown in Figure 2.15. The averages of plane-wave coherencies estimated from 20 events, 30 events, 50 events and 70 events of earthquakes are presented. The events are randomly selected for each category from the available 93 events. Once



**Figure 2.15** – Comparison between coherencies estimated from different numbers of earthquake events for 10m and 100m of separations

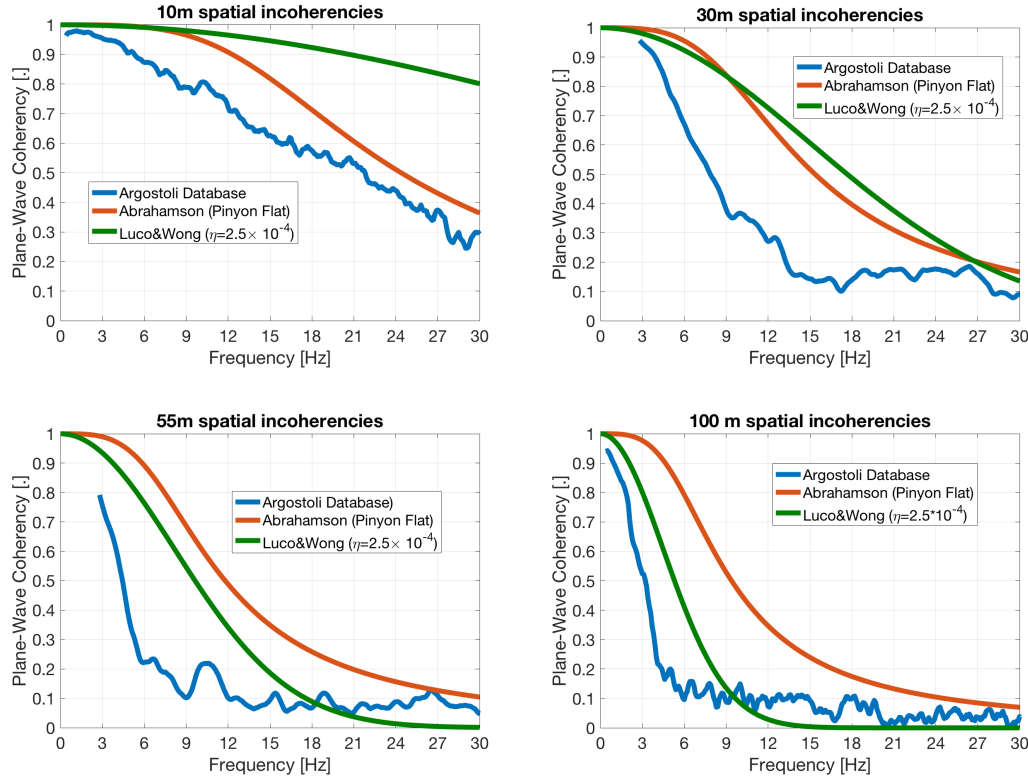
again, the station separations of 10 m and 100 m are selected to illustrate the results. It is shown that for 20 earthquake events, the average of plane-wave coherencies does not converge properly yet, while for 30 events, the average of plane-wave coherencies converges and has almost the same value to the cases of 50 events and 70 events. Consequently, it is concluded that only about 30 earthquake events can already give a good estimation of coherencies. To be noted also that for the same station separations, with the dense array presented in Figure 2.2, we have about 4 or 5 pairs of stations. This means that for 30 earthquake events, we have around 120 realisations of coherencies. This convergence properties might be applicable only in the case of plane-wave coherencies since all the signals are rotated to the direction of plane-wave propagation. This convergence properties should also be examined for other earthquake dense array because it is possible that the convergence properties change from one site to another site.

## 2.4 Comparison between insitu spatial coherency and existing coherency models

In this section, the plane-wave coherencies estimated from Argostoli database are compared with existing coherency models reviewed in the section 1.5.3. The coherency models which will be compared here are those of Abrahamson (equation 1.24), of Luco&Wong (equation 1.27) and the one of [Sato et al., 2012] (equation 1.59). Two comparisons are presented here. For the first one, the parameters of Abrahamson model are not changed and are the same to those given by Abrahamson [EPRI, 2007a] for Pinyon Flat rock dense array. The value each parameter is listed in Table 1.4. For the model of Luco&Wong, the parameter  $\eta$  were defined to be  $2.5 \times 10^{-4} \text{ s/m}$  since this value is recommended by Luco&Wong [Luco and Wong, 1986]. The model of [Sato et al., 2012] is not used for this first comparison because no one in the literature used this model for their studies yet and hence, we don't have any referent values of the literature to compare with the *insitu* coherencies of Argostoli database. Figure 2.16 illustrates that comparison. It is shown clearly that none of the two models (Abrahamson and Luco&Wong) can represent the coherencies estimated from Argostoli database if their parameters are not changed. The fact that coherencies estimated from Argostoli database are significantly smaller than coherencies of Abrahamson model (rock site) might be explained by the fact the shear-wave velocity of Argostoli site ( $V_{s30} \approx 830 \text{ m/s}$ ) is smaller than that of Pinyon Plate site ( $V_{s30} \approx 1030 \text{ m/s}$ ) which is the site used by Abrahamson for establishing his empirical model.

For the second comparison, the parameters of Abrahamson model are modified to fit the value





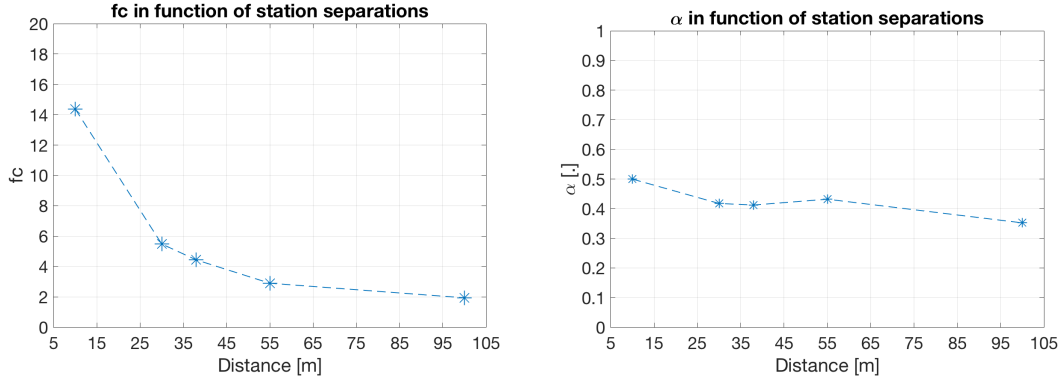
**Figure 2.16** – Comparison between coherencies estimated from Argostoli database and existing coherency models for 10m, 30m, 55m and 100m of separations

of coherencies estimated from Argostoli database. The parameter  $\alpha$  of the model of Luco&Wong is also estimated to fit the model with *insitu* coherencies. By using non-linear regression curve fitting, it is found that only the parameters  $f_c$  and  $n_1$  of Abrahamson model are needed to be changed to fit the model with Argostoli coherency. Other parameters stay the same to the case of Pinyon Flat database. The parameters of Abrahamson model which are fit to the Argostoli coherencies are listed in Table 2.1. The different values of  $f_c$  for different station separations are presented in Figure 2.17 (left).

For the coherency model of Luco&Wong (equation 1.25), as what is realized in [Konakli et al., 2013], it is found that the value of  $\alpha$  is not constant and can vary with respect to distance of station pair. The values of  $\alpha$  for different station separations are presented in Figure 2.17 (right). The shear-wave velocity used in this comparison is the shear-wave velocity of the top 30m which is about 830 m/s.

Parameters	Values fitted for Argostoli dense array
$a_1$	1.0
$a_2$	40
$a_3$	0.4
$f_c$	$23.1797 - 5.1567 \cdot \ln(d_{ij} + 1) + 2.4428 \cdot (\ln(d_{ij} + 1) - 3.6)^2$
$n_1$	$2.8634 + 0.0579 \cdot \ln(d_{ij} + 1) - 0.2226 \cdot (\ln(d_{ij} + 1) - 3.6)^2$
$n_2$	16.4

**Table 2.1** – Parameters of Abrahamson model for Argostoli dense array



**Figure 2.17** – The values of parameters used for fitting existing coherency models with Argostoli coherencies. Left:  $fc$  as a function of station separations (for Abrahamson model). Right:  $\alpha$  as a function of station separations (for the Model of Luco&Wong).

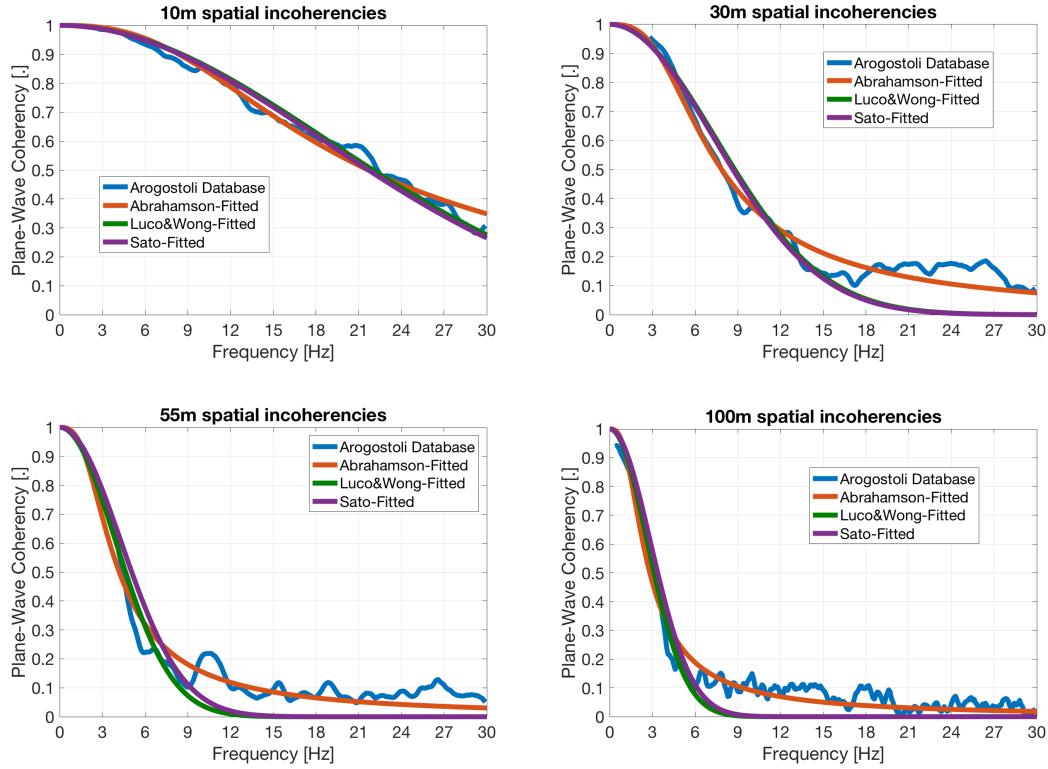
$d$	10	30	55	100
$Z$	115	120	230	500

**Table 2.2** – Fitted values of  $Z$  of Sato model for different station separations

In this second comparison, the model of [Sato et al., 2012] (equation 1.59) is also fitted to compared to the *insitu* coherencies of Argostoli database. The parameters of the model are  $\xi = COV, \ell_c, Z$  and  $V_o$ . For the velocity of wave propagation, like in the case of model of [Luco and Wong, 1986], it is considered to be the shear-wave velocity of the first 30m of the medium  $V_{s30} = 830m/s$ . About the two statistical parameters, based on literature, for this comparison, we use  $\xi = 20\%$  and  $\ell_c = 30m$ . Without any information about the depth of random heterogeneous media, for simplify our analyses, we chose to vary the parameter ( $Z$ ) to fit the model to the *insitu* coherencies. The fitted values of  $Z$  for different station separations is presented in Table 2.2. To be noted that, physically, the value of  $Z$ , which is the depth of the heterogeneous medium is a constant. The details about choosing to fit its value will be given in the Chapter 3.

Remark that, physically, the depth of the random heterogeneous media should not vary since it should be constant for all station separations. But the analyses about the influence of this parameter on the spatial variability of seismic ground motions by using numerical modelling, which will be presented in Chapter 3 of this manuscript will explain more about our choice here to choose  $Z$  as a variable depending on the station separations.

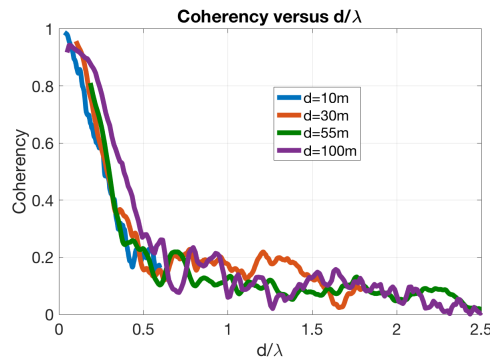
The fitted coherency models and Argostoli coherencies are presented in Figure 2.18. After these comparisons, it can be concluded that the functional form of Abrahamson model seems to be well adapted to the *insitu* coherencies, especially for high frequencies. Accurately, at high frequencies, the *insitu* coherencies do not approach quickly to zero which is adapted to Abrahamson model. It can be said as what should be observed too since the Abrahamson model is empirically constructed by real earthquake databases. For the model of Luco&Wong and that of Sato, it seems that the models tend to zero faster than experimental coherencies and the both models are almost the same after being fitted to *insitu* coherencies. Talking about the value of parameter  $\alpha$  of Luco&Wong model, by fitting exactly the *insitu* coherencies to the model,  $\alpha$  seems to vary significantly as seen in Figure 2.17-right. [Konakli et al., 2013] also found similar conclusions for the analysis of 2004 Parkfield earthquakes. About the parameter  $Z$  of the mode of [Sato et al., 2012], it is also seen that the value varies strongly depending on station separation distances.



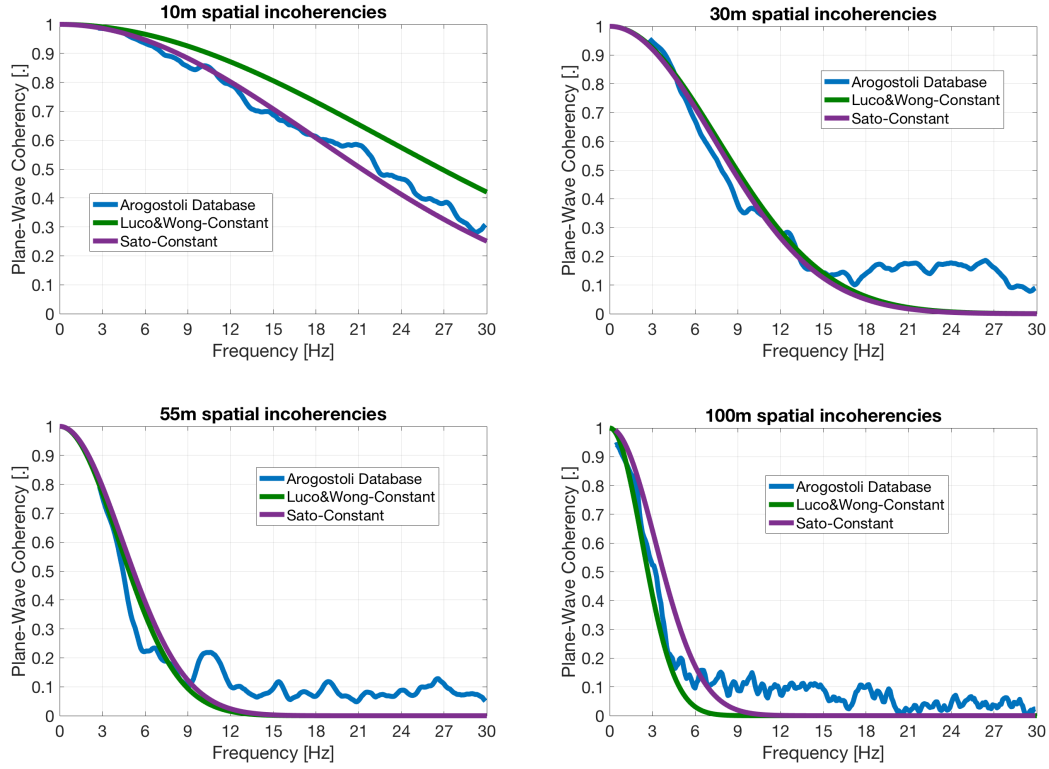
**Figure 2.18** – Comparison between coherencies estimated from Argostoli database and modified (fitted) coherency models for 10m, 30m, 55m and 100m of separations

If we investigate the coherencies as a function of the ratio between the station separation ( $d$ ) and wavelength ( $\lambda$ ), an interesting result can be observed as presented in Figure 2.19. The wavelength presented here is simply a ratio between shear-wave velocity ( $V_{s30}$ ) and frequency of signals. For frequency varying from 0 Hz to 30 Hz, the value of  $(1/\lambda)$  can vary from 0 to  $0.036m^{-1}$ . For different station separations, it seems that all the coherencies are approximately the same. With this investigation, one can conclude that the functional form of the semi-empirical coherency model should be taken as a function of  $d/\lambda$ . The functional form of the model of Luco&Wong (equation 1.25) and of Sato (equation 1.59) are consistent with this conclusion, but we need to observe more precisely about the value of parameter  $\alpha$  and about the power of  $(d/\lambda)$ .

For the first investigation about the model of [Luco and Wong, 1986] and that of



**Figure 2.19** – Coherencies with respect to  $d/\lambda$



**Figure 2.20** – Comparison between coherencies estimated from Argostoli database and constant-parameter coherency models for 10m, 30m, 55m and 100m of separations

[Sato et al., 2012], we can observe the following cases. Since it is reported by [Luco and Wong, 1986] and [Luco and Mita, 1987] that parameter  $\alpha$  is a constant, with its variation presented in figure 2.17-right, we can test it by estimating the value of  $\alpha$  as the average of all its values for different distances. Hence, we add the last comparison where *insitu* coherencies of Argostoli database are compared to the model of [Luco and Wong, 1986] with  $\alpha$  constant ( $\alpha = 0.41$ ). For the model of [Sato et al., 2012], with what we can observe from Table 2.2, by choosing to fit the value of  $Z$ , it seems like  $Z$  does not vary when  $d \leq \ell_c$  ( $Z \sim 4 \times \ell_c$ ) and its value changes when  $d \geq \ell_c$  ( $Z \sim 4 \times d$ ). These considerations will be explained again in Chapter 3 to validate the coherency model of [Sato et al., 2012]. This last comparison is presented in Figure 2.20.

One can observe from the last comparison that, with  $\alpha$  constant ( $\alpha = 0.41$ ), the model of [Luco and Wong, 1986] can give almost a good prediction of coherency when the station separation distances are larger than 30m while the *insitu* coherencies are less than those given by the model when  $d \leq 30m$ . About the model of [Sato et al., 2012], when we consider that  $Z = 4 \times \ell_c$  for the case that  $d \leq \ell_c$  and that  $Z = 4 \times d$  for the case that  $d \geq \ell_c$ , the model seems to give a better prediction in coherencies.

## 2.5 Conclusions on spatial coherency of Argostoli earthquake database

The analysis of spatial coherencies of seismic ground motions estimated from Argostoli database for small separation distances is presented. In term of influence of signal components on coherencies, it is remarked that there is no significant difference between the coherencies estimated from

horizontal component and those from vertical component. Since the coherencies are estimated from strong motion windows of earthquake signals, two other analyses are realized. Firstly, the differences between coherencies estimated from strong motion windows and those from coda parts of signals are analysed. For Argostoli database, it is shown that both parts of signals give the same coherencies. The result of this analysis is interesting in term of engineering applications since the coherencies can be estimated by knowing only coda parts of signals. This conclusion needs to be observed on other *rock* sites. Secondly, the analyses of influence of strong motion durations are presented. Consequently, it is recommended that the coherencies should be estimated from strong motion windows which can be defined from Arias Intensity by considering the moments when  $AI = 0.5$  and  $AI = 0.95$  as respectively the beginning and the end of strong motion windows so that high resolutions in frequencies for coherency estimations are obtained. Regarding the convergence of coherency, the statistical analyses show that only about 30 earthquake events can already give a good estimation of spatial coherencies.

Finally, the most important analysis of these studies is to compare the coherencies estimated from Argostoli database with some existing coherency models in the literature. The coherency models which are used to be compared here are those of Abrahamson, Luco&Wong and the one introduced in [Sato et al., 2012]. It is shown that neither Abrahamson model nor Luco&Wong model can represent the coherencies of Argostoli database if their parameters are not modified. For small separations, it seems that Abrahamson model is comparable to coherencies of Argostoli database but the difference becomes important for large separations. For the model of Luco&Wong, the difference is significant for small separations but becomes closer to the Argostoli coherencies for large separations. This result shows clearly that existing coherency models may provide unsatisfactory estimations of the actual site-specific coherency values.

Nevertheless, by changing the value of some parameters, both coherency models seem to represent better the *insitu* coherencies. The most important conclusions of these analyses should be:

- (1) Although Abrahamson model [EPRI, 2007a] was normally used in literature to represent the coherencies of rock sites, some of its parameters should be modified by using *insitu* results before being used in soil-structure interaction applications.
- (2) For the model of Luco&Wong [Luco and Wong, 1986], the first conclusion from fitting with *insitu* coherencies is that the parameter  $\alpha$  varies moderately with respect to station separations, and the value of  $\alpha = 0.41$  should be selected for the Argostoli database
- (3) For the model of Sato [Sato et al., 2012] it is necessary to know some statistical parameters like  $\ell_c$  and  $\xi = COV$  of the random heterogeneous media. This model will be examined more clearly in Chapter 3 based on the numerical modelling studies to search for the possibility of validating that coherency model.

## Chapter 3

# Numerical modelling of seismic wave propagation in heterogeneous media

*“An approximate answer to the right problem is worth a good deal more than an exact answer to an approximate problem.”*

JOHN TUKEY

### 3.1 Introduction

This chapter aims to analyse the influence of the physical and statistical properties of random heterogeneous media on the spatial coherency of seismic ground motions. The analyses are based on numerical modelling of seismic wave propagation in random heterogeneous media. It aims to analyse the possibility of the validation of the coherency model of Sato. Many numerical case-studies of seismic waves propagation in random heterogeneous media are realized by using Spectral Element Method (SEM), implemented in software SEM3D. The ground motion signals obtained by numerical modelling (synthetic signals) are used to evaluate the spatial coherency (plane-wave coherency). The chapter begins with a brief description of spectral element method and software SEM3D, followed by a simple case-study to show the validation and performance of the software. In the section 3.3, the analyses of the influence of statistical and physical properties are pointed out. The comparison between the coherency estimated from synthetic earthquake signals and the coherency model of Sato is presented. Finally, the numerical analyses of seismic wave propagation in the site of Argostoli (presented in the Chapter 2) are realized to define its statistical properties. The statistical properties obtained from the numerical modelling are used in the coherency model of Sato to be compared with the *insitu* coherencies presented in the Chapter 2 to get a full validation of the coherency model.

### 3.2 Introduction to the Spectral Element Method and Software SEM3D

This section presents briefly the numerical methods of software SEM3D used for modelling the wave propagation in random heterogeneous media.

SEM3D [Aubry, 2016] is a software developed in the framework of SINAPS@ Project ([www.institut-seism.fr/projets/sinaps/](http://www.institut-seism.fr/projets/sinaps/)) [BergeThierry et al., 2016] in order to analyse the seismic wave propagation in random heterogeneous non-linear media. SEM3D is developed based on the Spectral Element Method which is presented in what follows.

The spectral method is a discretization method for the approximate solution of partial differential equations expressed in a weak form, based on high-order Lagrangian interpolants used in conjunction with particular quadrature rules. The solution is written as a series of polynomial form functions which can approximate the solution well in some norms as the polynomial degree tends to infinity.

The spectral element method [Komatitsch, 1997] is a high-order finite element technique that combines the geometric flexibility of finite elements with the high accuracy of spectral method. This spectral element method exhibits several favourable computational properties, such as the use of tensor products, natural diagonal mass matrices, and adequacy to implementations in a parallel computer system. Due to these advantages, the spectral element method is a viable alternative to the currently popular methods such as finite volume and finite element methods.

In the following, we introduce briefly the uses of spectral element method in the resolutions of elastodynamic problems, especially, in wave propagation in random heterogeneous media. Some more details about mathematical formulations of the method can be found in Appendix D.

### 3.2.1 Generalities on software SEM3D

Software SEM3D solves the problem of elastic wave propagation in a medium described by :

$$\nabla_{\mathbf{x}} \boldsymbol{\sigma}(\mathbf{x}) + \mathbf{f} = \rho(\mathbf{x}) \frac{\partial^2 \mathbf{u}(\mathbf{x}, t)}{\partial t^2} \quad (3.1)$$

where  $\boldsymbol{\sigma}$  is the Cauchy stress tensor,  $\rho(\mathbf{x})$  is the local density of the medium at a position  $\mathbf{x} = (x, y, z)$ , and  $\mathbf{u}$  is the displacement field.  $\mathbf{f}$  represents all external forces applying on the motions.

Like the classical finite element method, the spectral element also uses the weak formulation of the elasto-dynamic equilibrium equations. The displacement field can be written in each element or mesh on the base of Lagrange polynomials which are defined on the point of Gauss-Lobatto-Legendre (GLL). A sample of positions of GLL points is shown in Figure D.2 in Appendix D. One of the originalities of the method is about the choice of GLL points which give the diagonal mass matrix. It can reduce the simulation time since it does not need time for inverting the mass matrix.

With the numerical method implemented in SEM3D, the numerical error is controllable and minimized when the time step of simulation is smaller than the critical time step ( $\Delta t \leq \Delta t_{cr}$ ) which is the ratio between the smallest element size ( $\Delta l$ ) and the velocity of dilatation wave ( $c_L$ ):

$$\Delta t \leq \Delta t_{cr} = \frac{\Delta l}{c_L} \quad (3.2)$$

To do the numerical modelling of a full space or a half space, Software SEM3D uses the Perfectly Match Layers (PML). The latter is a particular material which has role to absorb the waves when waves arrive at the border of the interested domain. It does not permit the reflections of waves back to the domain.



### 3.2.2 Generation of random heterogeneous properties of the media

To get random heterogeneous media, the random properties of media need to be generated. In literature, several algorithms are developed to generate the random properties of material, and the one used in SEM3D is introduced by [Shinozuka and Deodatis, 1991]:

$$q(\mathbf{x}) = \sum_{n=0}^N \hat{R}^{1/2}(\mathbf{k}_n) \exp(i\mathbf{k}_n \cdot \mathbf{x}) \sqrt{\Delta_n} \xi(n) \quad (3.3)$$

where  $\xi = \xi(n) : n \leq N$  is the white noise,  $\mathbf{k}_n \in \Omega_n$  for all  $n \leq N$ ,  $(\Omega_n)_{0 \leq n \leq N}$  is a partition of  $\Omega$  and  $\Delta_n$  is the Lebesgue measure of  $\Omega_n$ .

A library for generating stochastic fields was established in the framework of a Ph.D thesis (see [de Carvalho Paludo et al., 2016] for instance) sponsored by SINAPS@ project. The importance of that library is about its capacity to generate the random properties of a large heterogeneous medium by superposition of independent fields based on the notion of multi-processor interface (MPI). With that library, for instance, the parameters which can be generated as a stochastic field to represent the random heterogeneous media are  $(\kappa, \mu, \rho)$  or  $(\lambda, \mu, \rho)$  where  $\kappa$  is the bulk modulus,  $\mu$  is the shear modulus (Lamé constant),  $\rho$  is the mass density of the medium,  $\lambda$  is another Lamé constant. In all numerical case-studies realized in this Ph.D thesis, these parameters are considered to follow the log-normal statistic law whose probability density is defined by

$$f(x) = \frac{1}{x\sigma\sqrt{2\pi}} \exp\left(-\frac{(\ln x - m)^2}{2\sigma^2}\right), \quad (3.4)$$

where  $x$  represents the elastic properties ( $\lambda, \mu, \kappa$  or  $\rho$ ),  $m$  and  $\sigma$  are respectively average value and standard deviation of elastic properties.

About the correlation model of the random media, it is noted that for all numerical modellings realized in these studies, the Gaussian correlation model is used (see Table 1.1).

### 3.2.3 Representation of earthquake source in numerical modelling

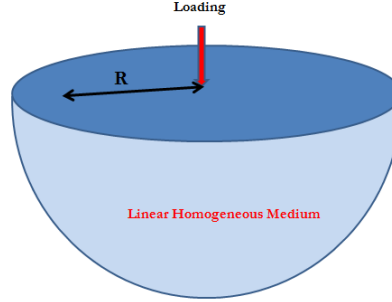
Many possible ways can be found in literature to represent the earthquake sources in the numerical modelling. Among available methods used in literature, two source terms are often considered. The first one is simply a point source and the second one is, after [Komatitsch et al., 1999], an equivalent body force, derived from a seismic moment density tensor distribution, which represents the equivalent stress distribution associated with seismic sources. The later one is generally called "moment tensor". The moment tensor is a simple mathematical description of the seismic waves produced by a complex rupture involving displacements varying in space and time on an irregular fault. More details about mathematical formulations to represent the earthquake sources in numerical modelling are reported in Appendix D.

It should be noted that for all numerical modelling case-studies of seismic wave propagation realized in these studies, and presented in the next section, the moment tensor is used to represent the earthquake sources.



### 3.2.4 A simple case-study with SEM3D

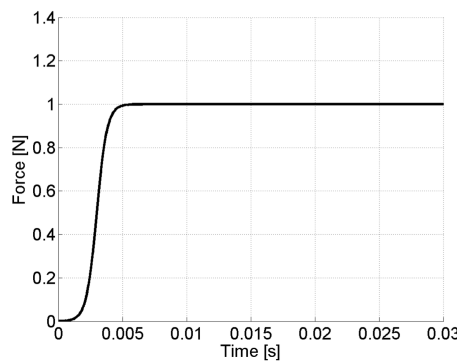
The first simple case-study to verify the solution of SEM3D software is to consider a linear homogeneous half-space with an impulse applied on the free surface (see Figure 3.1). The goal of this case-study is simply to validate the performance of the software SEM3D by comparing the displacement given by the numerical simulation with the analytical solution.



**Figure 3.1** – Free surface elastic homogeneous medium

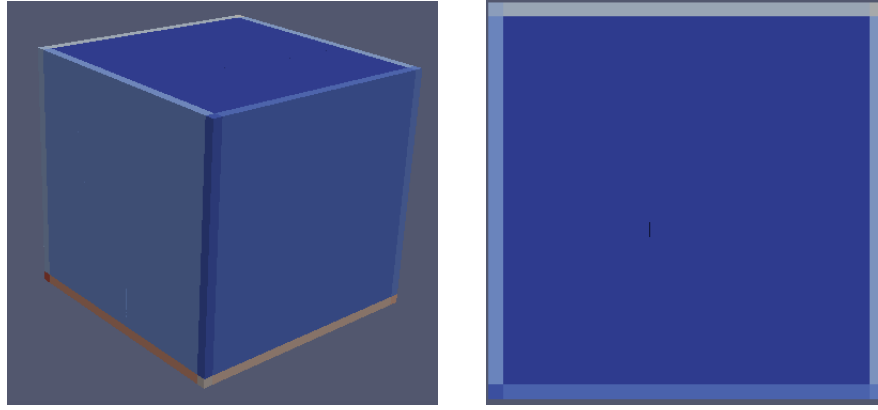
The loading is applied vertically on the free surface in form of an impulse of "Heaviside Step Function" defined by equation 3.5. The loading function is smoothed to avoid the numerical error due to the brutal change in loading. The loading function after being smoothed is presented in Figure 3.2.

$$f(t) = P \begin{cases} 0 & \text{for } t < 0.0015 \\ 0,5 & \text{for } t = 0.0015 \\ 1 & \text{for } t > 0.0015 \end{cases} \quad (3.5)$$



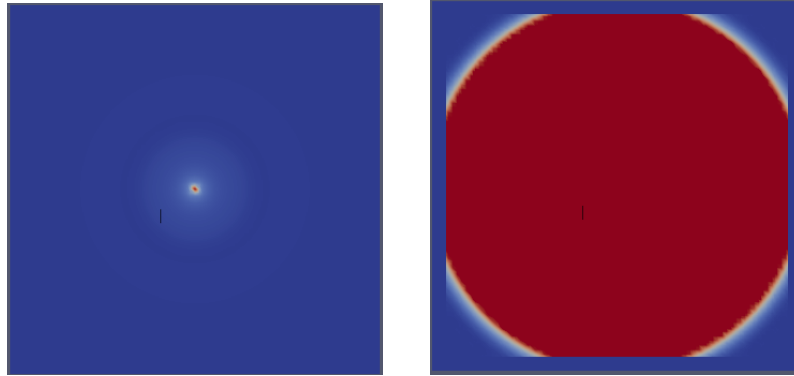
**Figure 3.2** – Smoothed Heaviside Step Function to be applied on the free surface of the medium

With SEM3D, the half space medium is modelled as a cube of size  $(100 \times 100 \times 100m^3)$  surrounded by PML except the above surface which free (see Figure 3.3). The size of finite element mesh is  $(4 \times 4 \times 4m^3)$  for the elastic properties :  $Vp = 6123.7m/s$ ;  $Vs = 2500m/s$ ;  $\rho = 2000Kg/m^3$ . We use 5 GLL points in each element as well as in PML.



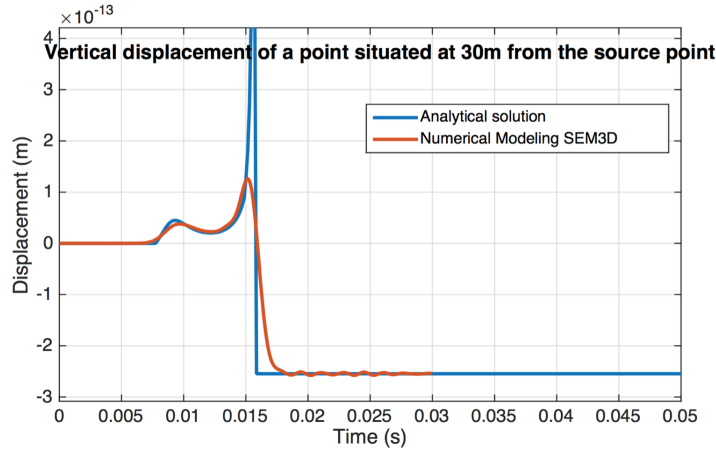
**Figure 3.3** – Half space medium surrounded by PML (left) and the free surface seen from above (right)

Figure 3.4-left and 3.4-right present the magnitude of displacement seen from above of the free surface for instants  $t = 0.0025$  (just after the loading starts) and  $t = 0.015$  (when the loading already arrives at maximum). We can also remark that there is no reflection waves due to the presence of PML.



**Figure 3.4** – Magnitude of displacement at  $t = 0.0025$  (left) and  $t = 0.015$  (right)

The available analytical solutions for this problem can be found in [Kausel, 2006]. It is about the vertical displacement of any points on the free surface. Hence, the vertical displacement of a point located at 30m from the loading point is chosen to be compared with the analytical solution. That comparison can be presented in Figure 3.5. The good agreement can be found between the both solutions while some differences can be due to the fact that the Heaviside Step Function is smoothed before applying for numerical modelling. It should be noted that the size of finite element mesh and the number of GLL points are selected to be conform to the the criteria of time step which are important for the stability in the numerical resolution and for decreasing the numerical error.



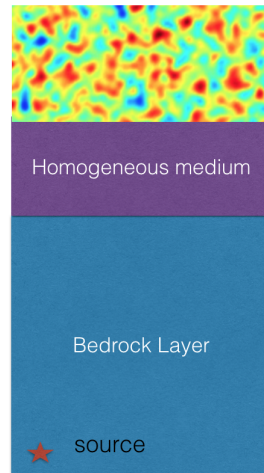
**Figure 3.5** – Comparison between analytical solution with the solution given by SEM3D modelling

### 3.3 Influence of the physical and statistical parameters of soil properties on the spatial coherency of earthquake ground motions

This section is devoted to the analyses of the influence of the physical and statistical parameters of soil properties on the spatial coherency of seismic ground motions, based on numerical modellings by using software SEM3D. The goal of these analyses is to verify the coherency function defined by theoretical considerations presented in the section 1.5.4, which is called in this manuscript as the coherency model of [Sato et al., 2012]. Since there are four important parameters (beside frequency and station separation) which are  $\ell_c$ ,  $\xi$ ,  $Z$  and  $V_o$  existing in the coherency function (equation 1.59), the analyses of the influence of each parameter will be presented one after another one. For each analysis, the coherency curves obtained by numerical modelling with SEM3D are also compared to the coherency model defined previously.

To simplify the analyses, all the case-studies presented here are modelled with the media which is composed of 3 layers : the bed rock layer, the homogeneous layer just above the bedrock layer, and the top one is the random heterogeneous layer interested in our analyses (Figure 3.6). The homogeneous layer between the bedrock layer and the random heterogeneous layer is considered to avoid the brutal change in velocity which can lead to some phenomena (such as interference, for example) influencing the result of our analyses.

To be noted also that with the lack knowledge of P-wave velocity, the Poisson ratio is considered to be 0.4 for soft soil, and 0.25 for the rock site, which leads to the ratio between the P-wave velocity and S-wave velocity of respectively : 1.73 and 2.45. To simplify the analyses, it is also considered that for all the case-studies presented in what follows, the mass density is  $\rho = 2000 \text{ Kg/m}^3$ . The coefficient of variation of shear wave velocity is normally considered to be 15% for all cases except the section 3.3.3 where it is changed to analyse its influence on the spatial incoherence. The size of analysed domain (Figure 3.6) are respectively  $1000\text{m} \times 1000\text{m} \times 2000\text{m}$  for the bedrock layer,  $1000\text{m} \times 1000\text{m} \times 600\text{m}$  for the second homogeneous layer, and  $1000\text{m} \times 1000\text{m} \times Z$  for the random heterogeneous layer, in which  $Z$  can vary for the first analysis (section 3.3.1). For other analyses,  $Z = 300\text{m}$  is considered. About the shear wave velocity, except the section 3.3.2 where the influence of  $V_s$  is analysed, the value of  $V_s = 700\text{m/s}$  is considered. The size of finite element mesh can vary



**Figure 3.6** – The representation of the medium modelled in SEM3D for analysing the influence of physical and statistical parameters on the spatial variability of earthquake ground motions

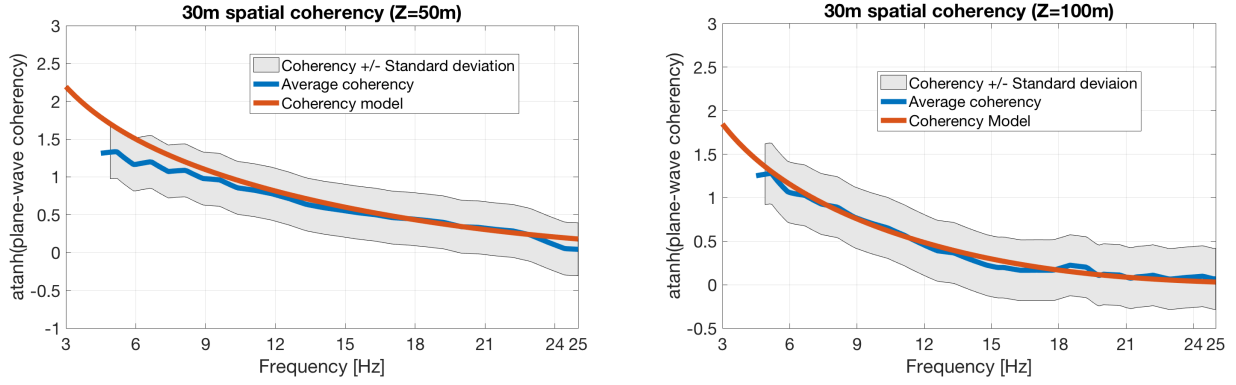
from case to case to respect the time step criteria and to optimize the simulation time. It can, hence, vary from  $5m$  to  $20m$  for different case-studies. Finally, for the correlation length, for most of the cases, the value of  $\ell_c = 40m$  is used. We do not use its constant value for all cases since its influence is observed to be irregular for different station separations and for different sizes of heterogeneous medium. This affirmation will be clarified in details in this following of this section.

It is necessary to remark that the plane-wave coherencies presented in what follows are obtained from the average of coherencies of different station pairs recorded on the free surface of the media. For each station separation distance, we have at least more than 50 station pairs for station separations more than  $50m$  and more than 100 station pairs with station separations between  $10m$  to  $50m$ . The average of coherencies are obtained by the mean of  $\tanh^1$  transfers as what is realised for the Argostoli database (see Figure 3.7 and Figure 3.11).

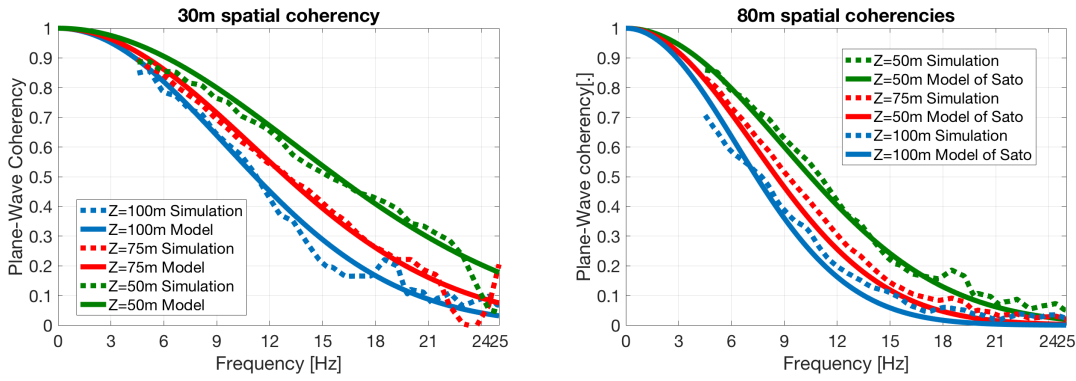
Finally, all the analyses presented are realized for station separation distances from  $10m$  to  $100m$  which conformed to the industrial applications.

### 3.3.1 Influence of the depth of heterogeneous layer

For the first case-study about the influence of possible parameters on the spatial coherency of earthquake ground motions, we are interested in how the depth of the heterogeneous layer can influence the spatial coherency. To do so, first of all, 3 cases are realized :  $Z = 50m$ ;  $Z = 75m$  and  $Z = 100m$ . The spatial coherency for  $30m$  of station separations estimated from synthetic signals given by SEM3D modellings are presented in Figure 3.7. With many different realizations of coherencies, we present the average coherency accompanied by its standard deviation. The average coherencies are also compared to the coherency model of Sato. For both cases of  $Z = 50m$  and  $Z = 100m$ , it is shown that the coherency model (equation 1.59) represents very well the coherencies given by numerical simulations. Figure 3.8 presents the comparison between the synthetic spatial coherency given by numerical modelling with SEM3D and the coherency model given by theoretical considerations of [Sato et al., 2012]. It can be said that the coherency model provides a good agreement with the numerical results. Physically, it is just obvious to mention that for a large



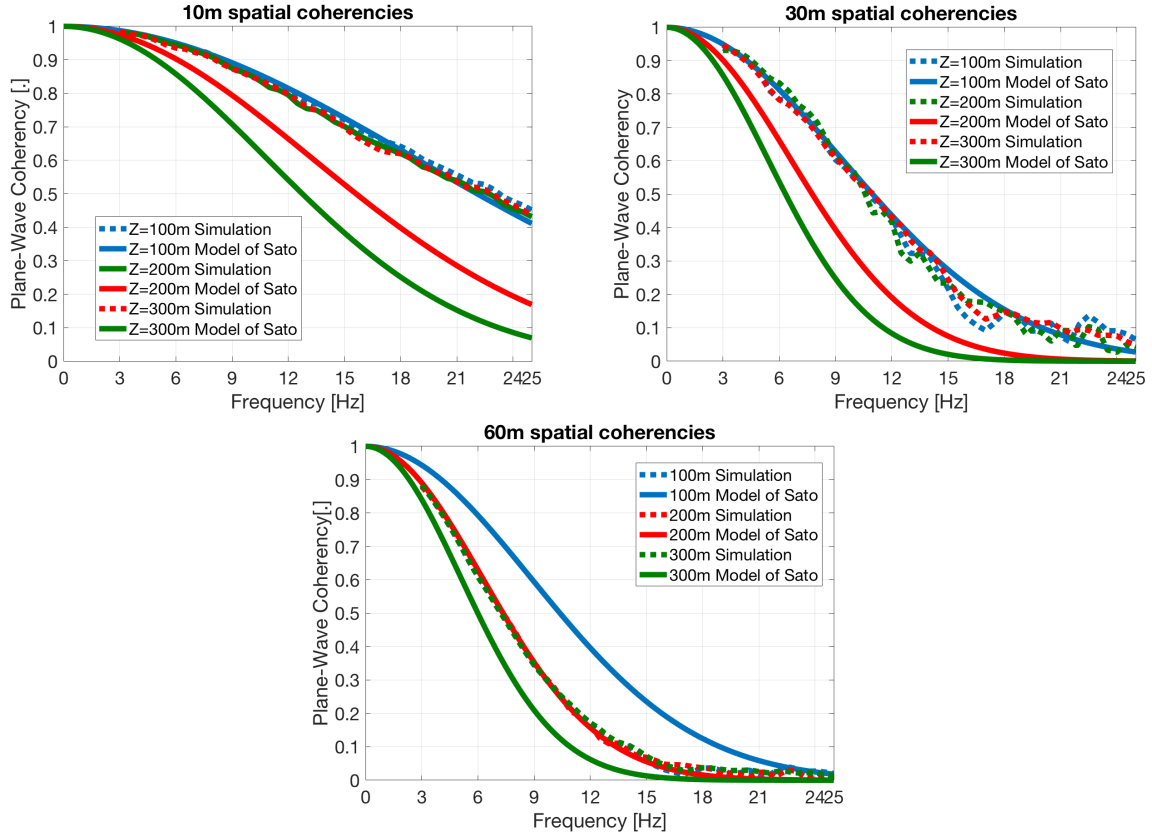
**Figure 3.7** – 30m spatial coherencies for the case of  $V_s = 700\text{m/s}$ ;  $\ell_c = 40\text{m}$ ,  $COV = 15\%$  and  $Z = 50\text{m}$  (left) or  $Z = 100\text{m}$  (right)



**Figure 3.8** – Influence of  $Z$  on the spatial coherency of earthquake ground motions and comparison between synthetic coherencies and theoretical coherency

heterogeneous medium, propagation of waves will provide significant scattering because of many fluctuations created by heterogeneous properties, while a small heterogeneous medium will not provide a huge scattering and it results in the fact that the coherency is much more bigger than the case of large heterogeneous media.

Nevertheless, for these three cases, the value of  $Z$  is not high enough since it is not evident to consider the real depth of a random medium in the real applications. Therefore, several more case-studies are realized to discuss on the value of  $Z$ . It is about the higher values of  $Z$  for this time. Three additional case-studies are realized. Remark that the value of  $\ell_c$  is changed from the previous case-studies because we wish to investigate the case that  $Z$  is large enough compared to the value of correlation length of the medium. The three values of  $Z$  for these three cases are  $100\text{m}$ ;  $200\text{m}$  and  $300\text{m}$ . Figure 3.9 presents the comparisons between the synthetic coherencies and the coherency model. It can be seen clearly that, for higher values of  $Z$ , the coherency model cannot represent well the numerical results. It seems like the coherency becomes independent of  $Z$  when the later one arrives at certain value. A parametrical study by using the synthetic coherencies given by SEM3D modellings shows that it is possible that the value of  $Z$  can be replaced by other parameters which can be  $\ell_c$  and  $d$  when  $Z$  is large enough compare to  $\ell_c$ . The first conclusion from that parametrical study suggests to take the value of  $4 \times \ell_c$  to be the limit of value of  $Z$  for which the model of [Sato et al., 2012] (equation 1.59) is valid. For the case that  $Z \geq 4 \times \ell_c$ , the value of  $Z$  does not influence the coherency any more and needs to be replaced by other parameters. Our conclusion from many case-studies with numerical modelling with the help of the comparison to



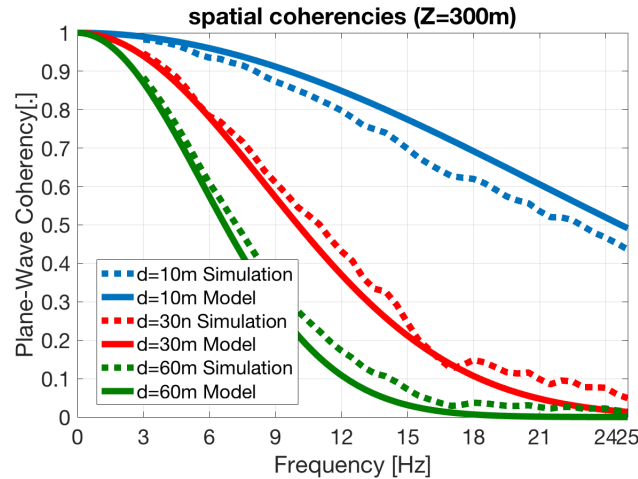
**Figure 3.9** – Influence of  $Z$  on the spatial coherency of earthquake ground motions and comparison between synthetic coherencies and theoretical coherency for the case of big value of  $Z$  (for  $V_s = 700\text{m/s}$ ;  $\ell_c = 40\text{m}$ ,  $\text{COV} = 15\%$ )

*in situ* coherencies of Argostoli database, presented in Chapter 2, is that  $Z$  can depend not only on the distance of station separations  $d$  but also on the correlation length  $\ell_c$  of the medium. Our suggestion from these studies is to propose a small modification of Model of [Sato et al., 2012], which is:

$$\gamma(d, f) = \exp \left\{ -\sqrt{\pi} \xi^2 \ell_c Z_{eq} \frac{(2\pi f)^2}{V_{s30}^2} \left[ 1 - \exp \left( -\frac{d^2}{\ell_c^2} \right) \right] \right\} \quad \text{for } Z_{eq} = \begin{cases} Z & \text{for } Z \leq 4 \cdot \ell_c \\ 4 \cdot \ell_c & \text{for } Z \geq 4 \cdot \ell_c, d \leq \ell_c \\ 4 \cdot d & \text{for } Z \geq 4 \cdot \ell_c, d \geq \ell_c \end{cases} \quad (3.6)$$

The independence between  $Z$  and spatial coherencies might be explained the hypothesis on the single mean free path of the random heterogeneous media. Mean free path here refers to the average distance travelled by a moving particle (wave propagation) between successive impacts (collisions) which modify its direction or energy or other particle properties. Physically, when the size of the random heterogeneous medium is larger than the mean free path of the medium, the wave scattering does not depend on the size of the medium any more. The new comparison between the synthetic coherencies and the coherency model for the case that  $Z \geq 4 \times \ell_c$  is presented in Figure 3.10.

For the next case-studies analysing the influence of other parameters, the height of the random heterogeneous layer is always considered to be large enough compared to the correlation length ( $Z \geq 4 \times \ell_c$ ). Therefore, the coherency model which will be compared to the synthetic coherencies is the equation 3.6 with the second and third conditions. It means that there is no dependence of



**Figure 3.10** – Comparison of synthetic coherencies with the model of Sato in the case that  $Z \geq 4 \times \ell_c$  (for  $V_s = 700\text{m/s}$ ;  $\ell_c = 40\text{m}$ ,  $\text{COV} = 15\%$ )

$Z$  in the coherency model any more.

### 3.3.2 Influence of shear-wave velocity

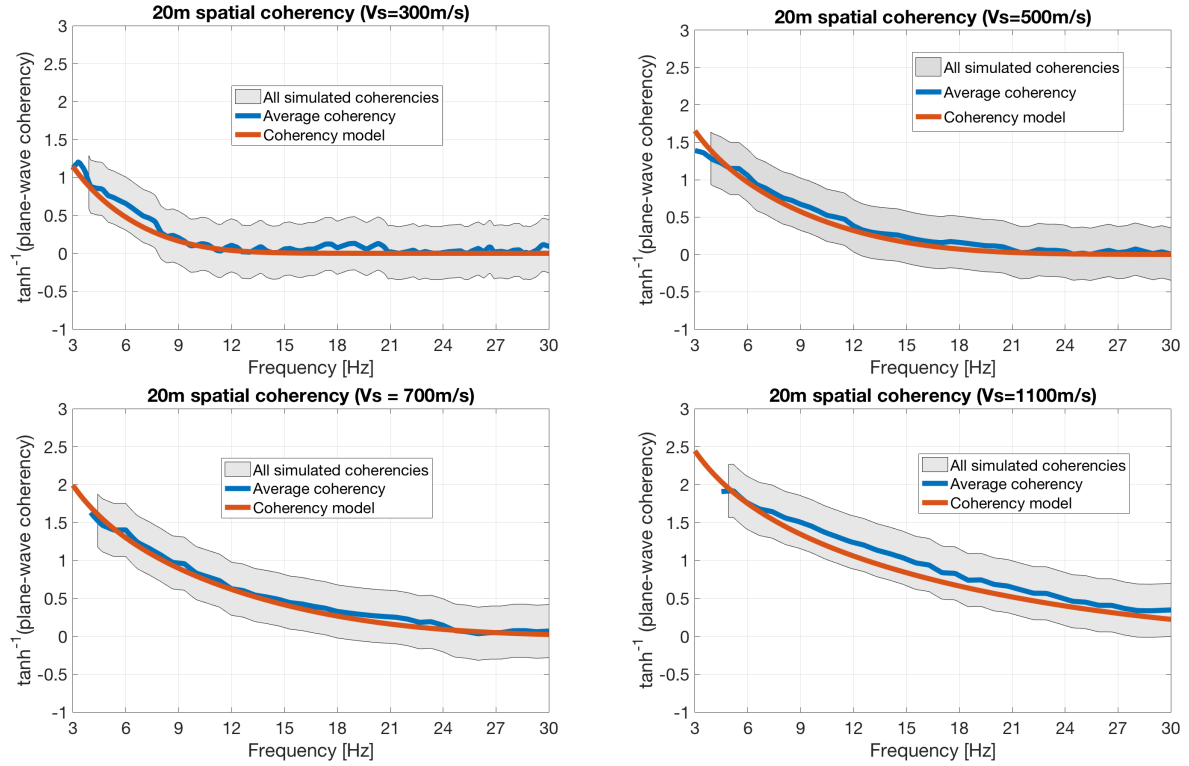
The second analysis is to observe the influence of shear-wave velocity on spatial variability of seismic ground motions. To do so, as what presented in the case of the influence of  $Z$ , different values of  $V_s$  are used for the modelling. First of all, the average coherencies are presented with the standard deviation (Figure 3.11). The synthetic coherencies are also compared to the new modified coherency model (equation 3.6). It is obviously seen that the modified coherency model gives almost a perfect agreement with the synthetic coherencies obtained from the numerical modellings with SEM3D.

Figure 3.12 presents the influence of shear-wave velocity on spatial variability of seismic ground motions for 20m, 30m and 40m of separations. The results show clearly its influence: the coherency decreases when the shear-wave velocity decreases. This result is conform to the experimental results as well as the conclusions in the literature.

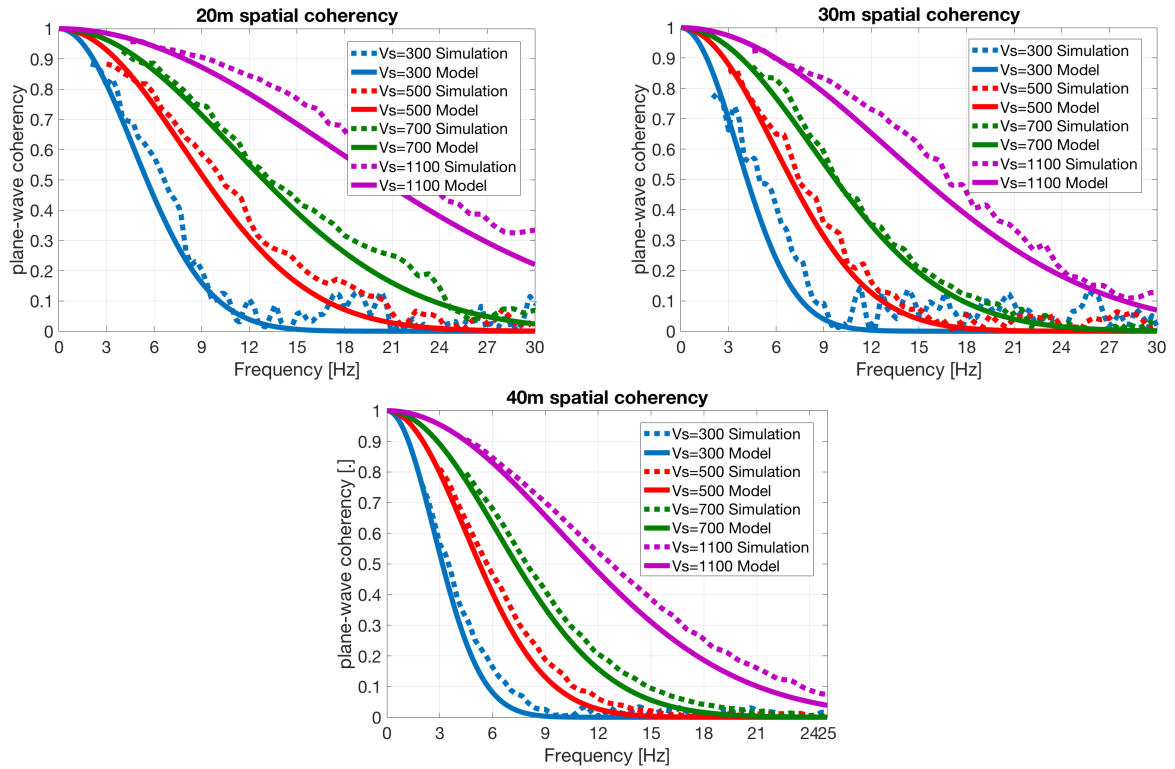
### 3.3.3 Influence of coefficient of variation of elastic properties

The another parameter to be analysed about its influence on the spatial coherency of earthquake ground motions is a statistical parameter called coefficient of variation (COV) of elastic properties. In this analyse, the COV of shear-wave velocity is considered. Three coefficients of variation are considered : 10%, 20%, 40%. Figure 3.13 presents the comparison of coherencies estimated from 3 media with different COV of shear-wave velocity. One can see the influence of COV on spatial coherency of earthquake ground motions: the coherency decreases while the COV increases. This result is physically reasonable since one can suppose that whenever the fluctuation of elastic properties in the medium is small, the medium is less heterogeneous, and the coherency is greater than the case of a medium with important fluctuations of elastic properties. The comparisons between the synthetic coherencies and the modified coherency model are also presented and the conclusion shows once again that the coherency model gives a satisfactory result.



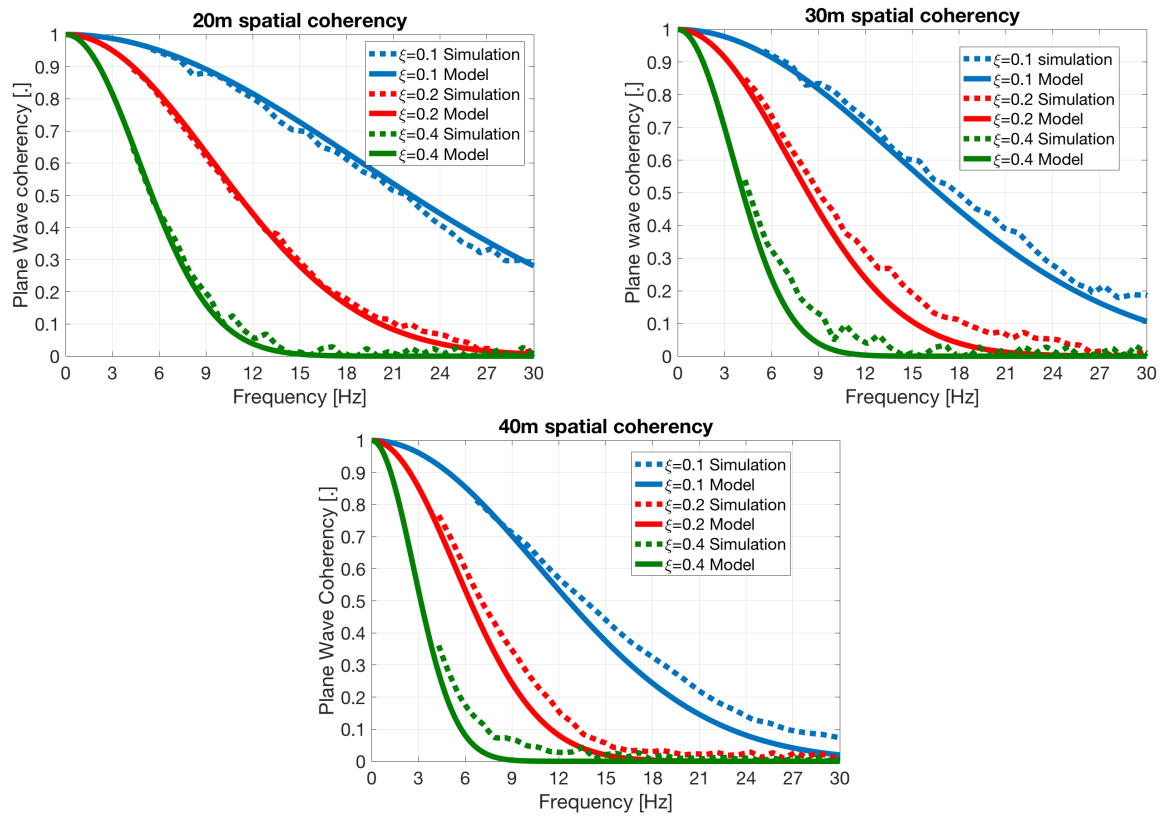


**Figure 3.11** – 20m spatial coherencies for different shear-wave velocities presented with standard deviations and compared to the modified coherency model

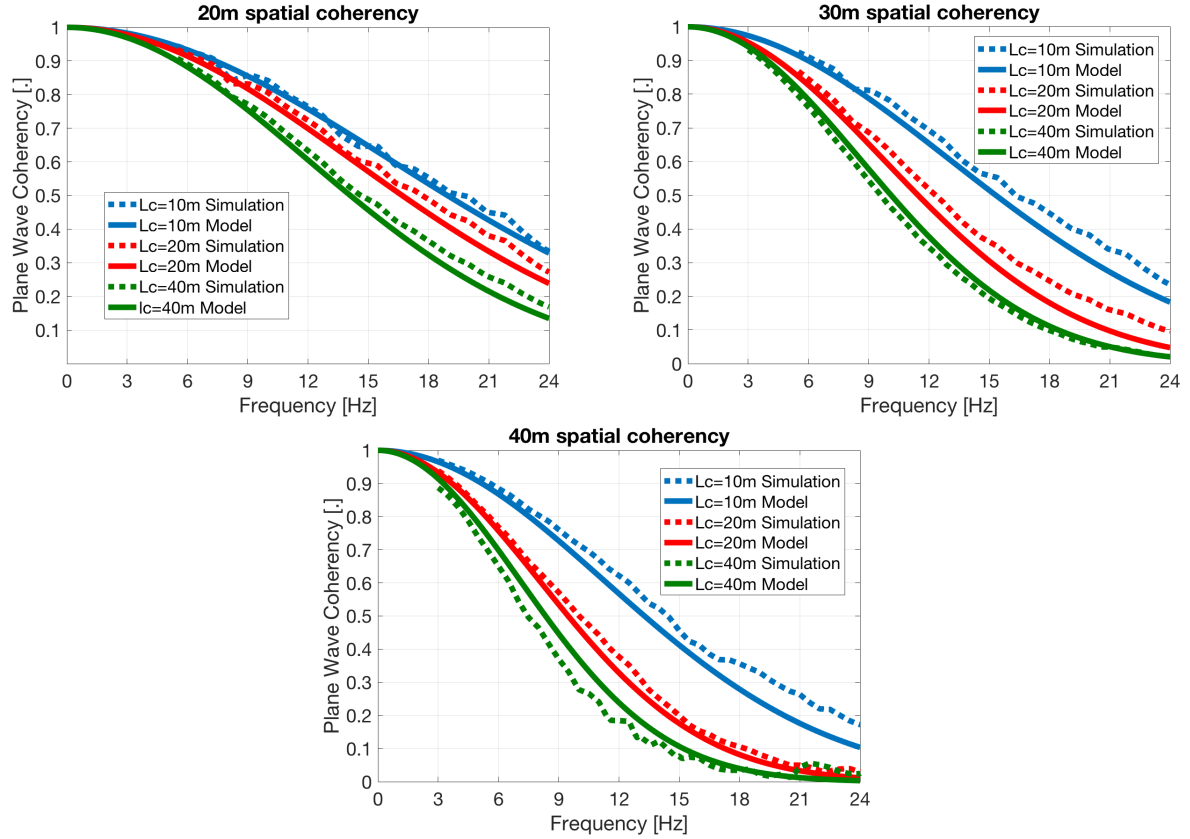


**Figure 3.12** – influence of shear-wave velocity on spatial coherency for soil site for 20m, 30m and 40 of separations (for  $\ell_c = 30m$ ;  $\xi = 0.15$ )





**Figure 3.13** – influence of coefficient of variation (COV) of random properties on spatial coherency for soil site for 20m, 30m and 40 of separations (for  $\ell_c = 30\text{m}$ ;  $V_s = 800\text{m/s}$ )



**Figure 3.14** – influence of correlation length on spatial coherency for soil site and rock site (for  $V_s = 800\text{m/s}$ ;  $\xi = 0.15$ )

### 3.3.4 Influence of correlation length of medium

The last parameter existing in the coherency model of Sato is the correlation length of the random medium. This section is devoted to the analysis of its influence on the spatial coherency of seismic ground motions. To do so, different values of correlation length ( $\ell_c$ ) are used for the numerical modelling while other parameters are kept to be constant. Figure 3.14 presents the influence of the correlation length of medium on the spatial coherency of seismic ground motions. One can remark clearly that even for short separation of station pairs, the coherency decrease when the correlation length increase. An important information from the results is that this property is true when the correlation length is in the same order of magnitude of wavelength. When the value of correlation length becomes too small or too big compared to wavelength, it is not possible to conclude on that influence. Once again, the coherency model gives a satisfactory result when it is compared to the the synthetic coherencies.

## 3.4 Modelling of spatial variability of seismic ground motions for Argostoli dense array

After analysing the influence of the physical and statistical parameters on spatial coherency of seismic ground motions, in this section, we try to identify the values of the statistical parameters ( $\ell_c$  and  $\xi$ ) of Argostoli site by comparing the spatial coherency of seismic ground motions obtained

$(\ell_c, \xi)$	10 m	30 m	55 m	100 m
20 m, 0.2	0.0420	0.2266	0.8844	0.9908
20 m, 0.3	0.3062	0.5047	0.6094	0.7763
20 m, 0.4	0.5233	0.7456	0.8346	0.9526
<b>30 m, 0.2</b>	<b>0.0419</b>	<b>0.2230</b>	<b>0.5090</b>	<b>0.5589</b>
30 m, 0.3	0.3327	0.5317	0.7560	0.9160
30 m, 0.4	0.5464	0.7658	0.9359	0.9921
40 m, 0.2	0.0499	0.2328	0.5694	0.6315
40 m, 0.3	0.3421	0.4864	0.8184	0.9696
40 m, 0.4	0.5545	0.7315	0.9619	0.9986
40 m, 0.1	0.3111	1.1096	2.0286	2.3005

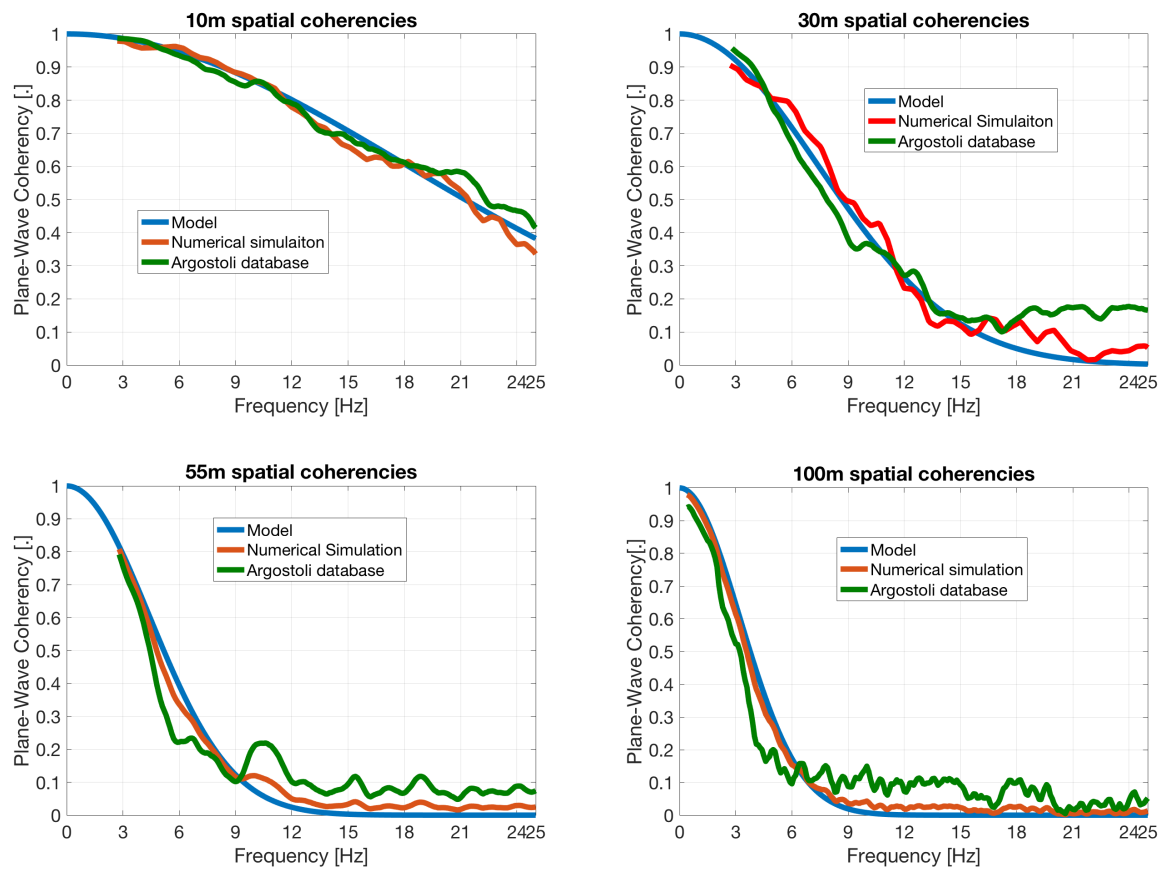
**Table 3.1** – Relative error in  $\mathbb{L}^2$  between *insitu* coherencies and synthetic coherencies obtained by each couple of statistical parameter. The bold numbers are the smallest relative errors.

from experimental data, with the results of numerical modellings. The profile of shear-wave velocity of Argostoli site is presented in Figure 2.7. The density is considered to be constant and equal to  $2000 \text{ Kg/m}^3$  (the same to what are realized for the previous numerical studies presented in the last section) and the ration of velocities for this case is considered to be equal to 2 ( $V_p = 2 \cdot V_s$ ).

A parametrical study is realized to determine the values of statistical parameters  $\ell_c$  and  $COV = \xi$  which give the closest coherencies to the *insitu* spatial coherencies of Argostoli database. The methodology for this parametrical study is to estimate the spatial coherencies from the synthetic signals given by numerical modelling of seismic wave propagation in the random heterogeneous media corresponding to the given statistical parameters  $\ell_c$  and  $COV = \xi$ . Ten couples of  $(\ell_c, \xi)$  are tested :  $(\ell_c = 20\text{m}, \xi = 0.2)$ ,  $(\ell_c = 20\text{m}, \xi = 0.3)$ ,  $(\ell_c = 20\text{m}, \xi = 0.4)$ ,  $(\ell_c = 30\text{m}, \xi = 0.2)$ ,  $(\ell_c = 30\text{m}, \xi = 0.3)$ ,  $(\ell_c = 30\text{m}, \xi = 0.4)$ ,  $(\ell_c = 40\text{m}, \xi = 0.2)$ ,  $(\ell_c = 40\text{m}, \xi = 0.3)$ ,  $(\ell_c = 40\text{m}, \xi = 0.4)$  and  $(\ell_c = 40\text{m}, \xi = 0.1)$ . The coherencies estimated from the synthetic signals given by each couple are compared to the coherencies of Argostoli database. To determine the couple who gives the closest coherencies, we calculate the relative errors (in  $\mathbb{L}^2$  norm) which are simply the differences between the Argostoli coherencies and the synthetic coherencies given by different statistic parameters. Mathematically, the error is defined for all frequencies by:

$$error = \sqrt{\frac{\sum_{f_i} (Coh_{insitu}(f_i) - Coh_{syn}(f_i))^2}{\sum_{f_i} (Coh_{insitu}(f_i))^2}} \quad (3.7)$$

The relative error for each couple of statistical parameters is presented in Table 3.1. By comparing the relative errors, it is obvious to see that the couple  $(\ell_c = 30\text{m}, \xi = 0.2)$  gives the smallest error. We selected, hence, the couple  $(\ell_c = 30\text{m}, \xi = 0.2)$  for comparing the coherency model of Sato to the *insitu* coherencies of Argostoli database. These comparisons are presented in Figure 3.15. Anyway, as seen in Table 3.1, it seems that, for Argostoli case, the correlation length does not influence significantly the spatial coherencies, i.e, the couple  $(\ell_c = 40\text{m}, \xi = 0.2)$  also gives small relative errors. It should be noted that the correlation length in the vertical direction is taken to be equal to 3 m for any case presented in that table. This value is selected based on the numerical and experimental observation : the correlation length in the vertical direction is normally 10 times smaller than that of the horizontal direction in the real site with significant stratifications of soil properties.



**Figure 3.15** – Comparisons between the *insitu* coherencies of Argostoli database, the synthetic coherencies estimated from synthetic signals of SEM3D and the modified coherency model

### 3.5 Conclusions on validation of coherency model and numerical assessment of spatial variability of seismic ground motions

The model of [Sato et al., 2012] which is selected to be analysed in our studies, after being slightly modified, provides a satisfactory result in terms of coherency prediction after being compared to the *insitu* coherencies as well as synthetic coherencies obtained by numerical simulations.

The conclusion of this chapter is to give a validation of coherency model of Sato which is represented by equation 3.6. All the case-studies presented previously show that this coherency model gives a satisfactory result since it always gives a good agreement with the synthetic coherencies. To be noted that the coherency model are validated in these studies for the station separations between 10m and 100m which is conformed to the industrial applications.

The numerical case-studies also permits to determine the statistical parameters of the random heterogeneous media on the site of Argostoli. Correlation length  $\ell_c$  and coefficient of variation  $\xi$  of the medium are identified by comparing the coherencies estimated from numerical case-studies to the *insitu* coherencies of Argostoli database.

Nevertheless, the parameters existing in that coherency model are not easy to be defined. Beside the shear wave velocity which generally used in seismology and earthquake engineering, the correlation length and the coefficient of variation of elastic properties are still a mystery. There are not many studies yet in the literature which provide the satisfactory conclusion on the determinations of those statistical parameters.

Another remarkable point is about the coefficient 4 which exists in the coherency model. It is obtained empirically by analysing the numerical results without any theoretical judgement. This should be examined clearly to get a full theoretical model of coherency which can be adapted to all earthquake sites. More investigations by comparing this value to the mean free path of the random heterogeneous medium need to be realised. As a matter of fact, after [Khazaie et al., 2016], the mean free path of a random heterogeneous medium is defined by :

$$\ell_m = \frac{4\ell_c^3}{\pi^2 \cdot \xi^2 \cdot \lambda^2} \quad (3.8)$$

which is approximated to  $\approx 4 \cdot \ell_c$  with the parameters used for our numerical modelling. By using this reason, we can deduce two different regimes of wave scattering which influence the spatial coherencies :

- When  $Z_{eq} \leq \ell_m$  : single scattering
- When  $Z_{eq} \geq \ell_m$  : multiple scattering.

## Chapter 4

# Spatial variability of seismic ground motion in soil-structure interaction analysis

*“There are only two worlds - your world, which is the real world, and other worlds, the fantasy. Worlds like this are worlds of the human imagination: their reality, or lack of reality, is not important. What is important is that they are there. These worlds provide an alternative, provide an escape, provide a threat, provide a dream, and power; provide refuge, and pain. They give your world meaning. They do not exist; and thus they are all that matters.”*

NEIL GAIMAN, in The Books of Magic

### 4.1 Introduction

This chapter is devoted to the industrial case-studies which consist to the demonstrations of the importance of taking into account spatial variability of seismic ground motions in the analyses of soil-structure interactions by using coherency models. The goal of this chapter is to show the influence of spatial variability of seismic ground motions on the structural responses (floor response spectra). A nuclear power plant reactor building in Japan is selected for the analyses : the Kashiwasaki-Kariwa power plant. This building is selected for our studies since it has already been analysed in the framework of Karisma benchmark, and also in the framework of SINAPS@ project. The chapter begins with the descriptions of the Kashiwasaki-Kariwa power plant reactor building, the soil surrounding the building and the earthquake signals. After that, the methodology of taking into account the spatial variability of seismic ground motions in the soil-structure interaction analyses with software Code\_Aster (an open source software developed and used by EDF R&D) are presented. Finally, the comparisons of the floor structural responses for the case of coherent input motions and incoherent input motions are presented to show the influence of the spatial variability of earthquake ground motions on the structural responses.



**Figure 4.1** – Kashiwazaki and Kariwa Nuclear Power Plant, in Japan [IDN, 2015]

## 4.2 Descriptions of the case-study

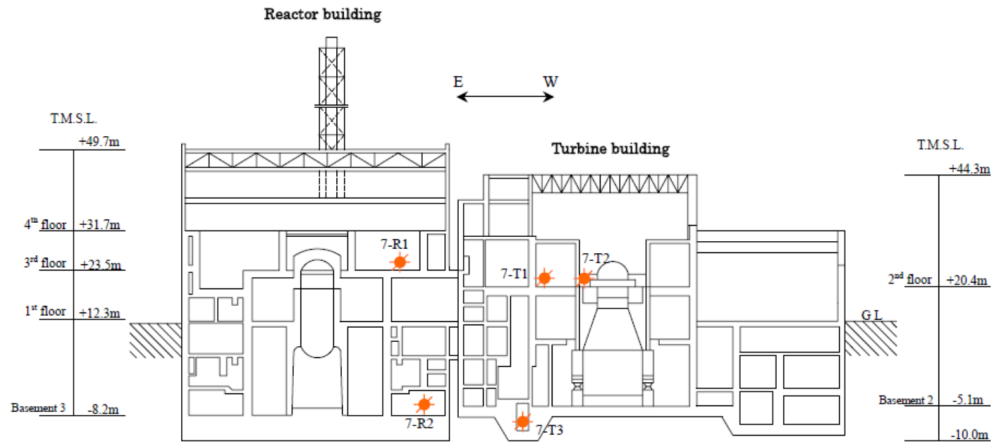
This section gives a general description of our case-study, the Kashiwazaki-Kariwa power plant reactor building used for the analyses of soil-structure interaction, the structural properties, the soil properties as well as the finite element mesh used for numerical modelling. The earthquake signals recorded during the earthquakes in 2007 which will be used as input motion for the analysis of soil-structure interaction are also presented at the end of this section. More general detailed description about Kashiwazaki-Kariwa power plant and some structural analyses of its building after earthquakes in 2007, might be found in [IAEA, 2012].

The Niigata Chuetsu-Oki earthquakes (NCO) destroyed some parts of the Niigata region in Japan on July 16th, 2007. The first one of NCO, with magnitude of 6.6 Mw, happened in the sea at the depth of between 10 and 15 km, and the distance of around 10 km from the coast. The second one happened just several hours after the first one with magnitude of 6.8 Mw.

The NCO earthquakes led to the lost of around 5 millions dollars of economy and the death of 10 people. The damages are significant in all the region, particularly, the Kashiwazaki-Kariwa (KK) nuclear power plant (see Figure 4.1) which is situated at around 15 km from the earthquake fault [Pavlenko and Irikura, 2012]. The 4.2km square site is situated in the Niigata region city of Kashiwazaki and the town of Kariwa, roughly 135 miles North West of Tokyo, on the shoreline of the Sea of Japan. Kashiwazaki-Kariwa is also the world's fourth largest electric-generating station behind three hydroelectric plants; Itaipu on the Brazil Paraguay border, Three Gorges Dam in China and Guri Dam in Venezuela. Similar to all other nuclear power plants in Japan, Kashiwazaki Kariwa was built to severe earthquake confrontation principles. However, the NCO earthquakes caused the plant to dribble radioactive substances into the air and water. The plant, which has been in service since 1985, was stopped up until safety checks following the earthquake were completed. The plant was reopened in May 2009.

With the significant number of data and observations realized during the NCO earthquakes, an international benchmark KARISMA (Kashiwazaki-Kariwa Research Initiative for Seismic Margin Assessment) was established in 2009-2010, initiated by International Atomic Energy Agency (IAEA) [IAEA, 2012], [IAEA, 2013]. Among different parts of the benchmark, there is a part of structural analyses based on the responses of the Unit 7 reactor building of the KK nuclear power plant center (see Figure E.1). The Unit 7 is situated at North-West of the site, next to Unit 5 and Unit 6. Each





**Figure 4.2** – Y-Z view of Unit 7 [IAEA, 2013]

Unit is composed by a reactor building and a turbine building (see Figure E.2). The Y-Z view of Unit 7 is presented in Figure 4.2

The height of the building is  $63m$ , in which  $26m$  is embedded, and the size of the foundation is  $56,7 \times 59,3m^2$ . The building is composed of 9 floors including roof and apron. The X-Z view and Y-Z view on the only reactor building are shown in figure 4.3. The vertical coordinate of each floor is presented in Table E.1 in appendix. Some principal structural elements of reactor building are also given in Table E.2 in appendix E. The properties of materials used for the construction are given in Table E.3, also in appendix E.

#### 4.2.1 Finite element model of reactor building

The finite element model of reactor building was originally constructed by NECS [Mezher, 2009] and slightly modified by several other engineers to conform with their analyses. For all details about finite element model of the structure, reader is referred to [Banci et al., 2015] and [Mezher, 2009]. The finite element mesh of the reactor building is presented in Figure 4.4.

All materials are modelled in the case of linear elastics since the analyses of the building reported that there is no significant damage of the reactor building. The distribution of the mass inside the structure used for numerical modelling is presented in Table E.4 in the appendix.

#### 4.2.2 Modelling of soil surrounding the building

By using software MISS3D, actually integrated in Code\_Aster, for the case of linear soil-structure interactions, the soil does not need to be meshed. Only the surface interfaces between soil and building need to be taken into account in the analyses. Different layers of soil can be modelled in MISS3D without being meshed. This will be explained briefly in the next section, and for more details about this modelling, reader is referred to [Greffet, 2016].

As described previously, the building is embedded of  $26m$  in the ground. The interfaces between building and soil are presented in Figure 4.5. After [IAEA, 2012], the soil properties next to the



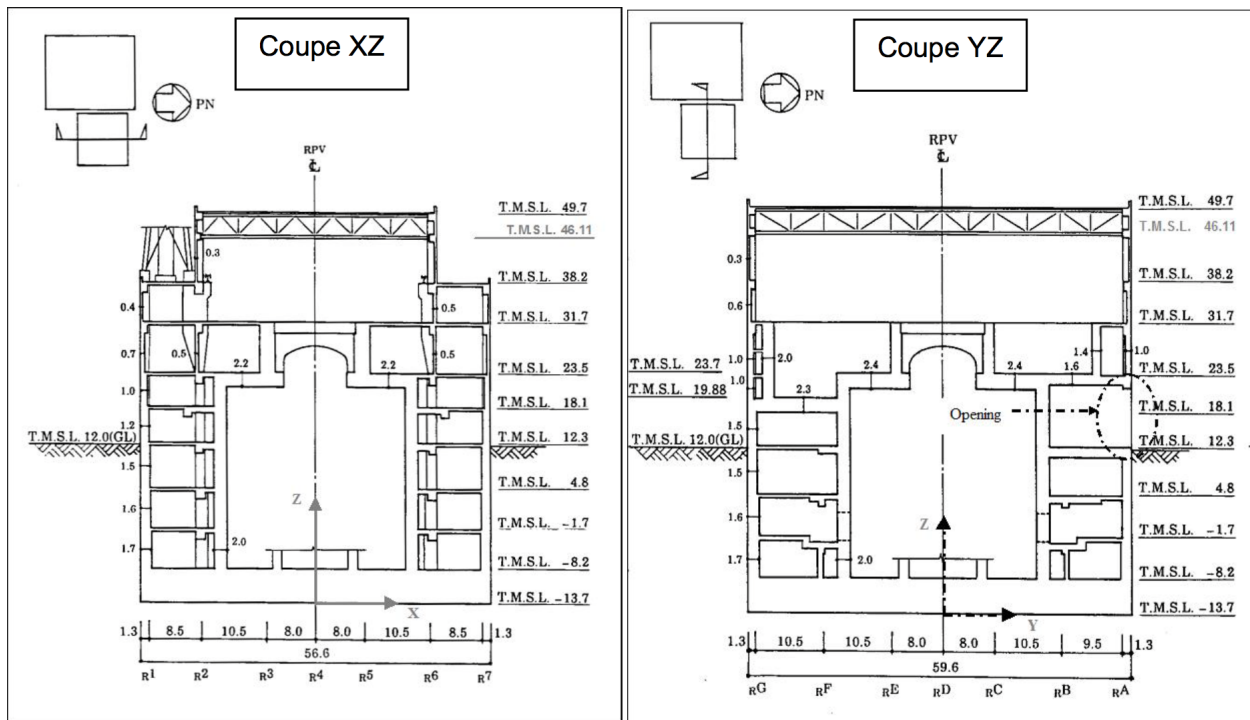


Figure 4.3 – X-Z and Y-Z views of reactor building in Unit 7 [IAEA, 2013]

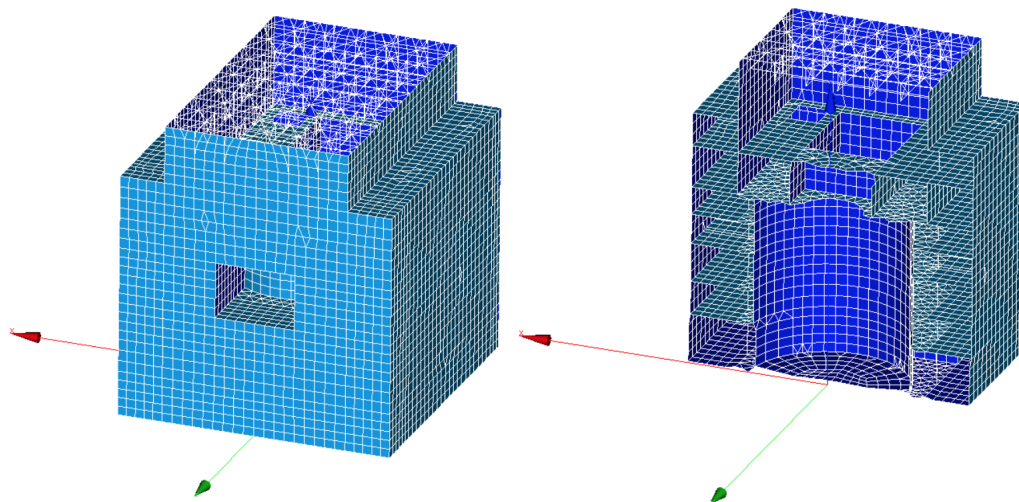
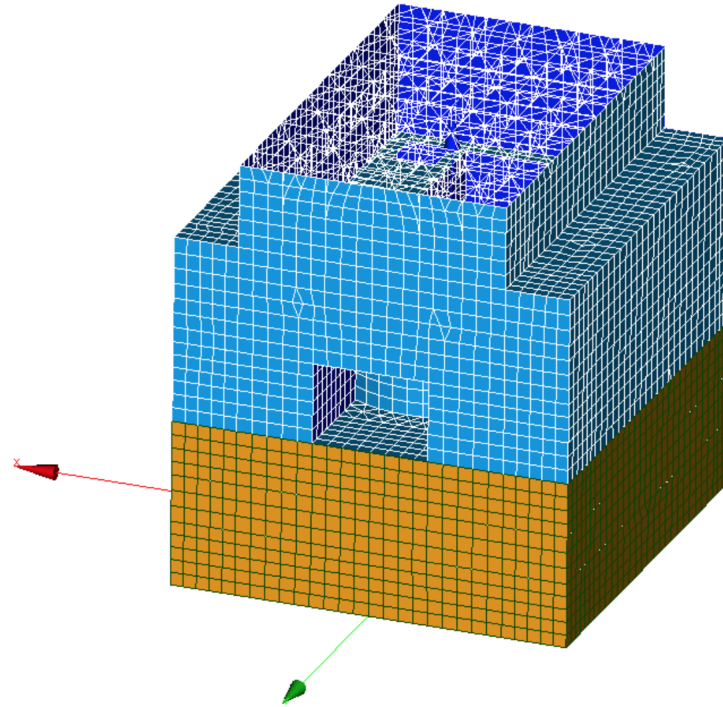


Figure 4.4 – Finite element mesh of reactor building



**Figure 4.5** – Interfaces between reactor building and soil

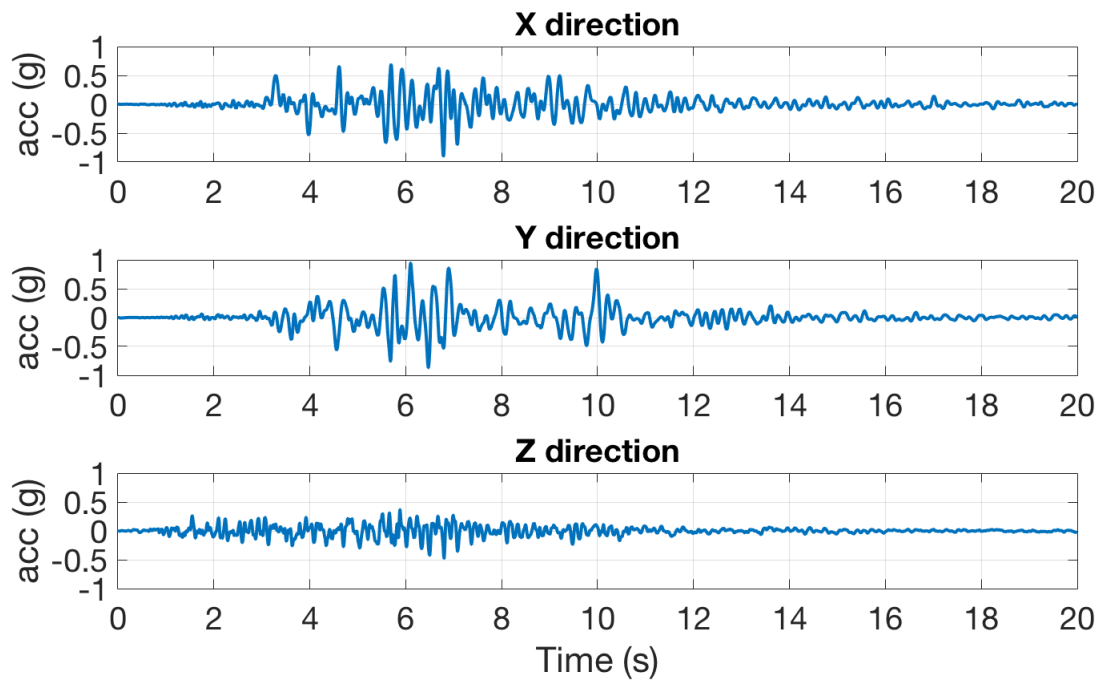
Unit 7 of KK power plant that can be used for soil modelling are presented in Table 4.1. More details about all soil properties of the site can be found in [Banci et al., 2015].

<b>Z (m) T.M.S.L</b>	<b>Type of soil</b>	<b>Vs (m/s)</b>	<b>Vp (m/s)</b>	<b>Density (kg/m<sup>3</sup>)</b>	<b>Poisson ratio</b>	<b>Shear Modulus (kPa)</b>
+12	Sand	150	310	1610	0,347	36 000
+8	Sand	200	380	1610	0,308	65 700
+4	Clay	330	1240	1730	0,462	192 000
-6	Rock	490	1640	1700	0,451	416 000
-33	Rock	530	1700	1660	0,446	475 000
-90	Rock	590	1710	1730	0,432	614 000
-136	Rock	5650	1790	1930	0,424	832 000
-155	Substratum	720	1900	1990	0,416	1 050 000

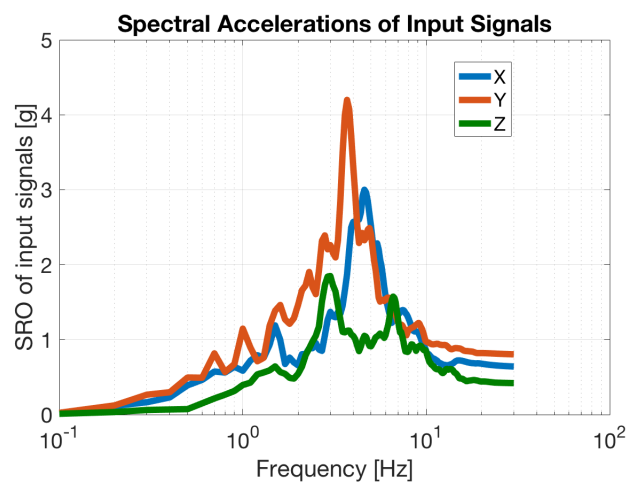
**Table 4.1** – Stratigraphy of Unit 7 of KK site [IAEA, 2012]

### 4.2.3 Earthquake signals (input motion)

The 3 components of signal used as input motion in this study are plotted in Figure 4.6 and their spectral accelerations are plotted in Figure 4.7. These signals are provided in the framework of Karisma benchmark.



**Figure 4.6** – Three components of signals used for input motion



**Figure 4.7** – FFT of the three components of signals used for input motion

### 4.3 Methodology of Soil-Structure Interaction analysis accounting for incoherent input motions

This section presents briefly about the methodology implemented in software Code\_Aster for the soil-structure interaction analysis accounting for spatial variability of seismic ground motions (incoherent input motions). For more details about this methodology, readers are referred to [Zentner and Devesa, 2011] and [Zentner, 2016].

#### 4.3.1 Soil-Structure Interaction analysis in frequency domain

For the analysis of linear soil-structure interaction, in frequency domain, we use the methodology implemented in software MISS3D which is actually embedded in software Code\_Aster. More details about software MISS3D can be found in [Clouteau, 2005] and [Clouteau, 2007].

With MISS3D, the propagation of linear elastic waves in a stratified soil (unbounded domain) is solved by a boundary element method. The methodology for the analysis of soil-structure interaction is based on dynamic sub-structuring where only interfaces of substructures require to be meshed by boundary element. The dynamic sub-structuring method (see Figure 4.8) consists of a decomposition of the analysed physical domain into 3 parts : interface ( $V_i$ ) between structure and soil, the principal part of structure ( $V_o$ ) and the soil domain. With the decomposition method of Craig-Bampton [Roy et al., 1968], the sub-structuring method calculates the dynamic modes  $\varphi$  of the domain  $V_o$  and the static modes of  $\psi$  of the interface  $V_i$ . These two types of modes are combined to form a generalized basis  $\phi$  defined as:

$$\phi = [\varphi \ \psi] \quad (4.1)$$

and the displacement field ( $u$ ) of structure can be written by:

$$u = \sum \alpha_n \varphi_n + \beta_n \psi_n \quad (4.2)$$

where coefficients  $\alpha_n$  and  $\beta_n$  are respectively the factors of participations of each dynamic mode and each static mode.

Based on these generalised coordinates, the problem of soil-structure interaction can be reduced to the resolution of the harmonic problem :

$$[\mathbf{K}_b + i\omega\mathbf{C}_b - \omega^2\mathbf{M}_b + \mathbf{K}_s(\omega)]\hat{\mathbf{q}}(\omega) - \hat{\mathbf{f}}_s(\omega) = 0 \quad (4.3)$$

where  $\mathbf{K}_b$ ,  $\mathbf{C}_b$  and  $\mathbf{M}_b$  are the generalized stiffness, damping and mass matrices of the structure, and  $\hat{\mathbf{q}}(\omega) \in \mathcal{C}^M$  is the generalized vector of displacement in the frequency domain (Note that  $M = N_I + N_S$  where  $N_I$  is the number of interface degree of freedom and  $N_S$  is the number of retained eigen modes of the structure).

$\mathbf{K}_s(\omega)$  and  $\hat{\mathbf{f}}_s(\omega)$  are respectively the frequency dependent soil impedance matrix and seismic load vector. The later two can be calculated with MISS3D.

In the following, we define a complex transfer function of displacement  $\mathbf{H}(\omega)$  by:

$$\mathbf{H}(\omega)\hat{\mathbf{f}}_s(\omega) = \hat{\mathbf{q}}(\omega) \quad (4.4)$$

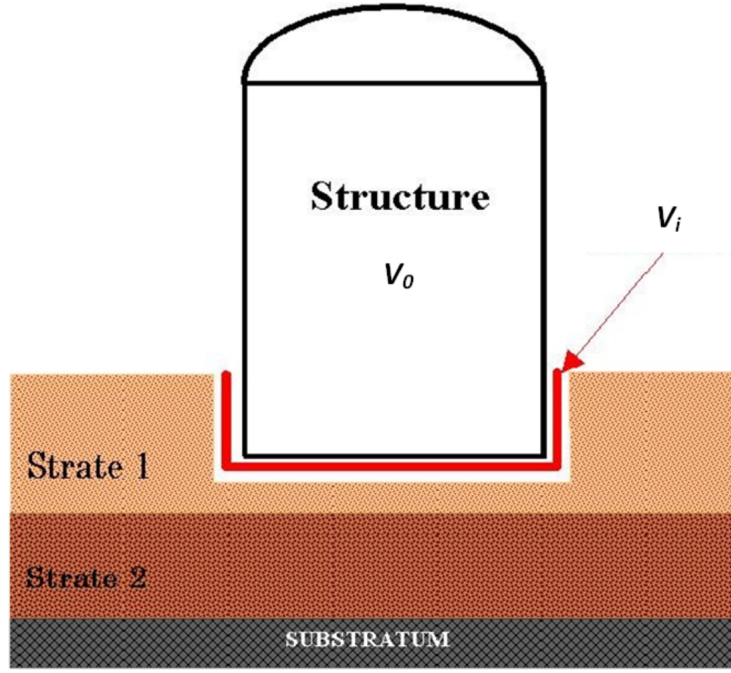


Figure 4.8 – Dynamic sub-structuring method

If the input motion (excitations) is supposed to be a Gaussian stationary stochastic process, the structural response is also a Gaussian stationary stochastic process since the transfer function can be considered to be a linear filtering. We can construct a relation between the power spectral density of seismic force (input motions) ( $\mathbf{S}_f(\omega)$ ) and that of structural responses ( $\mathbf{S}_q(\omega)$ ) by:

$$\mathbf{H}(\omega)\mathbf{S}_f(\omega)\mathbf{H}^*(\omega) = \mathbf{S}_q(\omega) \quad (4.5)$$

where  $\mathbf{H}^*$  is the transposed conjugate of  $\mathbf{H}$ .

#### 4.3.2 Accounting for spatial variability of seismic ground motions

To account for spatial variability of seismic ground motions represented in probabilistic framework by a coherency function  $\gamma(x_k, x_l, \omega)$ , the cross spectral density of soil movement in free field is defined by:

$$S_u(x_k, x_l, \omega) = \gamma(x_k, x_l, \omega)S_o(\omega) \quad (4.6)$$

where  $x_k$  and  $x_l$  represent two different point on the interface between soil and structure, and  $S_o$  is the one point power spectral density of free field ground motion.

For all couple of points  $x_k$  and  $x_l$  on the interface, the matrix of cross spectral densities ( $\mathbf{S}_u(\omega)$ ) is defined by:

$$\mathbf{S}_u(\omega) = \mathbf{\Gamma}(\omega)S_o(\omega) \quad (4.7)$$

where  $\mathbf{\Gamma}$  is a coherency matrix of dimension  $M \times M$  whose each element is

$$\Gamma_{kl}(\omega) = \gamma(x_k, x_l, \omega) \quad (4.8)$$

In the case of coherent input motions (without spatial variability), all elements of the coherency matrix are equal to one. Generally, in linear seismic soil structure analysis, the seismic incident

field is considered to be homogeneous, which means that the stochastic description depends only on the distance ( $d = |x_k - x_l|$ ) but does not depend on the location of  $x_k$  and  $x_l$ .

For the case that the ground motion is modelled by non stationary, evolutive power spectral density (which is not carried out in our studies here), the equation 4.7 can be simply written as:

$$\mathbf{S}_u(\omega, t) = \mathbf{\Gamma}(\omega) S_o(\omega, t) \quad (4.9)$$

The principle of superposition, for linear analysis, allows to separate the seismic excitation in the three directions  $x, y$  and  $z$ . Consequently, equation 4.7 needs to be constructed according to the configuration and the coefficient  $M$  is equal to the number of nodes on the interfaces finite element mesh. In this case, equation 4.7 can be further written as:

$$\mathbf{S}_u(\omega) = \mathbf{\Phi}(\omega) \mathbf{\Lambda}(\omega) \mathbf{\Phi}^*(\omega) S_o(\omega) \quad (4.10)$$

where  $\mathbf{\Phi}(\omega)$  is the matrix containing the eigen vectors ( $\phi_n$ ) of the coherency matrix  $\mathbf{\Gamma}(\omega)$  and  $\mathbf{\Lambda}(\omega)$  is a diagonal matrix containing all eigen values ( $\lambda_n$ ) of the coherency matrix.

By writing  $\mathbf{S}_u(\omega) = \sum_{n=1}^M \mathbf{s}_u^n(\omega) \mathbf{s}_u^{n*}(\omega)$ , we can write from 4.10 :

$$\mathbf{s}_u^n(\omega) = \phi_n(\omega) \sqrt{\lambda_n(\omega)} \sqrt{S_o(\omega)} \quad (4.11)$$

If  $\mathbf{G}(\omega)$  is the transfer function matrix linking the seismic ground motion ( $\mathbf{S}_u(\omega)$ ) to seismic load ( $\mathbf{S}_f(\omega)$ ) in equation 4.5), which is:

$$\mathbf{S}_f(\omega) = \mathbf{G}(\omega) \mathbf{S}_u(\omega) \mathbf{G}^*(\omega) \quad (4.12)$$

and by writing  $\mathbf{S}_f(\omega) = \sum_{n=1}^M \mathbf{s}_f^n(\omega) \mathbf{s}_f^{n*}(\omega)$ , we can obtain the power spectral density of seismic loading :

$$\mathbf{s}_f^n(\omega) = \mathbf{G}(\omega) \phi_n(\omega) \sqrt{\lambda_n(\omega)} \sqrt{S_o(\omega)} \quad \text{for } n = 1, \dots, N \leq M \quad (4.13)$$

### 4.3.3 Power spectral density of structural responses and transfer function

As written in equation 4.5, the power spectral density of structural responses can be obtained by linear filtering:

$$\mathbf{s}_q^n(\omega) = \mathbf{H}(\omega) \mathbf{s}_f^n(\omega) \quad (4.14)$$

The transfer function  $\mathbf{H}(\omega)$  can be computed for unitary input motion ( $S_o(\omega) = 1$ ), and by computing the power spectral density of structural response in physical domain ( $\mathbf{V}_{\mathbf{o}}$  in Figure 4.8). We consider then the diagonal terms of the power spectral density of the structural responses that correspond to particular degree of freedom of the finite element model and evaluate the transfer function as  $\sqrt{[\mathbf{S}_{V_o}^N]_{ii}}$ .



#### 4.3.4 Transient analysis of structural responses

To get structural responses in time domain from power spectral density which is in frequency domain, the spectral representation theorem is used. The theorem says that there exists an orthogonal increment process  $\zeta(\omega)$  such that, for fixed time  $t$ :

$$\mathbf{u}(t) = \int_{\omega} e^{i\omega t} d\zeta(\omega) \quad (4.15)$$

where the complex vector process  $\zeta$  is centred and verifies :

$$\mathbb{E}[d\zeta(\omega_1)d\zeta(\omega_2)] = \begin{cases} 0 & \text{if } \omega_1 \neq \omega_2 \\ \mathbf{S}_{\mathbf{u}}(\omega)d\omega & \text{if } \omega_1 = \omega_2 \end{cases} \quad (4.16)$$

in which

$$d\zeta(\omega) = \mathbf{\Phi}(\omega)\mathbf{\Lambda}(\omega)^{1/2}\sqrt{S_o(\omega)}d\mathbf{W} \quad (4.17)$$

where  $\mathbf{W}$  is a vector-valued Wiener process, and  $\mathbb{E}$  is the mathematical expectation operator.

With this theorem, and by using the power spectral density of structural responses, the structural responses in time domain can be expressed as:

$$\mathbf{q}^N(t) = \sum_{n=1}^N \sum_{p=1}^P e^{i\omega_p t} \mathbf{H}(\omega_p) \mathbf{s}_f^n(\omega_p) \varepsilon_n(\omega_p) \sqrt{\Delta\omega} \quad (4.18)$$

where  $\varepsilon_n$  are complex independent centred Gaussian random variables of unit variance and  $\Delta\omega$  is the frequency step.

This expression can be evaluated by using Fast Fourier Transform (FFT) algorithm. Effectively, in frequency domain, we can write:

$$\hat{\mathbf{q}}^N(\omega) = \sum_{n=1}^N \mathbf{H}(\omega) \phi_n(\omega) \sqrt{\lambda_n(\omega)} \hat{u}_o(\omega) \quad (4.19)$$

where  $\hat{u}_o(\omega)$  is the Fourier transform of the given accelerogram  $u_o(t)$ .

Finally, the structural responses in time domain can be computed by the inverse Fourier transform of the frequency domain responses.

### 4.4 Influence of spatial variability of seismic ground motions on the responses of KK reactor building

The methodology to take into account the spatial variability of seismic ground motion in the soil-structure interaction analyses, by using coherency function was implemented in software Code\_Aster [Zentner, 2016] with the operator DYNA\_ISS\_VARI.

The analyses of soil-structure interaction are realized by using the coupling software Code\_Aster-MISS3D. The structure parts are analysed with Code\_Aster and the soil parts (impedance and seismic loading) are analysed with MISS3D. The finite element mesh, the properties of structural materials, the soil properties, as well as the input motions (earthquake signals) are presented in the section 4.2.



In this section, we present the influence of the spatial incoherence of seismic ground motions on the responses of linear SSI analysis of a Kashiwasaki-Kariwa reactor building (Unit 7). The comparisons between the structural responses for the case of coherent motions and incoherent motions are presented.

For the case of incoherent motions, 3 coherency models are used to represent the spatial variability of seismic ground motions. With the soil profile presented in Table 4.1, it is shown clearly that the site of Kashiwasaki-Kariwa power plant can be considered to be a soil site with the shear wave velocity for the first 30m of around 250m/s. Hence, the model of Abrahamson for soil site (equation 1.24 with the parameters in Table 1.5) is used for the analysis. But the building is embedded for 26m under the ground surface. The incoherent motions to be analysed need to be counted from that depth. For such case, the shear wave velocity for the first 30m counted from the foundation of the building needs to be evaluated. By using Table 4.1, the shear wave velocity for that case is 528m/s. Therefore, the media can be considered to be between the soft soil and the hard rock. The model of Abrahamson rock site (equation 1.24 with the parameters in Table 1.4) is also used for this analysis. The third coherency model is the model of [Sato et al., 2012], re-examined and validated in this Ph.D thesis. Without any knowledge of its parameters, the model of [Luco and Wong, 1986] is not used to analyse the structural response here, but in any case, with what is shown and discussed in Chapter 2 and Chapter 3, it can be said that the model of [Luco and Wong, 1986] is almost the same to the one of [Sato et al., 2012]. We cannot also get any knowledge about statistical properties of random media in the site of Kashiwasaki-Kariwa power plant. With what we can get from literature, and based on our analyses with numerical simulations presented in Chapter 3 (especially for the case of Argostoli site), the values of  $\ell_c = 30m$  and  $\xi = COV = 20\%$  are used for the model of [Sato et al., 2012] for this case-study.

For analysing the influence of spatial variability of seismic ground motions on the structural responses, we present the spectral acceleration of several points on the structure. The first point whose spectral accelerations in direction X and direction Y are presented in Figure 4.9 is a point situated at the top of internal structure. Another point presented in Figure 4.10 is about the point R1 (see Figure 4.2 for its location). One can remark clearly that the spectral accelerations of the case with incoherent input motions are smaller than those with coherent input motions. It is simply confirmed to what is found in the literature. Between the structural responses given by incoherent input motion using both Abrahamson models and model of [Sato et al., 2012], it is shown that the model of [Sato et al., 2012] gives the spectral accelerations slightly smaller than those given by two other models. The Abrahamson model of hard rock always gives the spectral accelerations greater than other two coherency models. The differences between the responses given by different coherency models could be explained by Figure 4.11 where we compare the coherencies of different models for several separation distances. It can be remarked clearly that except the case of  $d = 10m$ , the coherency model of Sato always gives the coherency smaller than the two models of Abrahamson.

## 4.5 Conclusion on the industrial application case study

The methodology to take into account the spatial variability, developed and implemented in open software Code\_Aster by [Zentner and Devesa, 2011], is summarised and presented. This methodology is used to analyse the structural responses in terms of spectral accelerations of a reactor building of the Kashiwasaki-Kariwa nuclear power plant. As expected, based on literature, the structural responses of the case with incoherent input motions (represented by coherency functions) are always smaller than the case with coherent motions.

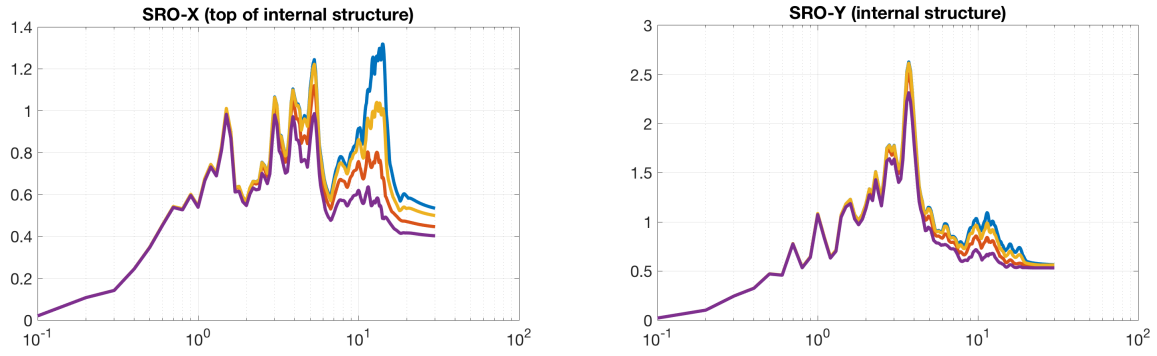


Figure 4.9 – spectral accelerations of a point at the top of internal structure

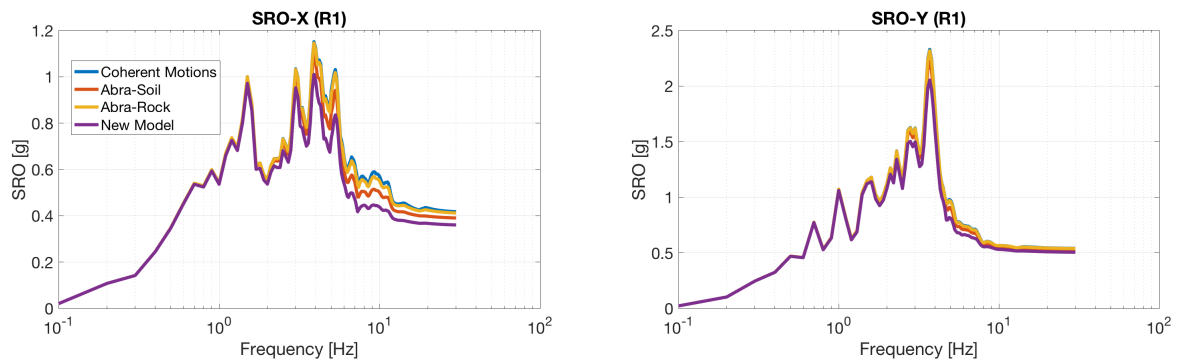


Figure 4.10 – spectral accelerations of the point R1

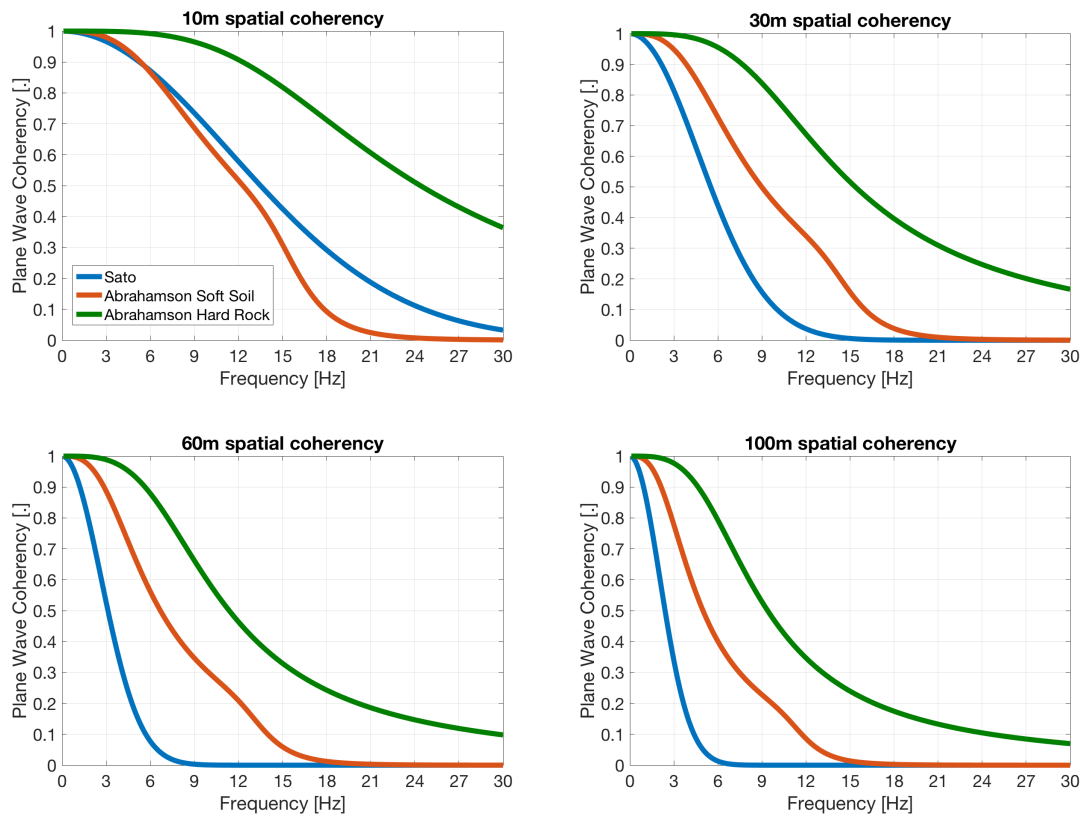


Figure 4.11 – Comparison between the coherencies obtained from different coherency models

Three coherency models are used for this analysis : the two models of Abrahamson for hard rock and for soft soil and the model of Sato. Without any available informations about the statistical properties of the soil in the media, we selected some reasonable parameters based on our literature reviews and numerical simulation studies. Those parameters give significantly small values of coherencies for model of Sato. But in terms of structural responses, although the structural responses obtained by using Abrahamson model are greater those obtained by using model of Sato, the difference is not completely significant. This can be due to the fact that the input signals at high frequencies are not important. Reminding that the spatial variability of earthquake ground motions can have significant influence on the structural response spectra at high frequencies. In our case-study here, the amplitude of Fourier transforms of input signals are almost zero when frequencies are higher than even  $10Hz$ .

Anyway, although the input motions possess of only small frequency signals, still the structural responses obtained by taking into account the spatial variability of seismic ground motions are smaller than the case of coherent input motions, even for such building size.



# Summery and Conclusions

*“In human affairs of danger and delicacy successful conclusion is sharply limited by hurry.”*

JOHN STEINBECK

The principal objective of this Ph.D thesis is to analyse the possibility of providing a parametrical coherency model of the spatial variability of seismic ground motions for using in the analyses of soil-structure interaction, and to show the importance of taking into account the spatial variability of seismic ground motions in such analysis.

Based on the coherency models existing in the literature, and on theoretical considerations to define a coherency function from seismic wave propagation in random heterogeneous media, several coherency models are selected to be analysed in our studies. Reminding that the three tasks identified to be realised in this Ph.D thesis are : (1) theoretical analyses of seismic wave propagation in random heterogeneous media to define a parametrical coherency function, (2) analyses the available earthquake signals to define the empirical coherency functions (in which we use Argostoli database), and (3) numerical analysis to understand more profoundly about the physical aspects of the influence of the physical and statistical properties of random heterogeneous media on the spatial variability of seismic ground motions and to validate the selected coherency model.

For the first task, we start by analysing the existing coherency models in the literature. Although many models are proposed and used in these last three decades, there are always some cases that the models cannot be used, and there are always several studies showing the limitations of those models. Among all of the models proposed, we selected two models to be analysed more precisely by using the *insitu* coherencies estimated from Argostoli which is realised in the second task. They are the model of Abrahamson and the model of Luco&Wong. These are the most used models in literature. With almost the same functional form of the model of Luco&Wong, we give a brief description of theoretical considerations to define a coherency function from seismic wave propagation in random heterogeneous media, introduced by [Sato et al., 2012], and we call the coherency model extended from that theoretical analysis as the model of Sato. Because of the existence of theoretical analyses with good understanding in physical as well as statistical aspects, this model is finally selected to be analysed profoundly in this Ph.D thesis, by comparing to the *insitu* coherencies (realised in the second task), and also by using numerical simulations (realised in the third task).

For the second task, the empirical (*insitu*) coherencies are estimated from Argostoli database. Many analyses are realised to understand which statistical and physical factors can influence the estimated coherencies. But in many case, it is interesting to conclude in this part that there is no significant influence of earthquake signal components, epicentral distances, strong motion durations, and selected signal window, on the estimated average spatial coherencies. It is also concluded that for around 100 to 150 realisations of coherency, we can already get a good estimation of average coherencies. The most interesting results of that part is about the fact that there is no significant

difference between the coherencies estimated from strong motion windows and those estimated from the coda of signals. We can mention that it is an important remark in this study, which should be verified for other earthquake sites to see if this conclusion is always correct. Finally, the last important conclusion of this second part, is about the comparison between *insitu* coherencies of Argostoli database and the coherency models of Abrahamson, Luco&Wong, and Sato. We can state that without any modifications, the three models cannot provide a satisfactory result in term of coherencies when they are compared to the Argostoli coherencies. But, one of the most interesting remark about it is that by modifying slightly their parameters, the coherency models can provide a satisfactory result. About the model of [Luco and Wong, 1986], the conclusion from this comparison is that the parameter  $\alpha$  is not constant (or constant only for some intervals station separation distances) which was also remarked by other studies in the literature. About the model of [Sato et al., 2012], it seems that with some modifications of its parameters, based on the help of the third task in numerical simulations, the model gives a satisfactory result of coherencies.

With the conclusion of the first and the second task, the coherency model of Sato is selected to be analysed with numerical case-studies, by using spectral element method, implemented in software SEM3D. The goal of numerical assessment realised in these studies is to model numerically the seismic wave propagation in random heterogeneous media, in order to get synthetic seismic signals on the ground surface. The conclusion about this analysis is that the spatial coherencies of seismic ground motions can depend on the velocity of seismic wave propagation in the media (which is the shear-wave velocity, in our studies here), the degree of fluctuation of random properties (coefficient of variation), the correlation length of the media, and the depth of random media. The latter one can influence the coherencies only in the case that its value is not important compared to correlation length of the media. When it becomes important, based on our analysis, this parameter should be replaced by correlation length of the heterogeneous media. In each analysis, we also compare the synthetic coherencies to the coherency model of [Sato et al., 2012]. By modifying slightly the parameter  $Z$ , as what is just mentioned, we can conclude on the validation of this model. The coherency model validated in these studies are for the station separations between 10m and 100m which is conformed to the industrial applications.

By knowing some physical profiles of the site of Argostoli, we also perform a numerical simulation of seismic wave propagation in random media of Argostoli site. Based on the coherencies estimated from Argostoli database, we realised a parametrical study, with numerical simulations, to define the statistical properties of the media. The goal of that study is to define which couple of  $(\ell_c, COV)$  can provide the coherencies that are closest to the *insitu* coherencies. From this analysis, it is found that the couple of  $(\ell_c = 30m, COV = 20\%)$  is the best couple to give the most satisfactory coherencies. The statistical properties obtained from that analysis is used for comparing the coherency model of Sato to the *insitu* coherencies of Argostoli to give a full validation of the coherency model.

Last, but not least, we perform an analysis of seismic soil-structure interaction with taking into account the spatial variability of seismic ground motions. The spatial variability is represented by a coherency function in probabilistic framework. We perform an analysis of a reactor building of the Kashiwasaki-Kariwa nuclear power plant. The validated coherency model is used for accounting for the incoherent ground motions in the soil-structure interaction analyses. As what is found in literature, although the input signals do not possess of significant high frequency contents, the difference in term of spectral accelerations between the coherent input motions and incoherent input motions is still significant. This result encourage the analyses of soil-structure interactions to consider the effects of spatial variability of seismic ground motions.

# Perspectives

*“Most misunderstandings in the world could be avoided if people would simply take the time to ask, “What else could this mean?” ”*

SHANNON L. ALDER

The coherency model validated in this Ph.D thesis has some statistical parameters (correlation length  $\ell_c$  and coefficient of variation  $COV$ ) which are not easily defined on the arbitrary sites. It is therefore not practical to apply the model without having any knowledge about these two parameters. These two parameters should be evaluated clearly in order to be used for the coherency model.

It is also seen that there exists a coefficient 4 which is until now not clarified about its origin. In our studies realized in this Ph.D thesis, it is selected to be conform with not only numerical results but also experimental results, but it should be proved theoretically. More theoretical analyses might be needed to clarify this coefficient based on the notion of the mean free path of the random heterogeneous media.

Another important remark might be dedicated to the non-linear case. All numerical analyses presented here are realized with the linear properties of the media. The coherency model validated in this Ph.D thesis can be used for a site with linear properties of the soil. Further analyses should be realized to see if the non-linear properties of the soil can also influence the spatial coherencies of seismic ground motions.





# Appendices



## Appendix A

# Spectral densities of seismic signals and their smoothing

Mathematically, power spectral densities ( $S_{jj}$  and  $S_{kk}$ ) and cross spectral density ( $S_{jk}$ ) can be respectively determined by Fourier transform of auto-covariance functions  $R_{jj}(\tau)$ ,  $R_{kk}(\tau)$  and cross covariance function  $R_{ij}(\tau)$  of time series  $a_j(t)$  and  $a_k(t)$  :

$$R_{jj}(\tau) = \begin{cases} \frac{1}{T} \int_0^{T-|\tau|} a_j(t) a_j(t+\tau) dt & \text{for } |\tau| \leq T \\ 0 & \text{for } |\tau| > T \end{cases} \quad (\text{A.1})$$

$$R_{jk}(\tau) = \begin{cases} \frac{1}{T} \int_0^{T-|\tau|} a_{jk}(t) a_k(t+\tau) dt & \text{for } |\tau| \leq T \\ 0 & \text{for } |\tau| > T \end{cases} \quad (\text{A.2})$$

where  $T$  indicates the duration of the analysed segment of the time series.

The power spectra are defined by:

$$S_{jj}(\omega) = \frac{1}{2\pi} \int_{-\infty}^{+\infty} R_{jj}(\tau) e^{-i\omega\tau} d\tau \quad (\text{A.3})$$

$$S_{jk}(\omega) = \frac{1}{2\pi} \int_{-\infty}^{+\infty} R_{jk}(\tau) e^{-i\omega\tau} d\tau \quad (\text{A.4})$$

By letting  $A_j(\omega) = \Lambda_j(\omega) \exp[i\Phi_j(\omega)]$  and  $A_k(\omega) = \Lambda_k(\omega) \exp[i\Phi_k(\omega)]$  be respectively the Fourier transforms of time histories  $a_j(t)$  and  $a_k(t)$ , one can evaluate directly the power spectral density  $S_{jj}(\omega)$  and cross spectral density  $S_{jk}(\omega)$  as following:

$$S_{jj}(\omega) = \frac{2\pi}{T} A_j^*(\omega) A_j(\omega) \quad (\text{A.5})$$

$$S_{jj}(\omega) = \frac{2\pi}{T} \Lambda_j^2(\omega) \quad (\text{A.6})$$

$$S_{jk}(\omega) = \frac{2\pi}{T} A_j^*(\omega) A_k(\omega) \quad (\text{A.7})$$

$$S_{jk}(\omega) = \frac{2\pi}{T} \Lambda_j(\omega) \Lambda_k(\omega) \exp[i\{\Phi_k(\omega) - \Phi_j(\omega)\}] \quad (\text{A.8})$$

where  $*$  denotes complex conjugate.

The smoothed spectral densities can be obtained by smoothing the spectral densities with a window function  $w(\tau)$  :

$$\bar{S}_{jj}(\omega) = \frac{1}{2\pi} \int_{-\infty}^{+\infty} w(\tau) R_{jj}(\tau) e^{-i\omega\tau} d\tau = \frac{1}{2\pi} \int_{-\infty}^{+\infty} \bar{R}_{jj}(\tau) e^{-i\omega\tau} d\tau \quad (\text{A.9})$$

where  $\bar{R}_{jj}(\tau) = w(\tau)R_{jj}(\tau)$  is the smoothed auto-covariance function and  $w(\tau)$  is a lag window with properties:

$$\begin{cases} w(0) = 1 \\ w(\tau) = w(-\tau) \\ w(\tau) = 0 \end{cases} \quad \text{for } |\tau| \geq T \quad (\text{A.10})$$

Equivalently, the smoothed spectral estimate can be evaluated directly in the frequency domain through the following convolution expression:

$$\bar{S}_{jj}(\omega) = \int_{-\infty}^{+\infty} W(u) S_{jj}(\omega - u) du \quad (\text{A.11})$$

where the spectral window  $W(\omega)$  and the lag window  $w(\tau)$  are Fourier transforms of each other, i.e.,

$$W(\omega) = \frac{1}{2\pi} \int_{-\infty}^{+\infty} w(\tau) e^{-i\omega\tau} d\tau \quad (\text{A.12})$$

and

$$w(\tau) = \int_{-\infty}^{+\infty} W(\omega) e^{i\omega\tau} d\omega \quad (\text{A.13})$$

The spectral window  $W(\omega)$  has the following properties:

$$\begin{cases} \int_{-\infty}^{+\infty} W(\omega) d\omega = w(0) = 1 \\ W(\omega) = W(-\omega) \end{cases} \quad (\text{A.14})$$

For discrete frequencies, the equation (30) takes the form:

$$\bar{S}_{jj}^M(\omega_n) = \sum_{m=-M}^{+M} W(m\Delta\omega) S_{jj}(\omega_n + m\Delta\omega) \quad (\text{A.15})$$

$$\bar{S}_{jj}^M(\omega_n) = \frac{2\pi}{T} \sum_{m=-M}^{+M} W(m\Delta\omega) \Lambda_j^2(\omega_n + m\Delta\omega) \quad (\text{A.16})$$

where  $\Delta\omega = 2\pi/T$  is the frequency step,  $\omega_n = n\Delta\omega$  is the discrete frequency,  $W(m\Delta\omega)$  is the spectral window,  $2M+1$  the number of frequencies over which the averaging is performed, and the superscript  $M$  indicates the dependence of the estimate on the length of the smoothing window.

With the same proofs, the cross spectral density can be evaluated by:

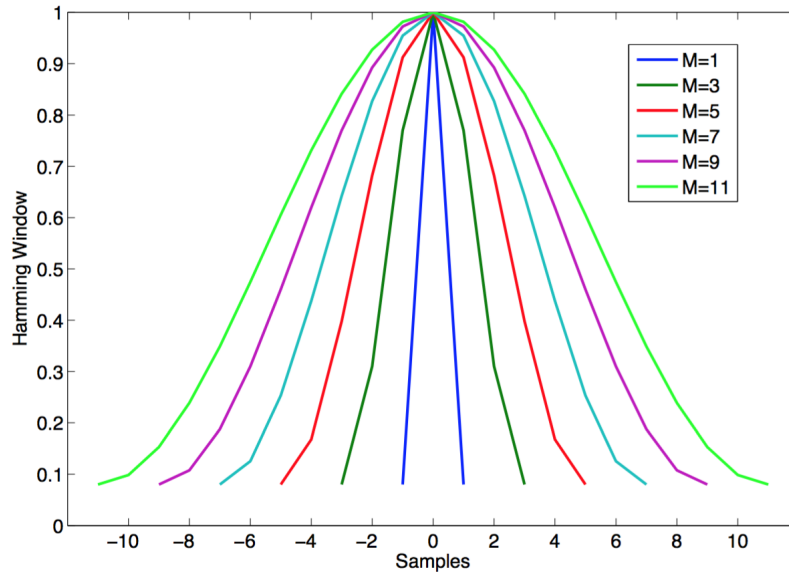
$$\begin{aligned} \bar{S}_{jk}^M(\omega_n) &= \frac{2\pi}{T} \sum_{m=-M}^{+M} W(m\Delta\omega) \Lambda_j(\omega_n + m\Delta\omega) \Lambda_k(\omega_n + m\Delta\omega) \\ &\quad \times \exp(i[\Phi_k(\omega_n + m\Delta\omega) - \Phi_j(\omega_n + m\Delta\omega)]) \end{aligned} \quad (\text{A.17})$$

From the available smoothing windows, the Hamming window is most commonly used for smoothing the seismic spectral estimates. The expression of this function is given by:

$$W(m) = 0.54 - 0.46 \cos\left(\frac{\pi(m+M)}{M}\right) \quad \text{for } m = -M, \dots, M \quad (\text{A.18})$$

The width of the window (or the number of points of window) is given by  $2M + 1$  for  $M = 1, 3, 5, 9, \dots$ . Figure A.1 illustrated the graphical representation of Hamming Window function for  $M = 1, 3, 5, 9$  and 11. The area underneath the Hamming window is  $1.08M$ . After [Zerva, 2009], if window is used in frequency domain it ought to satisfy the characteristics of spectral windows (equation A.14), hence, the area underneath the window needs to be equal to unity, i.e., the right-hand of equation A.18 needs to be divided by  $1.08M$ . The expression of Hamming window function in frequency domain for smoothing the seismic data becomes:

$$W(m) = \frac{0.54 - 0.46 \cos\left(\frac{\pi(m+M)}{M}\right)}{1.08M} \quad \text{for } m = -M, \dots, M \quad (\text{A.19})$$



**Figure A.1** – Hamming windows for  $M = 1, 3, 5, 7, 9$  and 11

An 11-point Hamming window was recommended by Abrahamson [Abrahamson et al., 1991] for smoothing in frequency domain for time windows with less than approximately 2000 samples, if the coherency estimates were to be used for analysis of structures with 5% critical damping.





## Appendix B

# Verification of coherency estimator

This appendix presents a simple test to verify the coherency estimator establish in a MATLAB code for estimating coherencies from earthquake signal database based on the methodologies presented previously in this section. The principal idea of this test, is to give a signal at a point on the ground surface and to generate the signals at other points by knowing a coherency function. The synthetic signals obtained from numerical simulations are used for estimating the coherencies. The average of synthetic coherencies is then compared to the coherency function which is used in signal generations in the beginning.

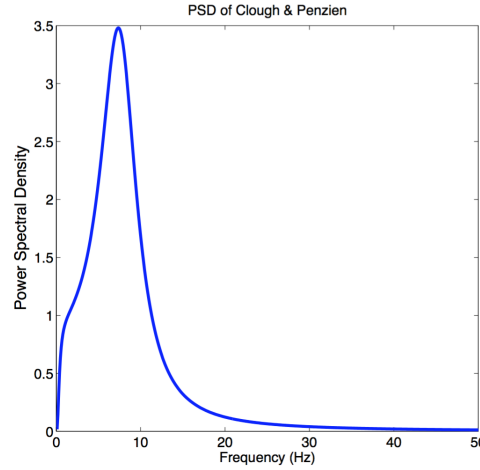
For the given signal, we consider that its power spectral density (PSD) is the analytical power spectral density of [Clough and Penzien, 1993]. The latter one is a modified model of the PSD of Kanai-Tajimi [Kanai, 1957], [Tajimi, 1960]. The parametrical expression of PSD of [Clough and Penzien, 1993] is often used by researchers to represents the PSD of seismic signals. The expression of the Clough&Penzien PSD is given by:

$$S(\omega) = \frac{\omega_g^4 + 4\xi_g^2\omega_g^2\omega^2}{(\omega_g^2 - \omega^2)^2 + 4\xi_g^2\omega_g^2\omega^2} S_o \cdot \frac{\omega^4}{(\omega_f^2 - \omega^2)^2 + 4\xi_f^2\omega_f^2\omega^2} \quad (\text{B.1})$$

with:

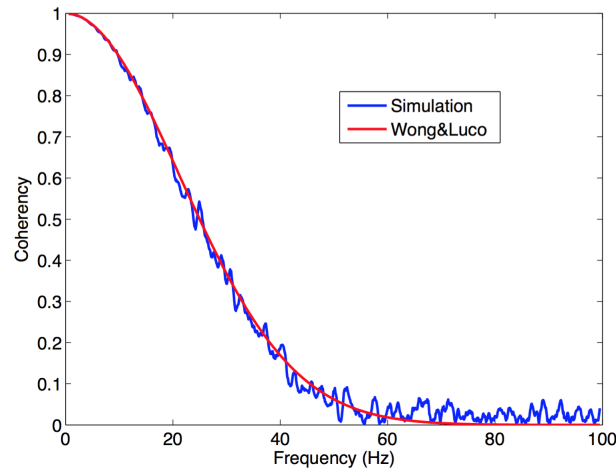
- $\omega_g = 2\pi f_g$  eigen frequency (circular) of soil
- $\xi_g$  damping ratio of soil
- $S_o$  white noise level before filtering
- $\omega_f$  circular frequency of high-pass filtering
- $\xi_f$  damping ratio of high-pass filtering

Note that the two parameters  $\omega_f$  and  $\xi_f$  were added to original model of Kanai-Tajimi which is described only by the first term of the right side in the equation B.1, in order to define the PSD when the frequency tends to zero. The PSD of Clough&Penzien for  $S_o = 1, \xi_g = 0.33, \xi_f = 1, f_g = 8Hz$  et  $f_f = 0.25$  is presented in Figure B.1 and considered in our study here.



**Figure B.1** – Power Spectral Density of Clough & Penzien

This PSD is used to generate two signals considered to be separated of 40m from each other. This generation is realized by using the "spectral representation method" and by considering that the spatial coherency of ground signals can be described by the coherency model of [Luco and Wong, 1986]. With the utilization of spectral representation method, the signals obtained will be stationary which correspond well to our statistic estimator. The two signals obtained from this generation are used to calculate the spatial plane-wave coherency by using the estimator implemented in MATLAB code. Figure B.2 presents the comparison between the coherency model of [Luco and Wong, 1986] and the coherency estimated from the generated signals by using the estimator presented above. The plane-wave coherency compared with coherency model here is simply an average of coherencies estimated from 100 pairs of signals (100 realisations).



**Figure B.2** – Comparison between the coherency model of Luco&Wong and the coherency estimated from simulated realizations

This figure shows clearly the agreement between the original coherency model of [Luco and Wong, 1986] used for the generation of signals and the coherency obtained by the estimator. This agreement can confirm that the MATLAB code used as a coherency estimator can give a good estimation of coherencies. That estimator is then used for the coherency estimations of Ar-

gostoli database (in Chapter 2) as well as of synthetic earthquake signals obtained from numerical modelling of wave propagation in random heterogeneous media (in Chapter 3).



## Appendix C

# Distributions of station pairs for different distances of separation of Argostoli dense array

With the dense array geometry presented in Figure [2.2](#), the station separations can be grouped to analyse the spatial coherencies of earthquake ground motions. The distributions of station pairs for different station separations are presented in Table [C.1](#).

09 m - 11 m	19 m - 21 m	29 m - 31 m	34 m - 36 m
B0R0-B1R1 (09.53 m)	B2R2-B2R1 (19.34 m)	B0R0-B2R2 (29.23 m)	B2R2-B3R2 (34.16 m)
B0R0-B2R1 (09.88 m)	B4R1-B4R2 (20.24 m)	B0R0-B3R2 (29.91 m)	B1R2-B2R2 (35.15 m)
B0R0-B3R1 (09.93 m)	B5R1-B5R2 (19.42 m)	B0R0-B4R2 (30.24 m)	B3R2-B4R2 (35.65 m)
B0R0-B4R1 (10.00 m)	B3R1-B5R1 (19.16 m)	B0R0-B5R2 (29.41 m)	B4R2-B5R2 (35.56 m)
B0R0-B5R1 (10.00 m)	B1R1-B1R2 (19.39 m)	B4R2-B5R1 (29.43 m)	-
37 m - 39 m	54 m - 56 m	64 m - 66 m	79 m - 81 m
B1R1-B4R2 (38.49 m)	B4R2-B4R3 (54.70 m)	B1R2-B1R3 (64.07 m)	B2R1-B2R3 (80.42 m)
B1R2-B4R1 (37.23 m)	B1R2-B4R2 (55.95 m)	B5R2-B5R3 (64.77 m)	B4R3-B5R2 (80.87 m)
B1R2-B3R1 (37.52 m)	B2R2-B5R2 (55.70 m)	-	-
B2R1-B4R2 (38.62 m)	-	-	-
B2R1-B5R2 (38.82 m)	-	-	-
B2R2-B5R1 (37.53 m)	-	-	-
B2R2-B4R1 (37.80 m)	-	-	-
B3R1-B5R2 (37.99 m)	-	-	-
B3R2-B5R1 (38.80 m)	-	-	-
84 m - 86 m	89 m - 91 m	94 m - 96 m	99 m - 101 m
B0R0-B4R3 (84.93 m)	B0R0-B2R1 (90.26 m)	B0R0-B5R3 (94.17 m)	B1R3-B4R1 (100.83 m)
B1R2-B2R3 (84.47 m)	B1R3-B2R1 (91.00 m)	B1R1-B3R3 (94.75 m)	B1R3-B3R1 (101.43 m)
B2R1-B3R3 (84.10 m)	B1R3-B2R2 (90.29 m)	B1R3-B1R4 (95.80 m)	B2R3-B4R1 (99.000 m)
B5R1-B5R3 (84.18 m)	B1R3-B5R1 (89.20 m)	-	-
B3R3-B4R1 (85.80 m)	B2R3-B2R4 (89.20 m)	-	-
B3R3-B4R2 (85.50 m)	B4R2-B5R3 (90.95 m)	-	-
B5R3-B5R4 (85.75 m)	-	-	-

Table C.1 – Distributions of station pairs for different separations

## Appendix D

# Introduction to spectral element method and software SEM3D

In the following, we introduce briefly the mathematical formulations of spectral element method in the resolutions of elastodynamic problems, especially, in wave propagation in random heterogeneous media.

### D.1 Equation of motions

The elastodynamic equilibrium equation of a motion describing the elastic wave propagation in an elastic medium of an open domain  $\Omega \subseteq \mathbb{R}^3$  (for  $\mathbf{x} = (x, y, z) \in \Omega$  and  $t \in [0, T]$ ) can be written by:

$$\nabla_{\mathbf{x}} \boldsymbol{\sigma}(\mathbf{x}) = \rho(\mathbf{x}) \frac{\partial^2 \mathbf{u}(\mathbf{x}, t)}{\partial t^2} \quad (\text{D.1})$$

in which,  $\boldsymbol{\sigma}$  is the Cauchy stress tensor,  $\rho(\mathbf{x})$  is the local density of the medium at a position  $\mathbf{x} = (x, y, z)$ , and  $\mathbf{u}$  is the displacement field. For an isotropic linear elastic medium, the stress tensor for the case of small strain tensor  $\boldsymbol{\epsilon}$  can be given by the Hook's law:

$$\boldsymbol{\sigma}(\mathbf{x}) = \mathbf{C}(\mathbf{x}) : \boldsymbol{\epsilon}(\mathbf{u}(\mathbf{x})) = \lambda(\mathbf{x}) \text{tr}[\boldsymbol{\epsilon}(\mathbf{u}(\mathbf{x}))] \mathbf{I} + 2\mu(\mathbf{x}) \boldsymbol{\epsilon}(\mathbf{u}(\mathbf{x})) \quad (\text{D.2})$$

and strain tensor  $\boldsymbol{\epsilon}$  is defined by:

$$\boldsymbol{\epsilon}(\mathbf{u}(\mathbf{x})) = \text{sym}(\nabla_{\mathbf{x}} \mathbf{u}(\mathbf{x})) = \frac{\nabla_{\mathbf{x}} \mathbf{u}(\mathbf{x}) + (\nabla_{\mathbf{x}} \mathbf{u}(\mathbf{x}))^T}{2} \quad (\text{D.3})$$

where  $\lambda(\mathbf{x})$  and  $\mu(\mathbf{x})$  are the local Lamé modulus, and  $\mathbf{C}(\mathbf{x})$  is the forth-order elastic tensor.

Replacing [D.2](#) and [D.3](#) into [D.1](#), one can obtain the elastic wave equation in an isotropic medium written as:

$$\rho(\mathbf{x}) \frac{\partial^2 \mathbf{u}(\mathbf{x}, t)}{\partial t^2} = (\lambda(\mathbf{x}) + 2\mu(\mathbf{x})) \nabla(\nabla \cdot \mathbf{u}(\mathbf{x}, t)) - \mu(\mathbf{x}) \nabla \times \nabla \mathbf{u}(\mathbf{x}, t) \quad (\text{D.4})$$

Applying the curl and divergence operators to both sides of [D.4](#), we can obtain equations for compressional waves (P-waves) and shear waves (S-waves) defined by:

$$\Delta(\nabla \cdot \mathbf{u}(\mathbf{x}, t)) - \frac{1}{v_p^2(\mathbf{x})} \frac{\partial^2(\nabla \cdot \mathbf{u}(\mathbf{x}, t))}{\partial t^2} = 0 \quad \text{for} \quad v_p(\mathbf{x}) = \sqrt{\frac{\lambda(\mathbf{x}) + 2\mu(\mathbf{x})}{\rho(\mathbf{x})}} \quad (\text{D.5})$$



and

$$\Delta (\nabla \times \mathbf{u}(\mathbf{x}, t)) - \frac{1}{v_p^2(\mathbf{x})} \frac{\partial^2 (\nabla \times \mathbf{u}(\mathbf{x}, t))}{\partial t^2} = 0 \quad \text{for} \quad v_s(\mathbf{x}) = \sqrt{\frac{\mu(\mathbf{x})}{\rho(\mathbf{x})}} \quad (\text{D.6})$$

where  $v_p$  and  $v_s$  are respectively the propagation velocities of P-waves and S-waves.

For the case of existence of any external forces  $\mathbf{f}$  applying at any point of the medium, [D.1](#) becomes:

$$\nabla_{\mathbf{x}} \boldsymbol{\sigma}(\mathbf{x}) + \mathbf{f} = \rho(\mathbf{x}) \frac{\partial^2 \mathbf{u}(\mathbf{x}, t)}{\partial t^2} \quad (\text{D.7})$$

## D.2 Weak formulation

For a displacement and velocity vector fields denoted respectively by  $\mathbf{u}(\mathbf{x}, t)$  and  $\mathbf{v}(\mathbf{x}, t)$ , the weak formulation of the elasto-dynamic equilibrium equations can be written for any test function  $\mathbf{w}$  by [\[Komatitsch et al., 1999\]](#):

$$\begin{cases} (\mathbf{w}, \rho \dot{\mathbf{v}})_{\Omega} = (\mathbf{w}, \mathbf{f})_{\Omega} - \mathbb{A}_{\Omega}(\mathbf{w}, \mathbf{u}) \\ (\mathbf{w}, \rho \dot{\mathbf{v}})_{\Omega} = (\mathbf{w}, \mathbf{v})_{\Omega} \end{cases} \quad (\text{D.8})$$

with initial conditions:

$$\begin{cases} (\mathbf{w}, \mathbf{u}(\mathbf{x}, t=0))_{\Omega} = (\mathbf{w}, \mathbf{u}_o)_{\Omega} \\ (\mathbf{w}, \mathbf{v}(\mathbf{x}, t=0))_{\Omega} = (\mathbf{w}, \mathbf{v}_o)_{\Omega} \end{cases} \quad (\text{D.9})$$

where the classical inner product  $(\cdot, \cdot)_{\Omega}$  and  $\mathbb{A}_{\Omega}(\mathbf{w}, \mathbf{u})$  are defined by:

$$(\mathbf{w}, \mathbf{u})_{\Omega} = \int_{\Omega} \mathbf{w} \cdot \mathbf{u} dV \quad (\text{D.10})$$

$$\mathbb{A}_{\Omega}(\mathbf{w}, \mathbf{u}) = \int_{\Omega} \nabla_{\mathbf{x}} \mathbf{w} : \mathbf{C} : \text{sym}(\nabla_{\mathbf{x}} \mathbf{u}) dV \quad (\text{D.11})$$

## D.3 Spatial discretizations

Like in finite element methods, the physical domain  $\Omega$  is partitioned into a finite ensemble of non-overlapping elements  $\Omega_e$  such that  $\cup_{e=1}^{n_{el}} \Omega_e = \Omega$  where  $n_{el}$  is the total number of elements. With this partition, the integral on the whole domain can be written as :

$$(\mathbf{w}, \mathbf{u})_{\Omega} = \sum_{e=1}^{n_{el}} (\mathbf{w}^e, \mathbf{u}^e)_{\Omega}^e = \sum_{e=1}^{n_{el}} \int_{\Omega_e} \mathbf{w}^e \cdot \mathbf{u}^e dV^e \quad (\text{D.12})$$

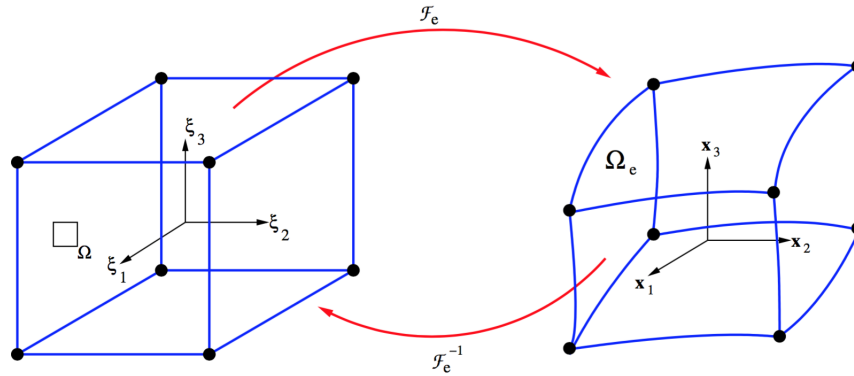
Considering  $\square_{\Omega} = [-1, 1]^3$  is the reference volume. For each element  $\Omega_e$  we suppose that there exists an invertible mapping function  $\mathcal{F}_e$  between the reference volume  $\square_{\Omega}$  and a local coordinate system  $\boldsymbol{\xi}$  of the element  $\Omega_e$ , defined as  $\mathcal{F}_e : \square_{\Omega} \rightarrow \Omega_e$  such that  $\mathbf{x}(\boldsymbol{\xi}) = \mathcal{F}_e(\boldsymbol{\xi})$  (see [Figure D.1](#)). This mapping can be used to go between the physical and the reference domain, and vice versa. Such a transformation can be defined from the multidimensional shape functions constructed by  $n$ -th Lagrange polynomial,  $l_i^n$ ,  $1 \leq i \leq n+1$ , associated with  $n+1$  points on the segment  $[-1, 1]$ . The point  $\mathbf{x}$  in element  $\Omega_e$  is uniquely related to the point  $\boldsymbol{\xi}$  in the reference element  $\square_{\Omega}$  via the invertible mapping:

$$\mathbf{x}(\boldsymbol{\xi}) = \mathcal{F}_e(\boldsymbol{\xi}) = \sum_{i=1}^{n_p} \mathbf{a}^i N_i(\boldsymbol{\xi}) \quad (\text{D.13})$$

where  $\{\mathbf{a}^i\}_{i=1,\dots,n_p}$  is the ensemble of the control points of  $\Omega_e$  and  $N_i$  is the tensor product of Lagrange polynomial associated to the control node  $\boldsymbol{\xi}_i$  de  $\square_{\Omega}$  ( $\mathbf{x}(\boldsymbol{\xi}^i) = \mathbf{a}^i$ ):

$$N_i(\boldsymbol{\xi}) = \otimes_{j=1}^d \mathbf{l}_i^{n_p}(\xi_j) \quad (\text{D.14})$$

for  $j \in \{1, 2, 3\}$ ,  $\xi_j \in [-1, 1]$ .



**Figure D.1** – 8-node hexahedral reference element and the mapping function

The Jacobian of the mapping can be written:

$$\mathbf{J} = \nabla_{\boldsymbol{\xi}} \mathbf{x} = \sum_{i=1}^{n_p} \mathbf{a}^i \frac{\partial N_{\mathbf{a}^i}(\boldsymbol{\xi})}{\partial \boldsymbol{\xi}} \quad (\text{D.15})$$

The order  $n$  is often considered to be small (1 for linear and 2 for quadratic), the shape function  $N$  is defined by :

$$N_{\mathbf{a}^j}(\boldsymbol{\xi}(\mathbf{a}^j)) = \delta_{ij} \quad (\text{D.16})$$

for which,  $\delta_{ij}$  is the Kronecker's delta function.

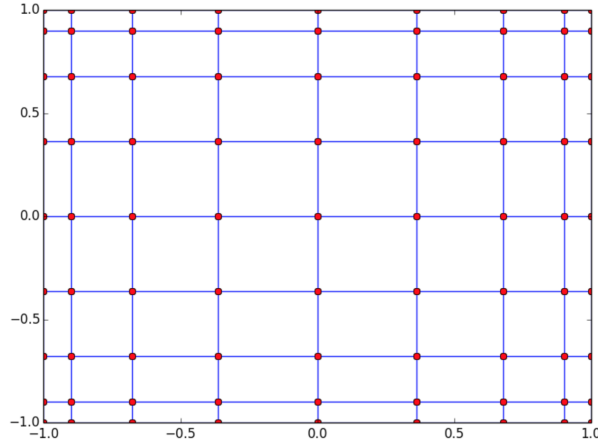
The Lagrange polynomials for  $n_p$  control points following each direction are defined by:

$$l_{\alpha}^{n_p}(\xi) = \frac{(\xi - \xi_1)(\xi - \xi_2) \cdots (\xi - \xi_{\alpha-1})(\xi - \xi_{\alpha+1}) \cdots (\xi - \xi_{n_p})}{(\xi_{\alpha} - \xi_1)(\xi_{\alpha} - \xi_2) \cdots (\xi_{\alpha} - \xi_{\alpha-1})(\xi_{\alpha} - \xi_{\alpha+1}) \cdots (\xi_{\alpha} - \xi_{n_p})} \quad (\text{D.17})$$

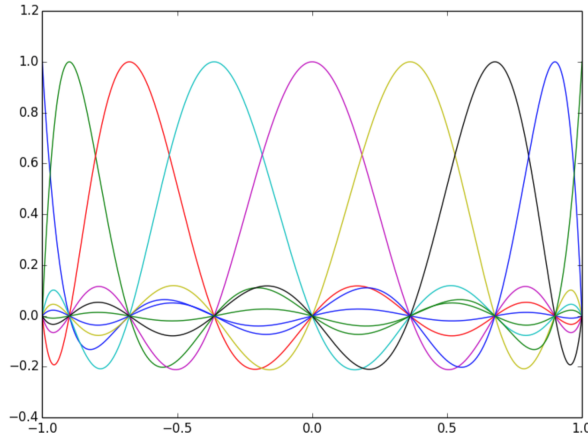
for  $\alpha = 1, 2, \dots, n_p$  and  $-1 \leq \xi_{\alpha} \leq 1$ .

In spectral element method, the Lagrange polynomial of degree 4 to 9 are normally used to interpolate the wave field (displacement  $\mathbf{u}(\mathbf{x}, t)$ ). After [Tromp et al., 2008], using 4th or 5th order Lagrange polynomial might provide a best trade-off between accuracy and computational time. The control points  $\xi_i (i = 1, \dots, n)$  needed in D.17 are the Gauss-Lobatto-Legendre points, which are the roots of equation:

$$(1 - \xi^2) \frac{P_n(\xi)}{d\xi} = 0 \quad (\text{D.18})$$



**Figure D.2** – Positions of GLL points on a 2D element of order 9 [Aubry, 2016]



**Figure D.3** – Lagrange polynomial of order 9 [Aubry, 2016]

where  $P_n$  denotes the Legendre polynomial of degree  $n$  defined by [Abramowitz and Stegun, 2012]:

$$P_n(\xi) = \frac{1}{2^n n!} \frac{d^n}{d\xi^n} ((\xi^2 - 1)^n) \quad (\text{D.19})$$

A sample of position of GLL points on a 2D element of 9th order is shown in Figure D.2, and an example of the 9th order Lagrange polynomials is shown in Figure D.3.

The displacement field  $\mathbf{u}(\mathbf{x})$  can be written in terms of Lagrange polynomials:

$$\mathbf{u}(\mathbf{x}(\xi_1, \xi_2, \xi_3)) = \sum_{\alpha=0}^n \sum_{\beta=0}^n \sum_{\gamma=0}^n \mathbf{u}(\mathbf{x}(\xi_\alpha^n, \xi_\beta^n, \xi_\gamma^n)) l_\alpha^n(\xi_1) l_\beta^n(\xi_2) l_\gamma^n(\xi_3) \quad (\text{D.20})$$

for which,  $(\xi_1, \xi_2, \xi_3) = \mathcal{F}_e^{-1}(\mathbf{x})$  are the coordinates in the referent element corresponding to the point  $\mathbf{x}$ ,  $\xi_\alpha^n, \xi_\beta^n, \xi_\gamma^n$  are respectively the coordinates of a node in the referent element  $\square_\Omega$  associated with the polynomials  $l_\alpha^n(\xi)$ ,  $l_\beta^n(\xi)$ ,  $l_\gamma^n(\xi)$ , and  $\mathbf{u}(\mathbf{x}(\xi_\alpha^n, \xi_\beta^n, \xi_\gamma^n))$  is the value of the desired field  $\mathbf{u}$  at GLL points.

## D.4 Diagonal mass matrix

The originality of the Spectral Element Method which the result of the choice of the quadrature for the numerical evaluation of the finite element formulation.

As in the classical Finite Element Method, the ordinary differential equation that governs the time dependence of the global system may be written in the form:

$$\mathbf{M}\ddot{\mathbf{U}} + \mathbf{K} \mathbf{U} = \mathbf{F} \quad (\text{D.21})$$

where  $\mathbf{U}$  denotes the displacement vector of the global system, which contains the displacement vector at all the grid points, in the global mesh, classically referred to the global degrees of freedom of the system,  $\mathbf{M}$  denotes the global mass matrix,  $\mathbf{K}$  is the global stiffness matrix and  $\mathbf{F}$  is the matrix of external forces.

In order to solve D.21, as in classical finite element method, the global mass matrix  $\mathbf{M}$  needs to be inverted. That global mass matrix  $\mathbf{M}$  can be obtained by assembling all the mass matrix of each element  $\mathbf{M}^e$  of the system:

$$\mathbf{M} = \bigoplus_{e=1}^{n_{el}} \mathbf{M}^e \quad (\text{D.22})$$

For each element  $\Omega_e$ , the mass matrix can be obtained by the tensor product:

$$\mathbf{M}^e = \mathbf{I}_d \otimes \widehat{\mathbf{M}}^e \quad (\text{D.23})$$

where  $\mathbf{I}_d$  is the identity matrix and  $\widehat{\mathbf{M}}^e$  is defined by [Delavaud, 2007] :

$$\widehat{M}_{ij}^e = \int_{\Omega_e} \rho(\boldsymbol{\xi}) N_{\mathbf{a}^i}(\boldsymbol{\xi}) N_{\mathbf{a}^j}(\boldsymbol{\xi}) d\boldsymbol{\xi} = \rho(\xi_\alpha^n, \xi_\beta^n, \xi_\gamma^n) |\mathbf{J}(\mathbf{x}(\xi_\alpha^n, \xi_\beta^n, \xi_\gamma^n))| \omega_\alpha^n \omega_\beta^n \omega_\gamma^n \delta_{ij} \quad (\text{D.24})$$

With that Kronecker delta  $\delta_{ij}$ , the matrix  $\widehat{\mathbf{M}}^e$  is a diagonal matrix which is the originality of the method and which gives an efficient parallel implementation as well as reduces the computation costs because of the inverse of the mass matrix.

## D.5 Time discretization

Generally, the equation D.21 can simply be written in another way as:

$$\mathbf{M}\ddot{\mathbf{U}} = \mathbf{F}^{ext}(t) - \mathbf{F}^{int}(\mathbf{u}, t) \quad (\text{D.25})$$

where  $\mathbf{F}^{ext}(t)$  and  $\mathbf{F}^{int}(\mathbf{u}, t)$  are respectively external and internal forces of the motions.

To solve numerically this equation, the time is discretized in short interval  $\Delta t : t_0, t_1, t_2, \dots$  with  $t_n = t_{n-1} + \Delta t$ . Denote  $\mathbf{u}_n, \mathbf{v}_n$  and  $\mathbf{a}_n$  be respectively the displacement, velocity and acceleration at the time step  $t_n$ . Consider three integration parameters  $\alpha, \beta, \gamma \in [0, 1]$ . The equation D.25 at time step  $t_{n+\alpha}$  can be written by [Komatitsch et al., 1999] :

$$\frac{1}{\Delta t} \mathbf{M}[\mathbf{v}_{n+1} - \mathbf{v}_n] = \mathbf{F}_{n+\alpha}^{ext} - \mathbf{F}^{int}(\mathbf{u}_{n+\alpha}, \mathbf{v}_{n+\alpha}) \quad (\text{D.26})$$

and we also have:

$$\mathbf{u}_{n+\alpha} = \alpha \mathbf{u}_{n+1} + (1 - \alpha) \mathbf{u}_n \quad (\text{D.27})$$

$$\mathbf{F}_{n+\alpha}^{ext} = \alpha \mathbf{F}_{n+1}^{ext} + (1 - \alpha) \mathbf{F}_n^{ext} \quad (\text{D.28})$$

$$\mathbf{u}_{n+1} = \mathbf{u}_n + \Delta t \left[ \left(1 - \frac{\beta}{\gamma}\right) \mathbf{v}_n + \frac{\beta}{\gamma} \mathbf{v}_{n+1} \right] + \Delta t^2 \left( \frac{1}{2} - \frac{\beta}{\gamma} \right) \mathbf{a}_n \quad (\text{D.29})$$

$$\mathbf{a}_{n+1} = \frac{1}{\gamma \Delta t} [\mathbf{v}_{n+1} - \mathbf{v}_n] + \left(1 - \frac{1}{\gamma}\right) \mathbf{a}_n \quad (\text{D.30})$$

These formulations can be said to be the numerical integration of Newmark with predictor and corrector:

For prediction ( $.^p$ ):

$$\mathbf{u}_{n+1}^p = \mathbf{u}_n + \Delta t \left(1 - \frac{\beta}{\gamma}\right) \mathbf{v}_n + \Delta t^2 \left( \frac{1}{2} - \frac{\beta}{\gamma} \right) \mathbf{a}_n \quad (\text{D.31})$$

$$\mathbf{v}_{n+1}^p = 0 \quad (\text{D.32})$$

$$\mathbf{a}_{n+1}^p = \left(1 - \frac{1}{\gamma}\right) \mathbf{a}_n - \frac{1}{\gamma \Delta t} \mathbf{v}_n \quad (\text{D.33})$$

to give the solution:

$$\frac{1}{\Delta t} \mathbf{M} \Delta \mathbf{v}^p = \mathbf{F}_{n+\alpha}^{ext} - \mathbf{F}^{int}(\mathbf{u}_{n+\alpha}^p, \mathbf{v}_{n+\alpha}^p) - \frac{1}{\Delta t} \mathbf{M} [\mathbf{v}_{n+1}^p - \mathbf{v}_n] \quad (\text{D.34})$$

and the correction ( $.^c$ ):

$$\mathbf{v}_{n+1}^c = \mathbf{v}_{n+1}^p + \Delta \mathbf{v}^p \quad (\text{D.35})$$

$$\mathbf{u}_{n+1}^c = \mathbf{u}_{n+1}^p + \frac{\beta \Delta t}{\gamma} \mathbf{v}_{n+1}^c \quad (\text{D.36})$$

$$\mathbf{a}_{n+1}^c = \mathbf{a}_{n+1}^p - \frac{1}{\gamma \Delta t} \mathbf{v}_{n+1}^c \quad (\text{D.37})$$

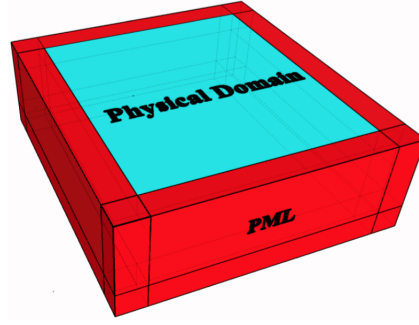
After [Simo et al., 1992], the values of  $\alpha = \beta = 1/2$  and  $\gamma = 1$  should be used to get a conditionally stable scheme. For [Cupillard et al., 2012], the accuracy and stability of the numerical method is ensured when:

$$d \leq \frac{n}{5} \lambda_{min} \quad (\text{D.38})$$

and when the CFL condition (Courant-Friedrichs-Lewy) is ensured:

$$\Delta t \leq C \left[ \frac{\Delta x}{v_p} \right]_{min} \quad (\text{D.39})$$

where  $d$  is the size of an element,  $n$  is the order of the polynomial,  $\lambda$  is the wavelength,  $v_p$  is the P-wave velocity, and  $C$  is the Courant number which is generally considered to be 0.4 for a 3D modelling.



**Figure D.4** – A half space domain surrounded by PML materials

## D.6 Perfect Match Layer (PML)

To do the numerical modelling of a full space or a half space, Software SEM3D adopts the Perfect Match Layers (PML) as the boundary conditions. Accurately, only the domain of interest will be modelled surrounded by the PML materials which have role to absorb the waves when the latter ones arrive at the borders of the domain of interest. An example of the half space domain surrounded by PML materials is presented in Figure D.4. When waves arrive at the free surface of the domain, they reflect and go back into the domain, while the reflections are not allowed when waves arrive at the borders between domain of interest and PML.

In frequency domain, a PML corresponds to an extension of the space of real coordinates in complex space. That extension is obtained by the following coordinate changes [Festa and Vilotte, 2005] :

$$\tilde{x} = x + \frac{\Sigma(x)}{i\omega} \quad (\text{D.40})$$

where  $\omega$  is the circular frequency and  $\Sigma(x)$  is an arbitrary function of  $x$  which increases regularly from the interface of the domain of interest to the external border of the PML.

For a plane-wave written in the form of:

$$\Phi(x, z, t) = A e^{i(\omega t - k_x x - k_z z)} \quad (\text{D.41})$$

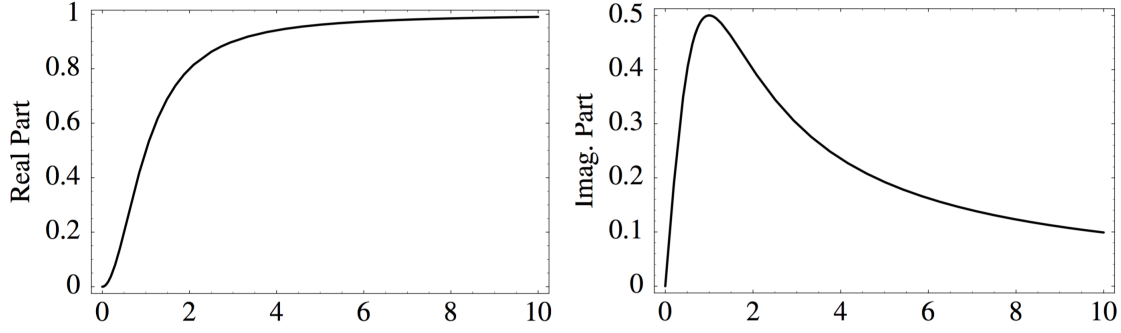
where  $A$  is the amplitude and  $k_x$  and  $k_z$  are respectively the wave numbers in  $x$  and  $z$  directions, will be transformed in the PML in  $x$  direction as:

$$\tilde{\Phi}(x, z, t) = \Phi(x, z, t) e^{-\frac{k_x}{\omega} \Sigma} \quad (\text{D.42})$$

which decreases exponentially independently of frequencies because of the ratio  $\frac{k_x}{\omega}$ .

Consider the decomposition in plane-wave of an Rayleigh wave propagating along the free surface ( $z = z_{max}$ ). The dependence along  $x$  direction of that wave will have the same characteristics as those of volume waves: they respect the same decreasing properties when they enter into the PML in  $x$  direction. Additionally, they preserve the characteristics of a surface wave, i.e. the movement is characterised by an exponential decreasing with the depth and an elliptic retrograde polarisation in the propagation plane on the surface, and prograde in the depth.

The classical choice of transformation in PML domain, as indicated in D.40 allows for a uniform decay, independent of frequencies inside the absorbing layer PML and a simplified description of the motions. More sophisticated expressions can lead to just as simple representations in the time



**Figure D.5** – Real and imaginary parts of the decay factor. The real parts controls the attenuation inside the absorbing layer and it is an increasing function reaching asymptotically the value 1. The imaginary part represents a phase shift, maximum at  $\omega = \omega_c$  and decreasing to zero for both  $\omega = 0$  and  $\omega \rightarrow \infty$  [Festa and Vilotte, 2005]

domain, with interesting properties inside the PML. If a real part is added to the frequency term, the pole of the stretching is moved away from the origin of the reference frame, into the imaginary axis, and the transformation can be written as:

$$\tilde{x} = x + \frac{\Sigma(x)}{i\omega + \omega_c} \quad (\text{D.43})$$

With this transformation, the compressional waves decrease in the PML following :

$$\tilde{\Phi}(x, z, t) = \Phi(x, z, t) e^{-\frac{k_x}{\omega} \frac{\omega^2 - i\omega\omega_c}{\omega^2 + \omega_c^2} \Sigma} \quad (\text{D.44})$$

where  $\omega_c$  is for instance, the circular cut-off frequency.

The transformation is finally dependent of frequencies through the factor  $\frac{\omega^2 - i\omega\omega_c}{\omega^2 + \omega_c^2}$ . Its real part contributes to the changes of the amplitude of decay, while its imaginary part is responsible of a phase shift. An example of the real part and imaginary part of the decay factor, plotted as functions of  $\omega/\omega_c$  is presented in Figure D.5 [Festa and Vilotte, 2005]. For the case of ( $\omega = 0$  and  $k_x/\omega$  finite), the real and imaginary parts tend to zero conducting to an elastic regime. When ( $\omega \rightarrow \infty$ ), the real part tends to 1, while the imaginary part vanishes. In this case, a PML standard is asymptotically found. Regarding the real part, the PML medium is like an elastic medium at low frequencies and a dissipative layer in high-range, the transition being described by a low pass filtering with a cut off frequency  $\omega_c$ . On the other hand, the imaginary part has a maximum for  $\omega = \omega_c$ , which corresponds to a phase shift.

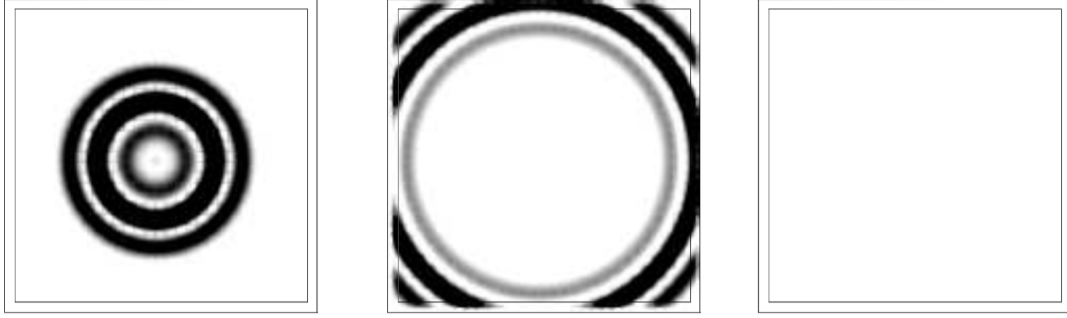
Figure D.6 [Festa and Vilotte, 2005] presents the modulus of velocity at three different instants : when waves propagate in the domain of interest, when waves arrive at the PML, and when waves are absorbed by PML. The source is simply an explosive Ricker at the center of the domain. It is shown that there is no visible reflections is seen to come back into the elastic medium.

## D.7 Stochastic field generations for random heterogeneous media

The equation describing the elastic wave propagation in elastic media can be expressed as:

$$\rho(\mathbf{x}) \frac{\partial^2 \mathbf{u}}{\partial t^2}(\mathbf{x}, t) - \nabla_x [\mathbf{C}(\mathbf{x}) : \nabla_x \otimes \mathbf{u}(\mathbf{x}, t)] = 0 \quad (\text{D.45})$$





**Figure D.6** – Modulus of the velocity at three different instants [Festa and Vilotte, 2005] to show about the absorbing properties of PML

where  $\rho(\mathbf{x})$  is the medium density,  $\mathbf{C}(\mathbf{x})$  is the forth-order elastic tensor and  $\mathbf{u}(\mathbf{x}, t)$  is the displacement field. To take into account the heterogeneities of the medium, we compute  $\mathbf{C}(\mathbf{x})$  replacing the properties by realization of a random field carrying inside its stochastic description.

The generation algorithm should meet the following specifications : (i) the time of generations should remain small compared to the simulation time and (ii) each generated sample should represent well the required statistics. One of the natural ways to sample a random field  $\{q(\mathbf{x}) : \mathbf{x} \in \Omega \subset \mathbb{R}^d\}$  with a given correlation function  $R$  is to search it as a linear combination of independent and identically distributed random seeds, where  $\Omega$  is the medium and  $d$  is the dimension of the domain of interest. The spectral representation is a classic way to sample Gaussian field :

$$q(\mathbf{x}) = \int_{\mathbf{k} \in \Omega} \hat{R}^{1/2}(\mathbf{k}) \exp(i\mathbf{k} \cdot \mathbf{x}) dW(\mathbf{k}) \quad (\text{D.46})$$

where  $\{W(\mathbf{k}) : \mathbf{k} \in \Omega\}$  is the Brownian motion,  $\hat{R}$  is the Fourier transform of  $R$ .

Several algorithm are developed to compute that stochastic integral and the one used in SEM3D is introduced by [Shinozuka and Deodatis, 1991]:

$$q(\mathbf{x}) = \sum_{n=0}^N \hat{R}^{1/2}(\mathbf{k}_n) \exp(i\mathbf{k}_n \cdot \mathbf{x}) \sqrt{\Delta_n} \xi(n) \quad (\text{D.47})$$

where  $\xi = \xi(n) : n \leq N$  is the white noise,  $\mathbf{k}_n \in \Omega_n$  for all  $n \leq N$ ,  $(\Omega_n)_{0 \leq n \leq N}$  is a partition of  $\Omega$  and  $\Delta_n$  is the Lebesgue mesure of  $\Omega_n$ .

A library for generating stochastic fields was established in the framework of a Ph.D thesis (see [de Carvalho Paludo et al., 2016] for instance) sponsored by SINAPS@ project. With that library, for instance, the parameters which can be generated as a stochastic field to represent the random heterogeneous media are  $(\kappa, \mu, \rho)$  or  $(\lambda, \mu, \rho)$  where  $\kappa$  is the bulk modulus,  $\mu$  is the shear modulus (Lamé constant),  $\rho$  is the mass density of the medium,  $\lambda$  is another Lamé constant. In all numerical case-studies realized in this Ph.D thesis, these parameters are considered to follow the log-normal statistic law whose probability density is defined by

$$f(x) = \frac{1}{x\sigma\sqrt{2\pi}} \exp\left(-\frac{(\ln x - m)^2}{2\sigma^2}\right), \quad (\text{D.48})$$

where  $x$  represents the elastic properties ( $\lambda, \mu, \kappa$  or  $\rho$ ),  $m$  and  $\sigma$  are respectively average value and standard deviation of of elastic properties.

About the correlation model of the random media, it is noted that for all numerical modellings realized in these studies, the Gaussian correlation model is used. This correlation function is given by:

$$R(d) = \xi^2 \exp\left(-\frac{d^2}{\ell_c^2}\right), \quad (\text{D.49})$$

where  $\xi$  is the coefficient of variation (COV) of elastic properties of the medium, and  $\ell_c$  is the correlation length of the medium.

## D.8 Earthquake source

In computational seismology, two simple source terms are often considered. The first one is simply a point source which is defined by:

$$\mathbf{f}(\mathbf{x}, t) = f_i \hat{\mathbf{e}}_i \delta(\mathbf{x} - \mathbf{x}_o) s(t - t_o) \quad (\text{D.50})$$

where  $f_i$  denotes the magnitude of the force applied at point  $\mathbf{x}_o$  at time  $t_o$  in the  $\hat{\mathbf{e}}_i$  direction;  $\delta(\mathbf{x} - \mathbf{x}_o)$  is the Dirac function and  $s(t - t_o)$  is an arbitrary function describing the force time variation.

The second one, after [Komatitsch et al., 1999], is an equivalent body force, derived from a seismic moment density tensor distribution, which represents the equivalent stress distribution associated with seismic sources:

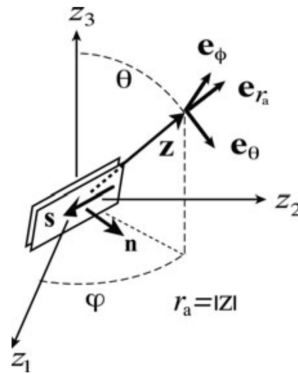
$$\mathbf{f}(\mathbf{x}, t) = -\text{div}[\mathbf{m}(\mathbf{x}, t)] \quad (\text{D.51})$$

where  $\mathbf{m}(\mathbf{x}, t)$  is the seismic moment density tensor at the location  $\mathbf{x}$  at time  $t$ . For simpler applications in literature, the seismic moment density is written similarly to a point source, which is :

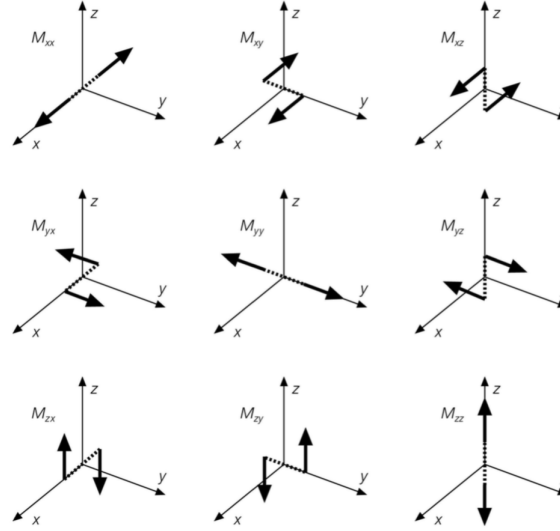
$$\mathbf{m}(\mathbf{x}, t) = \mathbf{M}(t) \delta(\mathbf{x} - \mathbf{x}_o) \quad (\text{D.52})$$

where  $\mathbf{M}$  is a symmetric tensor that has all the properties of a stress tensor. Figure D.7 presents an example of a share-dislocation point source which is normally represented by a moment tensor. That tensor can be normally written in the literature as a product between a constant moment tensor  $\mathbf{M}_o$  and an arbitrary time function  $s(t - t_o)$ :

$$\mathbf{M}(t) = \mathbf{M}_o s(t - t_o) \quad (\text{D.53})$$



**Figure D.7** – Geometry of a point shear-dislocation source, where  $\mathbf{n}$  is a normal to the fault and  $\mathbf{s}$  represents the fault slip direction



**Figure D.8** – Physical representation of each element of moment tensor matrix

The moment tensor is a simple mathematical description of the seismic waves produced by a complex rupture involving displacements varying in space and time on an irregular fault. With the moment tensor source, geometrically characterized by a unit vector  $\mathbf{n}$  normal to the fault plane and a unit vector  $\mathbf{s}$  parallel to the direction of fault slip as illustrated in Figure D.7, the far-field displacement vector in an infinite homogeneous elastic medium is related to the seismic-moment time function  $\mathbf{M}(t)$  representing the particle slip along the fault by [Madariaga, 2006]:

$$\mathbf{u}(\mathbf{z}, t) = B_r^P \mathbf{e}_{r_a} \frac{2}{\sqrt{15}} \frac{\dot{\mathbf{M}}(t - r_a/\alpha_o)}{4\pi\rho_o\alpha_o^3 r_a} + [B_\theta^S \mathbf{e}_\theta + B_\varphi^S \mathbf{e}_\varphi] \sqrt{\frac{2}{5}} \frac{\dot{\mathbf{M}}(t - r_a/\beta_o)}{4\pi\rho_o\beta_o^3 r_a} \quad (\text{D.54})$$

where  $(r_a, \theta, \varphi)$  are spherical coordinates of  $\mathbf{z}$ . Three orthogonal unit vectors of the spherical coordinate system are given by:

$$\mathbf{e}_{r_a} = \mathbf{z}/|\mathbf{z}| = \sin \theta \cos \varphi \mathbf{e}_1 + \sin \theta \sin \varphi \mathbf{e}_2 + \cos \theta \mathbf{e}_3 \quad (\text{D.55})$$

$$\mathbf{e}_\theta = \cos \theta \cos \varphi \mathbf{e}_1 + \cos \theta \sin \varphi \mathbf{e}_2 - \sin \theta \mathbf{e}_3 \quad (\text{D.56})$$

$$\mathbf{e}_\varphi = -\sin \varphi \mathbf{e}_1 + \cos \varphi \mathbf{e}_2 \quad (\text{D.57})$$


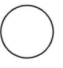










The first term in equation (13) is P-wave and the second term is S-wave in the far-field where the coefficients  $B_r^P$ ,  $B_\theta^S$  and  $B_\varphi^S$  are their radiation patterns :

$$B_r^P(\theta, \varphi, \mathbf{n}, \mathbf{s}) = \sqrt{15}(\mathbf{e}_{r_a} \mathbf{n})(\mathbf{e}_{r_a} \mathbf{s}) \quad (\text{D.58})$$

$$B_\theta^S(\theta, \varphi, \mathbf{n}, \mathbf{s}) = \sqrt{2.5}[(\mathbf{e}_\theta \mathbf{n})(\mathbf{e}_{r_a} \mathbf{s}) + (\mathbf{e}_\theta \mathbf{s})(\mathbf{e}_{r_a} \mathbf{n})] \quad (\text{D.59})$$

$$B_\varphi^S(\theta, \varphi, \mathbf{n}, \mathbf{s}) = \sqrt{2.5}[(\mathbf{e}_\varphi \mathbf{n})(\mathbf{e}_{r_a} \mathbf{s}) + (\mathbf{e}_\varphi \mathbf{s})(\mathbf{e}_{r_a} \mathbf{n})] \quad (\text{D.60})$$

With the moment tensor matrix  $\mathbf{M}_o$ , each element of the matrix represent different kinds of earthquake sources. Figure D.8 presents the different physical representation of each element of the tensor matrix, and the Figure D.9 presents the different kinds of earthquakes sources for different moment tensor matrix.

Moment tensor	Beachball	Moment tensor	Beachball
$\frac{1}{\sqrt{3}} \begin{pmatrix} 1 & 0 & 0 \\ 0 & 1 & 0 \\ 0 & 0 & 1 \end{pmatrix}$		$-\frac{1}{\sqrt{3}} \begin{pmatrix} 1 & 0 & 0 \\ 0 & 1 & 0 \\ 0 & 0 & 1 \end{pmatrix}$	
$-\frac{1}{\sqrt{2}} \begin{pmatrix} 0 & 1 & 0 \\ 1 & 0 & 0 \\ 0 & 0 & 0 \end{pmatrix}$		$\frac{1}{\sqrt{2}} \begin{pmatrix} 1 & 0 & 0 \\ 0 & -1 & 0 \\ 0 & 0 & 0 \end{pmatrix}$	
$\frac{1}{\sqrt{2}} \begin{pmatrix} 0 & 0 & -1 \\ 0 & 0 & 0 \\ -1 & 0 & 0 \end{pmatrix}$		$\frac{1}{\sqrt{2}} \begin{pmatrix} 0 & 0 & 0 \\ 0 & 0 & -1 \\ 0 & -1 & 0 \end{pmatrix}$	
$\frac{1}{\sqrt{2}} \begin{pmatrix} -1 & 0 & 0 \\ 0 & 0 & 0 \\ 0 & 0 & 1 \end{pmatrix}$		$\frac{1}{\sqrt{2}} \begin{pmatrix} 0 & 0 & 0 \\ 0 & -1 & 0 \\ 0 & 0 & 1 \end{pmatrix}$	
$\frac{1}{\sqrt{6}} \begin{pmatrix} 1 & 0 & 0 \\ 0 & -2 & 0 \\ 0 & 0 & 1 \end{pmatrix}$		$\frac{1}{\sqrt{6}} \begin{pmatrix} -2 & 0 & 0 \\ 0 & 1 & 0 \\ 0 & 0 & 1 \end{pmatrix}$	
$\frac{1}{\sqrt{6}} \begin{pmatrix} 1 & 0 & 0 \\ 0 & 1 & 0 \\ 0 & 0 & -2 \end{pmatrix}$		$-\frac{1}{\sqrt{6}} \begin{pmatrix} 1 & 0 & 0 \\ 0 & 1 & 0 \\ 0 & 0 & -2 \end{pmatrix}$	

**Figure D.9** – Different kinds of earthquake sources following different mement tensor matrix

For all the numerical studies presented in what follows, the moment tensor  $\mathbf{M}_o$  is considered to be of the form:

$$\mathbf{M}_o = -M_o \begin{bmatrix} 0 & 1 & 0 \\ 1 & 0 & 0 \\ 0 & 0 & 0 \end{bmatrix}$$

which corresponds to the case of a shear crack motion on a crack plane. It can be said as an idealized shearing source.

The time dependence function  $s(t)$  is considered to be a Ricker function defined by:

$$s(t) = \left(1 - 2(\pi f_c(t - \tau))^2\right) \exp\left(-(\pi f_c(t - \tau))^2\right), \quad (\text{D.61})$$

where  $f_c$  is the central frequency and  $\tau$  is the beginning of the signal.

## Appendix E

# Descriptions of reactor building of KK power plant

Some important characteristics of KK power plant as well as those of its finite element model used numerical modelling are presented here.

floor	T.S.M.L (vertical direction) in <i>m</i>
Inferior surface of apron	-13,7
3rd underground floor	-8,2
2nd underground floor	-1,7
1st underground floor	4,8
Ground floor	12,3
1st floor	18,1
2nd floor	23,5
3rd floor	31,7
4th floor	38,2
Roof	49,7

**Table E.1** – Vertical coordinate of each floor of the reactor building

Structural element	Characteristics (thickness)
Apron (reinforced concrete)	5,5 m
Floor (reinforced concrete)	50 cm to 2,3 m
External shell (reinforced concrete)	1,5 m to 1,7 m (foundation) 40 cm to 1,5 m (other parts)
Internal shell (reinforced concrete)	30 cm to 2,5 m
Containment (reinforced concrete)	2 m
Beams and Posts (reinforced concrete)	-
steal beam embedded in each floor	-
Steel trellis for supporting the roof	-

**Table E.2** – Principal structural components of reactor building

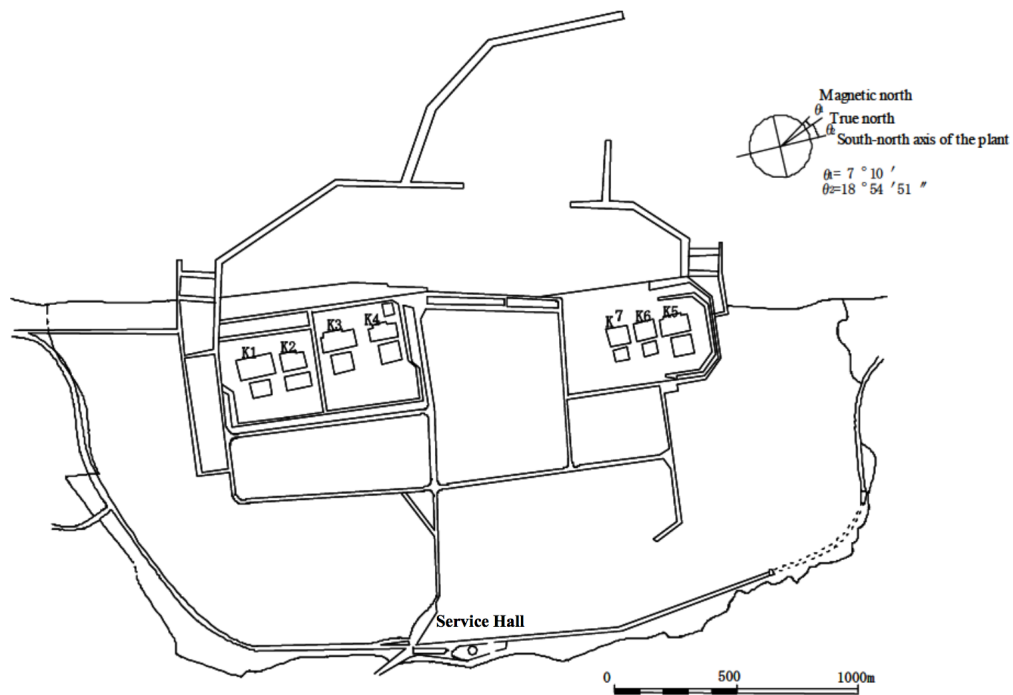


Figure E.1 – Maps of KK nuclear power plant [IAEA, 2012]

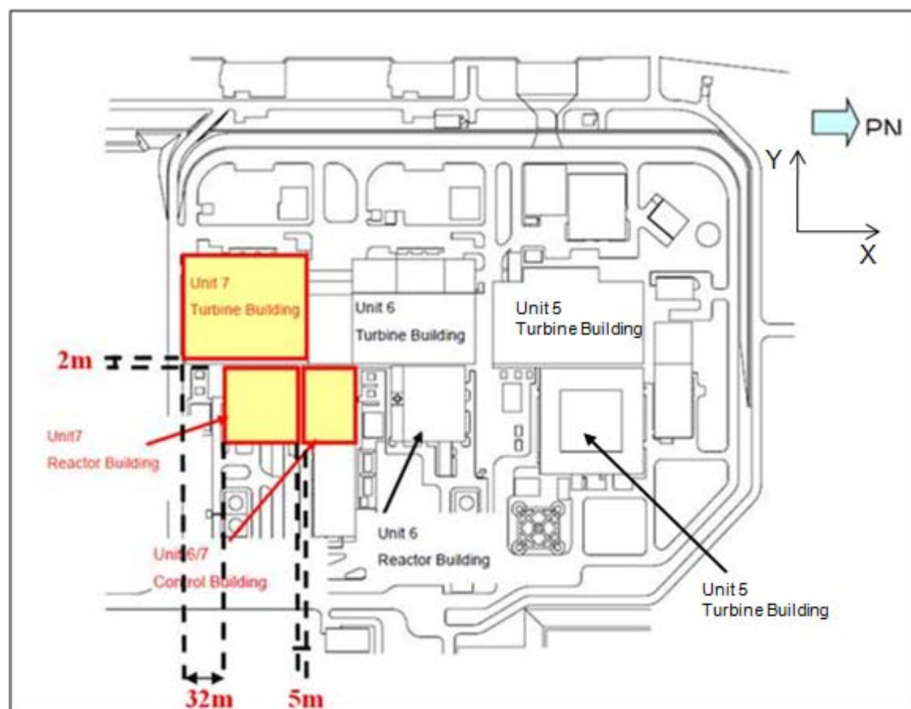


Figure E.2 – Maps of Unit 7 [IAEA, 2012]

Materials	Density ( $T/m^3$ )	Young modulus ( $MPa$ )	Poisson ratio	Compressive strength ( $MPa$ )	Tensile strength ( $MPa$ )
Concrete	2,4	31 300	0,2	33	-
Steel	7,8	205 000	0,3	-	240 (structural components) 350 (reinforce)
Steel for skewer model	0	192 000	0	-	-

**Table E.3** – Material properties used for the construction of reactor building

Structural components	Mass ( $T$ )	%Mass
Apron	45 996	22,99
floor (beside apron)	60 000	29,99
embedded external shell	20 837	10,41
external shell	12 778	6,39
Internal shell	31 916	15,95
Beams (reinforced concrete)	10 828	5,41
Posts (reinforced concrete)	8 430	4,21
Steel beam embedded in the floors	164	0,08
Beams and bars of the frame	389	0,19
NSSS	7 286	3,64
Equipments on the ground surface	507	0,25
Crane	270	0,13
Roof	664	0,33
<b>Total</b>	200 065	100,00

**Table E.4** – Distribution of mass inside the structural building





# Bibliography

- [Abrahamson, 1992] Abrahamson, N. (1992). Spatial variation of earthquake ground motion for application to soil-structure interaction. Technical Report TR-100463, EPRI.
- [Abrahamson, 1993] Abrahamson, N. (1993). Spatial variation of multiple support input. In *1st US Seminar on Seismic Evaluation of Retrofit of Steel Bridges, San Francisco, CA*.
- [Abrahamson et al., 1987] Abrahamson, N., Bolt, A. B., Darrah, R. B., Penzien, J., and Tsai, Y. B. (1987). The smart-1 accelerograph array (1980-1987): A review. *Earthquake Spectra*, (3):263–287.
- [Abrahamson et al., 1990] Abrahamson, N., Schneider, J. F., and Stepp, J. C. (1990). Spatial variation of strong ground motion for use in soil-structure interaction analyses. In *4th US-National Conference on Earthquake Engineering*, pages 317–326. Palm Springs CA.
- [Abrahamson et al., 1991] Abrahamson, N., Schneider, J. F., and Stepp, J. C. (1991). Empirical spatial coherency functions for application to soil-structure interaction analyses. *Earthquake Spectra*, 7(1):1–27.
- [Abramowitz and Stegun, 2012] Abramowitz, M. and Stegun, I. (2012). *Handbook of mathematical functions: with formulas, graphs, and mathematical tables*.
- [Ancheta et al., 2011] Ancheta, T., Stewart, J. P., and Abrahamson, N. (2011). Engineering characterization of earthquake ground motion coherency and amplitude variability. In *4th IASPEI/IAEE International Symposium*. University of California Santa Barbara.
- [Aubry, 2016] Aubry, L. (2016). *SEM Documentation*.
- [Banci et al., 2015] Banci, F., Greffet, N., Jacquet, M., Kham, M., Alves-Fernandes, V., and Nieto-Ferro, A. (2015). Projet omarisis2016 - méthodologies d’interaction sol-structure non-linéaire pour le cas d’application industrielle karisma. Technical report, Internal Technical Report of EDF R&D.
- [BergeThierry et al., 2016] BergeThierry, C., Svay, A., Laurendeau, A., Chartier, T., Perron, V., Guyonnet-Benaize, C., Kishta, E., Cottureau, R., Lopez-Caballero, F., Hollender, F., Richard, B., Ragueneaud, F., Voldoire, F., Banci, F., Zentner, I., Moussallam, N., Lancieri, M., Bard, P., Grange, S., Erlicher, S., Kotronis, P., Le-Maout, A., Nicolas, M., Regnier, J., Bonilla, F., and Theodoulidis, N. (2016). Toward an integrated seismic risk assessment for nuclear safety improving current french methodologies through the sinaps@ research project. *Nuclear Engineering and Design*.
- [Bi and Hao, 2013] Bi, K. and Hao, H. (2013). Numerical simulation of pounding damage to bridge structures under spatially varying ground motion. *Engineering Structures*, 46:62–76.
- [Clough and Penzien, 1993] Clough, R. W. and Penzien, J. (1993). *Dynamics of Structures*. McGraw-Hill, Inc., New York.
- [Clouteau, 2005] Clouteau, D. (2005). Manuel scientifique de miss. Technical report, MSSMAT, Ecole Centrale Paris.

- [Clouteau, 2007] Clouteau, D. (2007). Manuel utilisateur de miss. Technical report, MSSMAT, Ecole Centrale Paris.
- [Cupillard et al., 2012] Cupillard, P., Delavaud, E., Burgos, G., Festa, G., Vilotte, J. P., Capdeville, Y., and Montagner, J. P. (2012). Regsem: a versatile code based on the spectral element method to compute seismic wave propagation at the regional scale. *Geophysical Journal International*, 3(188):1203–1220.
- [Cushing et al., 2016] Cushing, E. M., Hollender, F., Guvonnet-Benaize, C., Perron, V., Imtiaz, A., Svay, A., Mariscal, A., Bard, P., Cottureau, R., Lopez-Caballero, F., Theodoulidis, N., Moiriat, D., and Gelis, C. (2016). Close to the lair of odysseurs cyclons: Sinaps@ postseismic campaign and accelerometric network installation on cephalonia island - site effect characterization experiment. In *7th International INQUA Meeting on Paleoseismology, Active Tectonics and Archeoseismology (PATA)*.
- [de Carvalho Paludo et al., 2016] de Carvalho Paludo, L., Bouvier, V., and Cottureau, R. (2016). Scalable parallel scheme for sampling of gaussian random fields over large domains. *Internaltional Journal for Numerical Methods in Engineering*.
- [Delavaud, 2007] Delavaud, E. (2007). *Simulation numérique de la propagation d’ondes en milieu géologique complexe : application à l’évaluation de la réponse sismique du bassin de Caracas (Venezuela)*. PhD thesis, Institut de Physique du Globe de Paris.
- [DerKiureghian, 1996] DerKiureghian, A. (1996). A coherency model for spatially varying ground motions. *Earthquake Engineering and Structural Dynamics*, 25:99–111.
- [DerKiureghian and Neuenhofer, 1992] DerKiureghian, A. and Neuenhofer, A. (1992). Response spectrum method for incoherent support motions. In *10th World conference on Earthquake Engineering, Madrid, Spain*.
- [EPRI, 2005] EPRI (2005). Effects of seismic wave incoherence on foundation and building response. Technical Update Report TR-1012966, EPRI.
- [EPRI, 2006a] EPRI (2006a). Program on technology innovation: Effects of seismic wave incoherence on foundation and building responses. Technical Report 1013504, EPRI.
- [EPRI, 2006b] EPRI (2006b). Program on technology innovation: Spatial coherency models for soil-structure interaction. Final Report 1014101, EPRI.
- [EPRI, 2006c] EPRI (2006c). Program on technology innovation: Spatial coherency models for soil-structure interaction. Technical Update Report 1012968, EPRI.
- [EPRI, 2007a] EPRI (2007a). Program on technology innovation: Effects of spatial incoherence on seismic ground motions. Technical Report 1015110, EPRI.
- [EPRI, 2007b] EPRI (2007b). Program on technology innovation: Validation of classi and sassi codes to treat seismic wave incoherence in soil-structure interaction (ssi) analysis of nuclear power plant structures. Final Report 1015111, EPRI.
- [Festa and Vilotte, 2005] Festa, G. and Vilotte, J. P. (2005). The newmark scheme as velocity-stress time-staggering: an efficient pml implementation for spectral element simulaitons of elastodynamics. *Geophysical Journal International*, 3(161):789–812.
- [Foti et al., 2014] Foti, S., Lai, C. G., Rix, G., and Strobbia, C. (2014). *Surface wave methods for near-surface site characterization*. CRC Press.
- [Ghiocel and Ostadan, 2007] Ghiocel, D. and Ostadan, F. (2007). Seismic ground motion incoherency effects on soil-structure interaction response of npp building structure. In *19th International Conference on Structural Mechanics in Reactor Technology (SMiRT19)*.
- [Ghiocel et al., 2010] Ghiocel, D. M., Stephen, S., and Hardy, G. (2010). Seismic motion incoherency effects for nuclear complex structures on different soil site conditions. In *OECD NEA Seismic SSI Workshop in Ottawa*.

- [Greffet, 2016] Greffet, N. (2016). Analyse sismique en iss et isfs avec le chaînage code\_aster-miss3d par la commande calc\_miss. Technical report, EDF Lab.
- [Hao et al., 1989] Hao, H., Oliveira, C. S., and Penzien, J. (1989). Multiple-station ground motion processin and simulaiton based on smart-1 array data. *Nuclear Engineering and Design*, 111:293–310.
- [Harichandran, 1988] Harichandran, R. S. (1988). Local spatial variation of earthquake ground motion, earthquake engineering and soil dynamics ii - recent advances in ground motion evaluation. *American Society of Civil Engineers, New York*, pages 203–217.
- [Harichandran, 1991] Harichandran, R. S. (1991). Estimating the spatial variation of earthquake ground motions from dense array recordings. *Structural Safety*, 10:219–233.
- [Harichandran, 1999] Harichandran, R. S. (1999). *SPATIAL VARIATION OF EARTHQUAKE GROUND MOTION, What is it, how do we model it, and what are its engineering implications?* Press of Michigan State University.
- [Harichandran and Vanmarcke, 1986] Harichandran, R. S. and Vanmarcke, E. (1986). Stochastic variation of earthauqke ground motion in space and time. *Journal of Engineering Mechanics, ASCE*, (112).
- [Hollender et al., 2015a] Hollender, F., Perron, V., Imtiaz, A., Svay, A., Mariscal, A., Bard, P., Cottureau, R., Lopez-Caballero, F., Cushing, E. M., Theodoulidis, N., and Moiriat, D. (2015a). Close to the lair of odysseurs cyclons: Sinaps@ post-seismic campaign and accelerometric network installation on cephalonia island. In *Proceedings of the 9th AFPS national meeting*.
- [Hollender et al., 2015b] Hollender, F., Perron, V., Imtiaz, A., Svay, A., Mariscal, A., Bard, P., Cottureau, R., Lopez-Caballero, F., Cushing, M., Theodoulidis, N., and Moiriat, D. (2015b). A deux pas du repaire du cyclope d’ulyse : la campagne post-sismique et le démarrage du réseau accélérométrique sinaps@ sur l’île de céphalonie. In *AFPS - Association Française du Génie Parasismique*. Marne la vallée, France.
- [Hong, 1993] Hong, H. (1993). Arch response to correlated multiple excitations. *Soil Dynamics and Earthquake Engineering*, 22:389–404.
- [IAEA, 2012] IAEA (2012). Guidance document part 1 : K-k unit 7r/b structure phase i, ii and revised iii. Technical report, International Agency of Atomic Energy.
- [IAEA, 2013] IAEA (2013). Review of seismic evaluation methodologies for nuclear power plants based a banchmark exercice. Technical Report IAEA-TECDOC-1722, International Agency of Atomic Energy.
- [IDN, 2015] IDN (2015). Top 10 nuclear power plants. *indiandefensenews*.
- [Jeremic et al., 2013] Jeremic, B., Tafazzoli, N., Ancheta, T., Orbovic, N., and Blahoianu, A. (2013). Seismic behavior of npp structures subjected to realistic 3d, inclined seismic motions, in variable layered soil/rock, on surface of embedded foundations. *Nuclear Engineering and Design*, 265:85–94.
- [Kanai, 1957] Kanai, K. (1957). Semi empirical formula for the seismic characteristics of the ground motion. *Bulletin of Earthquake Research Institute, University of Tokyo*, 35:309–325.
- [Kausel, 2006] Kausel, E. (2006). *Fundamental solutions in elastodynamics*. Cambridge.
- [Khazaie et al., 2016] Khazaie, S., Cottureau, R., and Clouteau, D. (2016). Influence of the spatial correlation structure of an elastic random medium on its scattering properties. *Journal of Sound and Vibration*, 370:132–148.
- [Klimes, 2002] Klimes, L. (2002). Correlation functions of random media. *Pure and Applied Geophysics*, (159):1811–1831.
- [Komatitsch, 1997] Komatitsch, D. (1997). *Méthodes spectrales et éléments spectraux pour l’équation de l’élastodynamique 2D et 3D en milieu hétérogène*. PhD thesis, Institut de Physique du Globe de Paris.

- [Komatitsch et al., 1999] Komatitsch, D., Vilotte, J., Vai, R., Castillo-Covarrubias, J., and Sanchez-Sesma, F. (1999). The spectral element method for elastic wave equations, application to 2d and 3d seismic problems. *International Journal for Numerical Methods in Engineering*, 9(45):1139–1164.
- [Konakli and DerKiureghian, 2011] Konakli, K. and DerKiureghian, A. (2011). Extended msrs rule for seismic analysis of bridges subjected to differential support motions. *Earthquake Engineering and Structural Dynamics*, 40:1315–1335.
- [Konakli et al., 2013] Konakli, K., Kiureghian, A. D., and Dreger, D. (2013). Coherency analysis of accelerograms recorded by the upsar array during the 2004 parkfield earthquake. *Earthquake Engineering and Structural Dynamics*, 43:641–659.
- [Loh, 1985] Loh, C. H. (1985). Analysis of the spatial variation of seismic waves and ground movements from smart-1 data. *Earthquake Engineering and Structural Dynamics*, (13):561–581.
- [Loh and Lin, 1990] Loh, C. H. and Lin, S. G. (1990). Directionally and simulation in spatial variation of seismic waves. *Engineering Structures*, 13:134–143.
- [Loh and Yeh, 1988] Loh, C. H. and Yeh, Y. T. (1988). Spatial variation and stochastic modelling of seismic differential ground movement. *Earthquake Engineering and Structural Dynamics*, 16:583–596.
- [Lou and Zerva, 2005] Lou, L. and Zerva, A. (2005). Effects of spatially variable ground motions on the seismic response of skewed, multi-span, rc highway bridge. *Soil Dynamics and Earthquake Engineering*, (25):729–740.
- [Luco and Mita, 1987] Luco, J. E. and Mita, A. (1987). Response of circular foundation to spatially random ground motion. *Journal of Engineering Mechanics*, 113(1).
- [Luco and Wong, 1986] Luco, J. E. and Wong, H. L. (1986). Response of a rigid foundation to a spatially random ground motion. *Soil Dyn. Earthqu. Engr.*, 14:891–908.
- [Madariaga, 2006] Madariaga, R. (2006). *Seismic source theory*, volume 4, chapter 2. Earthquake seismology.
- [Mezher, 2009] Mezher, N. (2009). Modélisation du bâtiment réacteur de l’installation nucléaire de kashiwazaki-kariwa - note de modélisation. Technical report, NECS.
- [Mezouer et al., 1998] Mezouer, N., Afra, H., and Silhadi, K. (1998). The effects of spatial variability ground motion on structures response. In *11th European Conference on Earthquake Engineering, Balkema, Rotterdam*.
- [Novak, 1987] Novak, M. (1987). Discussion of stochastic variation of earthquake ground motion in space and time by r. s. harichandran and e. h. vanmarcke. *Journal of Engineering Mechanics*, (1123):1267–1270.
- [Oliveira et al., 1991] Oliveira, C. S., Hao, H., and Penzien, J. (1991). Ground motion modelling for multiple input structural analysis. *Structural Safety*, 10:79–93.
- [Pavlenko and Irikura, 2012] Pavlenko, O. V. and Irikura, K. (2012). Nonlinear soil behavior at the kashiwazaki-kariwa nuclear power plant during the niigata chuetsu-oki earthquake (july 16, 2007). *Pure and Applied Geophysics*, 169:1777–1800.
- [Ramadan and Novak, 1993] Ramadan, O. and Novak, M. (1993). Coherency functions for spatially correlated seismic ground motions. Technical Report GEOT-9-93, Geotechnical Research Center, Ontario, Canada.
- [Rezaeian and DerKiureghian, 2011] Rezaeian, S. and DerKiureghian, A. (2011). Simulation of orthogonal horizontal ground motion components for specified earthquake and site characteristics. *Earthquake Engineering and Structural Dynamics*, 41:335–353.
- [Roy et al., 1968] Roy, R., Craig, J., and Bampton, M. C. (1968). Coupling of substructures for dynamic analysis. *AIAA Journal*, 6(7):1313–1319.

- [Sato et al., 2012] Sato, H., Fehler, M. C., and Maeda, T. (2012). *Seismic wave propagations and scattering in the heterogeneous earth: Second Edition*. Springer Edition.
- [Saxena et al., 2000] Saxena, V., Deodatis, G., and Shinozuka, M. (2000). Effect of spatial variation of earthquake ground motion on the nonlinear dynamic response of highway bridges. New Zealand. 12 WCEE.
- [Schneider et al., 1992] Schneider, J. F., Stepp, J. C., and Abrahamson, N. (1992). The spatial variation of earthquake ground motion and effects of local site conditions. In *Proceedings of the 10th Earthquake Engineering World Conference*.
- [Shinozuka and Deodatis, 1988] Shinozuka, M. and Deodatis, G. (1988). Response variability of stochastic finite element systems. *Engineering Mechanics*, 114(3):499–519.
- [Shinozuka and Deodatis, 1991] Shinozuka, M. and Deodatis, L. (1991). Simulations of stochastic process by spectral representations. *Applied Mechanics Reviews*, 44(4):191–205.
- [Simo et al., 1992] Simo, J., Tarnow, N., and Wong, K. (1992). Exact energy-momentum conserving algorithms and symplectic schemes for nonlinear dynamics. *Computer methods in applied mechanics and engineering*, 1(100):63–116.
- [Svay et al., 2017a] Svay, A., Perron, V., Imtiaz, A., Zentner, I., Cottureau, R., Clouteau, D., Bard, P., Hollender, F., and Lopez-Caballero, F. (2017a). Spatial coherency analysis of seismic ground motions from a rock site dense array implemented during the kefalonia 2014 aftershock sequence. *Earthquake Engineering and Structural Dynamics (Accepted)*.
- [Svay et al., 2015] Svay, A., Zentner, I., Cottureau, R., and Clouteau, D. (2015). Superposition of random effects and deterministic effects on spatial variability of seismic ground motions. In *CSMA, Presqu'île de Giens*.
- [Svay et al., 2016a] Svay, A., Zentner, I., Cottureau, R., and Clouteau, D. (2016a). Influence of physical and statistical properties of random heterogeneous media on spatial variability of seismic ground motions. In *ECCOMAS, Crete, Greece*.
- [Svay et al., 2016b] Svay, A., Zentner, I., Cottureau, R., and Clouteau, D. (2016b). Spatial coherency analysis of seismic ground motions from 2014-argostoli earthquake dense array. In *Annual meeting of Seismological Society of America, Reno, Nevada, USA*.
- [Svay et al., 2017b] Svay, A., Zentner, I., Cottureau, R., and Clouteau, D. (2017b). On the validation of a coherency model for spatial variability of earthquake ground motions based on numerical modelling of wave propagations in random heterogeneous media. *Soil Dynamics and Earthquake Engineering*.
- [Tajimi, 1960] Tajimi, H. (1960). A statistical method of determining the maximum response of a building structure during an earthquake. In *Proceeding of the 2nd World Conference on Earthquake Engineering*, pages 781–798, Science Council of Japan.
- [Theodoulidis et al., 2016] Theodoulidis, N., Karakostas, C., Lekidis, V., Makra, K., Margaritis, B., Morfidis, K., Papaioannou, C., Rovithis, E., Salonikios, T., and Savvaidis (2016). The cephalonia, greece, january 26 (m6.1) and february 3, 2014 (m6.0) earthquakes: near-fault ground motion and effects on soil and structures. *Bulletin of Earthquake Engineering*, 14:1–38.
- [Tromp et al., 2008] Tromp, J., Komatitsch, D., and Liu, Q. (2008). Spectral element and adjoint methods in seismology. *Communications in Computational Physics*, 1(3):1–32.
- [Tseng et al., 2013] Tseng, W., Lilhanand, K., Hamasaki, D., Garcia, J. A., and Srinivasan, R. (2013). Seismic soil-structure interaction with consideration of spatial incoherence of seismic ground motions : a case study. *Nuclear Engineering and Design*.
- [Valkaniotis et al., 2014] Valkaniotis, S., Ganas, A., Papathanassiou, G., and Papanikolaou, M. (2014). Field observations of geological effects triggered by the january-february 2014 cephalonia (ionian sea, greece) earthquakes. *Tectonophysics*, 630:150–157.

- [Verno et al., 1991] Verno, F., Fletcher, J., Carroll, L., Chave, A., and Sembera, E. (1991). Coherence of seismic body waves as measured by a small aperture array. *Journal of Geophysical Research*, 96:11981–11996.
- [Zentner, 2013] Zentner, I. (2013). Etude d’opportunité de la thèse "modélisation de la variabilité spatiale du champ sismique pour les études d’interaction sol-structure". Internal Report CR-AMA-13.131, EDF Lab.
- [Zentner, 2016] Zentner, I. (2016). Interaction sol-structure avec variabilité spatiale (opérateur dyna\_iss\_vari). Documentation de code\_aster, EDF Lab.
- [Zentner and Devesa, 2011] Zentner, I. and Devesa, G. (2011). A methodology for soil-structure interaction analysis accounting for spatially incoherent seismic free field motion. In *Proceedings of the 8th International Conference on Structural Dynamics, EUROODYN2011, Leuven, Belgium*.
- [Zerva, 2009] Zerva, A. (2009). *Spatial Variation of Seismic Ground Motions, Modelling and Engineering Application*. Boca Raton.
- [Zerva and Harada, 1997] Zerva, A. and Harada, T. (1997). Effect of surface layer stochasticity on seismic ground motion coherence and strain estimates. *Soil Dynamics and Earthquake Engineering*, 16(7-8):445–457.
- [Zerva and Zervas, 2002] Zerva, A. and Zervas, V. (2002). Spatial variation of seismic ground motions: an overview. *Applied Mechanics Reviews*, 55:270–297.
- [Zerva and Zhang, 1997] Zerva, A. and Zhang, O. (1997). Correlation pattern in characteristic of spatially variable seismic ground motions. *Earthquake Engineering and Structural Dynamics*, 26:19–39.



**Titre: Modélisation de la Variabilité Spatiale du Champ Sismique pour les Etudes d'Interaction Sol-Structure**

**Mots clés :** Variabilité spatiale, Interaction Sol-Structure, Fonction de Cohérence, Milieux hétérogènes aléatoires

**Résumé :** Dans les analyses d'interaction sol-structure (ISS), la pratique commune en génie civil est de considérer un mouvement uniforme du champ libre à tous les points situés à la surface du sol. Néanmoins, cette considération n'est pas tout à fait réaliste parce que les signaux sismiques sont spatialement différents grâce à l'effet de passage d'ondes, à l'effet de site et aussi aux dispersions et réflexions des ondes qui propagent dans des milieux hétérogènes aléatoires ("incohérence pure"). Ainsi, pour répondre aux problèmes de sécurité des bâtiments et équipements, il est important de faire une analyse d'interaction sol-structure dans la manière plus réaliste. Cela peut être acquis par prendre en compte la variabilité spatiale du champ sismique dans les études d'ISS. Un grand nombre d'études dans la littérature montrent que la prise en compte de la variabilité spatiale du champ sismique dans les études d'ISS peut avoir des effets importants sur la réponse de structures. L'incohérence spatiale du champ sismique due aux dispersions et réflexions des ondes (incohérence pure)

peut généralement être modélisée pour ce genre d'études dans le cadre probabiliste par une fonction de cohérence. Le but principal des études réalisées dans cette thèse de doctorat est de construire une description stochastique de la variabilité spatiale du champ sismique par un modèle de cohérence. Ce modèle devrait avoir une relation avec les propriétés physiques et statistiques de milieux considérés. En s'appuyant sur les analyses théoriques de la propagation des ondes sismiques dans des milieux hétérogènes aléatoires, les analyses des données expérimentales obtenues par des enregistrements sur des sites sismiques, ainsi que sur les modélisations numériques de propagation des ondes sismiques dans des milieux hétérogènes aléatoires, un modèle de cohérence est validé dans le cadre des études de cette thèse de doctorat pour représenter la variabilité spatiale du champ sismique dans les études d'interaction sol-structure. L'influence de la variabilité spatiale du champ sismique sur la réponse de structure est également analysée.

**Title : Modelling of Spatial Variability of Seismic Ground Motions for Soil-Structure Interaction Analysis**

**Keywords :** Spatial Variability, Soil-Structure Interaction, Coherency Function, Random heterogeneous media

**Abstract:** In seismic soil-structure interaction studies (SSI), the common practice in Civil Engineering is to consider a uniform movement of free field at any point on the ground surface. However, that assumption is not completely realistic since the seismic ground motions can vary spatially due to wave passage effects, dispersions and reflections of wave propagating in the random heterogeneous media "pure incoherence" and site effects. Therefore, in order to increase the security of buildings and equipment, it is important to do an analysis of seismic soil-structure interactions in the most realistic way. This can be achieved by taking into account the spatial variability of seismic ground motions. Several studies in the literature show that taking into account the spatial variability of seismic ground motions in SSI analyses can have remarkable effects on the structural responses. The spatial incoherence of seismic ground motions due to dispersions and reflections of wave "pure incoherence" can generally be modelled in such analysis by

a "coherency function" in frequency domain. The principal goal of this Ph.D thesis is to construct a stochastic description of spatial variability of seismic ground motions by means of coherency functions. Accurately, it aims to propose a parametrical coherency model of spatial variability of seismic ground motions. This later should be related to some physical and statistical properties of the soil at the application sites so that it can be applied in any types of sites. Based on theoretical considerations on coherency of seismic wave propagation in random heterogeneous media, on experimental data analyses, and on numerical modelling of seismic wave propagation in random heterogeneous media, a coherency model is validated and proposed for the analyses of soil-structure interactions. The influence of spatial variability of seismic ground motions on the structural responses are also pointed out by using the validated coherency model.

